C.P. No. 672

C.P. No. 672

MINISTRY OF AVIATION

AERONAUTICAL RESEARCH COUNCIL

CURRENT PAPERS

Wind Tunnel Tests at Supersonic Speeds on a Model of the Fairey Delta 2.

By

M.D. Dobson

LONDON: HER MAJESTY'S STATIONERY OFFICE

1964

PRICE 13s 6d NET

U.D.C. No. A.I.(42) Fairey Delta 533.6.013.1 : 533.6.011.5

C.P. No. 672

October 1962

WIND TUNNEL TESTS AT SUPERSONIC SPEEDS ON A MODEL OF THE FAIREY DELTA 2

by

M. D. Dobson

SUMMARY

Results are given of tests at Mach numbers from 1·42 to 2·00, on a 1/24 scale model of the Fairey Delta 2 aircraft. Lift, pitching moment, axial force, sideforce, yawing moment and rolling moment were measured, giving an assessment of the general stability characteristics, including the effects of airbrakes and a ventral fuel tank. Elevator effectiveness and aileron effectiveness were measured. Incremental values of drag were obtained resulting from separate addition of airbrakes and fuel tank, and the application of elevator and aileron. No absolute values of drag are presented owing to difficulties in measuring the internal drag of the intake system.

The model was stable in pitch and the position of the aerodynamic centre remained constant at 0·51 $\bar{c}$ (0·67 centre line chord) throughout the incidence range at all Mach numbers. The addition of airbrakes caused a rearward movement of the aerodynamic centre of 0·02 $\bar{c}$ at all Mach numbers.

In all configurations the model was directionally stable at low lift, though the stability decreased with increase of incidence and in some cases the model became directionally unstable at high incidence. Directional stability was appreciably improved by opening the airbrakes but was reduced by the addition of the ventral fuel tank.

Replaces R.A.E. Tech. Note No. Aero. 2844 - A.R.C.24,606

LIST OF CONTENTS

LIST OF ILLUSTRATIONS

LIST OF ILLUSTRATIONS (Contd.)

LIST OF ILLUSTRATIONS (Contd.)

1 INTRODUCTION

The Fairey Delta 2 is a research aircraft which is capable of supersonic flight up to a Mach number of at least 1·8. The aircraft, which is tailless, has a delta wing planform with a leading-edge sweepback angle of $\simeq 60^\circ$ and thickness-chord ratio of 0·04; the elevators are located inboard and the ailerons outboard on the unswept trailing-edge. It is powered by a single jet engine installed in the fuselage, the air for which passes through intakes at the wing roots. Two such aircraft have been built and they have been engaged in a considerable programme of flight research, see for example Refs.1 and 2.

As part of a research programme for the comparison of results as measured in flight and on representative models, a 1/24 scale model of the Fairey Delta 2 has been tested at supersonic speeds in the 3ft × 3 ft wind tunnel. This note gives the results of these tests.

In order to accommodate both the sting support and air flow through the model it was necessary to distort the fuselage shape, resulting in a slightly deeper fuselage with less boattailing at the base. No allowance has been made for these differences in the results presented.

Tests made at supersonic Mach numbers were required to provide information on:-

(a) lift and longitudinal stability of the model with various elevator settings;

(b) effects of airbrakes and ventral fuel tank on lift and longitudinal stability;

(c) drag increments of airbrakes, ventral fuel tank, elevator and aileron;

(d) lateral stability characteristics of the model with varying sideslip and incidence, including fin effectiveness, aileron effectiveness and the effects of airbrakes, elevator setting and the ventral fuel tank.

The basic experimental data are presented, together with some analysis but only a limited discussion of the results is included. A further report is to be written giving a comparison of fullscale and model results.

2 EXPERIMENTAL DETAILS

2.1 Model and balance

An outline drawing of the model is shown in Fig.1 and the principal dimensions are given in Table 1. Fig.2 is a photograph of the model mounted in the tunnel and details of the airbrakes and ventral fuel tank are given in Figs.3 and 4.

The model was made to 1/24 scale and the external shape is representative of the aircraft except for the following differences:-

(i) the model has a slightly different nose shape;

(ii) the fuselage is slightly deepened along its length;

(iii) the rear part of the fuselage is not boattailed to the extent which applies on the aircraft,

(iv) the model was designed from early drawings of the aircraft configuration, since when the fullscale intake area has been increased.

Thus the model has:-

(a) a projected side area 3% larger;

(b) a slightly shorter fuselage;

(c) a base area approximately four times greater than the aircraft with its reheat eyelids closed;

(d) air intakes which are approximately 10% small in area.

The external differences between the model and aircraft are shown in Fig.1.

Air was allowed to flow through the wing root intakes. The intakes and internal ducting are correctly represented as far as the engine face position, aft of which the air passage splits into two, leading the air above and below the faired internal drag balance and supporting sting, to exit at the annulus formed by the model base and the sting. The fuselage boundary-layer air was prevented from entering the intakes by bleed ducts inboard of the intakes. These ducts contained wedges to divert the air over the upper and lower surfaces of the wings in the region of the wing-body junctions. The port intake and boundary-layer duct may clearly be seen in Fig.2. It should be noted that there is a further difference between the model and aircraft concerning the bleed ducts in that, on the aircraft, air diverted downward by the wedges is ducted away and used for cooling purposes, later to be exhausted from the underside of the fuselage, well aft. In the present tests, the bleed air was exhausted onto the under surface in the wing-body junctions.

The wing was of composite construction and consisted of a hexagonal steel core which was covered with an epoxy resin and hand finished to the required profile. The steel core was manufactured in one piece with the rear fuselage. The basic model was completed by the intake section, canopy, nose, wing boundary-layer fences and tail bumper all of which were made of tufnol. The ventral fuel tank, airbrakes and fin were made detachable; the fin included the bullet at the root which houses the landing parachute on the aircraft.

Elevators and ailerons are represented on the model by cutting grooves in each surface of the wing along the control hingeline and deflecting the surfaces behind the grooves about the resulting spring centres. Previous laboratory tests had shown the safe life of such spring centres to be about two complete cycles, provided that the maximum deflection did not exceed 10°. Angular deflection of the control surfaces was measured by observing the displacement of the trailing-edge and in order to avoid cycling the spring centre more than necessary, bending ceased when the control surface was within ±0·2° of the desired value. To represent the basic aircraft configuration, the ailerons were set 3° up relative to the wing chordal plane for all the tests. Deflections of the ailerons are quoted relative to this setting.

The model was supported on a sting which incorporated a five component strain-gauge balance to measure normal force, sideforce, pitching moment, yawing moment and rolling moment.

Axial force was measured by a separate strain-gauge balance manufactured in one piece with the model. The arrangement is such that the

model is connected to the sting support through four flexible links on which the axial force gauges are bonded. These internal pieces (axial force balance and supporting sting) are arbitrarily faired so as to present as little as possible obstruction to the internal air flow. A drawing of a similar arrangement is shown in Fig.13 of Ref.3. It should be noted that the present model is a revised version of that indicated in this Ref.

2.2 Details of tests

Tests were made in the supersonic section of the tunnel[4] at Mach numbers 1·42, 1·61, 1·82 and 2·00. The tunnel total pressure was varied with Mach number, to give a Reynolds number, based on $\bar{c}$, of $1{\cdot}9 \times 10^6$ at M = 1·42 and $2{\cdot}7 \times 10^6$ at other Mach numbers. When incidence was varied the range was from -2° to 18° at M = 1·42 and -2° to 14° at other Mach numbers. When sideslip was varied the range was -2° to 8° at all Mach numbers. Tests were made with the model at constant angle of sideslip (of 0° or 4°) while incidence was varied and a constant angle of incidence (of 0°) while sideslip was varied; this involved the use of a cranked sting support.

Bands of distributed roughness were used to ensure that the boundary-layer on the model was turbulent. They consisted of a mixture of carborundum grains and thin aluminium point applied so that closely spaced individual grains projected from a paint base about 0·001 inch thick; grade 100 carborundum (average grain height 0·007 inch) was used for the tests. The distributed roughness was applied between 1·25 and 1·75 inch aft of the nose and between 0% and 10% of the local chord on the wings and fin.

Preliminary tests were made at each Mach number to determine the mass flow of air through the model intakes. Measurements were made with pitot and static pressure tubes positioned at the exit, in the plane of the base of the model and the mass flow was calculated from these. Results are presented in Figs.5 and 6. Fig.5 shows the variation of mass flow ratio with incidence and Mach number and indicates that under the test conditions the intake was running nearly full. Fig.6 shows the variation of the mass flow parameter $\frac{Q\sqrt{T}}{P_o S}$ (measured at zero incidence) with Mach number. It should be remembered that the intakes on the model are approx 10% small in area.

The following is a detailed table of the tests made:-

Test Mach number	α	β	η	ξ	Fin	Remarks
All four	Variable	0°	0°	0°	ON	
" "	"	"	"	"	OFF	
" "	"	"	-4°	"	ON	
" "	"	"	-10°	"	"	
" "	"	"	"	"	OFF	
" "	"	"	"	"	ON	Airbrakes on
" "	"	"	"	"	"	Ventral fuel tank on
1·61,1·82 & 2·00*	"	"	-4°	-5°	"	
1·42,1·82 & 2·00≠	"	4°	0°	0°	OFF	
All four	"	"	-10°	"	"	
" "	"	"	0°	"	ON	
" "	"	"	-10°	"	"	
" "	"	"	"	"	"	Airbrakes on
" "	"	"	"	"	"	Ventral fuel tank on
" "	0°	Variable	0°	"	"	
" "	"	"	"	"	OFF	
" "	"	"	-4°	"	ON	
" "	"	"	-10°	"	OFF	
" "	"	"	"	"	ON	
" "	"	"	"	"	"	Airbrakes on
" "	"	"	"	"	"	Ventral fuel tank on

* ≠ Tests were made at M = 1·42 and M = 1·61 respectively but the results are in error due to experimental faults.

The tests were not repeated as it was considered that the aerodynamic characteristics of the model had been well established and further tunnel time could not be spared.

2.3 Results and accuracy

The aerodynamic coefficients are based on aerodynamic mean chord, gross wing area and gross wing span with a moment reference point at 0·317 $\bar{c}$ (0·544 centre line chord). This last corresponds to the mean centre of gravity position used in the flight tests. The system of axes and the sign convention used for control deflections are shown in Fig.7.

Normal force, pitching moment, sideforce, yawing moment and rolling moment results are presented. For various reasons it was not possible to obtain accurately the internal drag of the intake without considerable additional experimental work, for which time was not available. Since the internal drag was a substantial part of the measured drag, this meant that the possible errors in experimental values of external drag of the model were too large to justify presentation. Hence only comparative drag results

have been included i.e. increments due to airbrakes, fuel tank, elevators and ailerons. For the computation of lift coefficient, measured axial force was used which could result in an error of up to $\frac{1}{2}\%$ of the maximum lift.

No corrections have been made to the results for deflection of the controls under aerodynamic loading but these deflections are estimated to be small for both elevators and ailerons. No tunnel flow corrections have been applied to the results as these are considered to be within experimental accuracy. The results have been corrected for balance interactions and sting deflections and are estimated to be accurate within the following limits:-

C_L	± 0·004	C_ℓ	± 0·0001	α	± 0·1°
C_Y	± 0·001	C_m	± 0·002	β	± 0·1°
ΔC_D	± 0·0001	C_n	± 0·0002		

3 DESCRIPTION OF RESULTS

3.1 Lift, longitudinal stability and drag

The variation of untrimmed lift coefficient with incidence and Mach number for the model with elevator settings of 0°, -4° and -10° is shown in Fig.8. Fig.9 shows the variation of trimmed lift (for $C_L \leq 0{\cdot}2$) with incidence and Mach number. The untrimmed lift curves are non-linear and show a reduction of lift curve slope with increasing incidence. Fig.10 shows the variation of untrimmed and trimmed lift curve slopes, measured at low lift, with Mach number. The untrimmed lift curve slope falls steadily with increase in Mach number from 2·77 at M = 1·42 to 1·95 at M = 2·00. The lift slope for the trimmed model is about 30% less than that for the untrimmed model at all Mach numbers.

Fig.11 shows the variation with Mach number of lift due to elevator. The effect of incidence on this is negligible for the test incidence range.

The variation of pitching moment coefficient with lift coefficient for elevator angles of 0°, -4° and -10° is shown in Fig.12. The curves have stable slopes and are linear within the lift range tested. There is little change in slope with change in either elevator setting or Mach number; thus the aerodynamic centre position remains virtually constant at 0·19 $\bar{c}$ aft of the test reference point, (Fig.13). Fig.14 shows the variation of $-\frac{\partial C_m}{\partial \eta}$, elevator effectiveness, with Mach number. This falls from 0·192 (measured per radian of control movement) at M = 1·42 to 0·114 at M = 2·00.

The effects which the airbrakes have on lift and pitching moment are small and are shown in Figs.15 and 16 respectively. The brakes produce little change in lift curve slope, below $\alpha \simeq 12°$, at all Mach numbers but do give a small positive increment in lift at constant incidence. They also produce a rearward shift of the aerodynamic centre position of about 0·02 $\bar{\bar{c}}$ at all Mach numbers. The effects of the ventral fuel tank on lift and pitching moment are shown in Figs.17 and 18. These are small, there being a slight forward movement of the aerodynamic centre (< 1% $\bar{\bar{c}}$) at Mach numbers of 1·61 and above.

Fig.19 shows the variation, with Mach number, of the drag increment measured at zero lift, resulting from the separate addition of the airbrakes, ventral fuel tank, elevator and aileron. Fig.19(a) shows that ΔC_{D_o} due to the airbrakes falls slightly with increasing Mach number and is of the order 0·05. The increment due to the tank is about 0·002 over the Mach number range.

Fig.19(b) shows the variations with Mach number of ΔC_{D_o} per radian of elevator and aileron movement.

3.2 Lateral stability

In order to obtain the variation of the sideslip derivatives, $\frac{\partial C_Y}{\partial \beta}$, $\frac{\partial C_n}{\partial \beta}$ and $\frac{\partial C_\ell}{\partial \beta}$, with incidence, tests were made with the model set at constant angles of sideslip of 0° and 4°, varying the angle of incidence. The derivatives were deduced assuming that the variations of the coefficients C_Y, C_n and C_ℓ were linear between the angles of sideslip tested. To check the validity of this assumption at low incidence further tests were made at each Mach number in which the model was set at zero incidence and the angle of sideslip varied. In this case the derivatives were obtained by measuring the slopes of the curves in the region $\beta \simeq 0°$. In the discussion of results the above techniques for obtaining derivatives are referred to as Method A and Method B respectively.

Curves showing the variation of sideforce coefficient with angle of sideslip for various model configurations are shown in Figs.20, 21 and 22. In general the curves are fairly linear over the sideslip range $0° < \beta < 4°$.

The differences in value of $-\frac{\partial C_Y}{\partial \beta}$ at zero incidence as obtained by the two methods are shown in Fig.23. The curves indicate that, in general, Method A gives values of $\frac{\partial C_Y}{\partial \beta}$ which are greater in magnitude by up to 10% than those given by Method B. This should be remembered when considering the variation of $\frac{\partial C_Y}{\partial \beta}$ with incidence in which $\frac{\partial C_Y}{\partial \beta}$ is obtained by Method A - the less accurate method.

The variation of $-\frac{\partial C_Y}{\partial \beta}$ with incidence for the various model configurations is shown in Fig.24. Fig. 25 shows the variation of $-\frac{\partial C_Y}{\partial \beta}$, at various values of incidence, with Mach number for the basic model with and without a fin and hence, by subtraction, the contribution of the fin. For the complete model sideforce falls with increase in Mach number and above M = 1·67 falls with increase of incidence. When the separate contributions of the body (i.e. model without fin) and fin are examined it may be seen that the sideforce on the body increases slightly with Mach number up to M = 1·8 and increases appreciably with increase of incidence at all Mach numbers, while the sideforce on the fin decreases appreciably with increase of both Mach number for M > 1·6 and incidence.

Figs.26, 27 and 28 show the variation of yawing moment coefficient with sideslip angle for the various configurations. Fig.29 shows the variation of $\left(\frac{\partial C_n}{\partial \beta}\right)_{\alpha=0°}$ obtained by the two methods A and B. In general, differences between the two methods are greater at low Mach number (M < 1·6) for the model with the fin on, when Method A may over-estimate the derivative by up to 20%, but with the exception of the case of the model with airbrakes, agreement is much closer for Mach numbers above M = 1·8. When the fin is removed agreement is good.

The variation of $\frac{\partial C_n}{\partial \beta}$ with incidence for the various model configurations is shown in Fig.30. For all configurations $\frac{\partial C_n}{\partial \beta}$ falls with increase of incidence and in some cases the model (with the fin on) becomes directionally unstable at high incidence. Fig.31 summarises the curves of $\frac{\partial C_n}{\partial \beta}$ against Mach number at zero incidence for the various configurations, as obtained by Method B. The curves for the model with $\eta = 0°$ and $-4°$ both show a steady decrease of $\frac{\partial C_n}{\partial \beta}$ with increase of Mach number. The curves for all configurations with the elevator set at $-10°$ however, show an increase in $\frac{\partial C_n}{\partial \beta}$ with Mach number up to $M \simeq 1{\cdot}8$, followed by a decrease above this Mach number. Thus below $M \simeq 1{\cdot}7$ the variation of $\frac{\partial C_n}{\partial \beta}$ with η is non linear and in fact changes sign between elevator angles of $-4°$ and $-10°$. Above $M \simeq 1{\cdot}7$ the variation of $\frac{\partial C_n}{\partial \beta}$ with Mach number is progressive with the stability increasing as the elevator is moved negatively between $0°$ and $-10°$. The curves for the model with airbrakes and ventral tank indicate that the brakes produce an increase in directional stability which varies from about 25% at $M = 1{\cdot}4$ to about 40% at $M = 1{\cdot}6$ and above while the ventral tank produces a decrease in stability of about 25% at all Mach numbers.

Fig.32 shows the variation of $\frac{C_n}{C_Y}$ (lateral centre of pressure position) with Mach number for the model at $\alpha = 0°$ and $\alpha = 10°$, both with and without a fin. Also included are curves for $\frac{\Delta C_n}{\Delta C_Y}$ (where ΔC_n and ΔC_Y are the differences in yawing moment and sideforce coefficients between the model configurations with and without a fin). This gives the position of the fin centre of pressure (including any interference effects concerning the fin) and is referred to as the "fin alone" case. The curves for the complete model show large forward movements of the lateral centre of pressure both with increase in Mach number for $M > 1{\cdot}6$ and with increase in incidence. The variations in the centres of pressure positions for the "fin off" and "fin alone" cases are small with variation in Mach number, thus the reduction in $\frac{\partial C_n}{\partial \beta}$ (Fig.31, $\eta = 0°$), results from the decrease in fin sideforce, as Mach number is increased above $M = 1{\cdot}6$, noted in Fig.25. The variations in centres of pressure position with incidence for the "fin off" and "fin alone" cases are fairly small and in each case in a stabilising direction, thus the reasons for the reduction in $\frac{\partial C_n}{\partial \beta}$ with increase of incidence (Fig.30), are the increase in body sideforce acting ahead of the moment centre and the reduction in fin sideforce noted in Figs.24 and 25, rather than any movements of their respective centres of pressure.

Curves showing the variation of rolling moment coefficient with sideslip angle for the various model configurations are shown in Figs.33, 34 and 35. Fig.36 shows the variation of $\left(\frac{\partial C_\ell}{\partial \beta}\right)_{\alpha=0°}$ with Mach number as obtained by the two methods A and B. Generally the results obtained by Method A appear to be greater up to $M \simeq 1{\cdot}7$ above which Mach number they are slightly

smaller. Curves showing the variation of $\frac{\partial C_\ell}{\partial \beta}$ with incidence for the various configurations are shown in Fig.37. Generally $\frac{\partial C_\ell}{\partial \beta}$ increases with increase in incidence but at M = 1·4 there is a local drop in $\frac{\partial C_\ell}{\partial \beta}$ at $\alpha = 14°$ which possibly may be attributed to the starboard wing tip stalling slightly before the port tip.

Fig.38 summarises the variation of the sideslip derivatives $\frac{\partial C_Y}{\partial \beta}$, $\frac{\partial C_n}{\partial \beta}$ and $\frac{\partial C_\ell}{\partial \beta}$ with Mach number for the model at trimmed lift coefficients of 0 and 0·2.

Fig.39 shows the variation of aileron effectiveness with incidence at Mach numbers of 1·61, 1·82 and 2·00. Figs.40 and 41 show the variation with incidence at these Mach numbers of sideforce and yawing moment due to aileron movement. Since these latter derivatives are established from fairly small differences the accuracy is low, in the extreme case being about ±30% and ±20% for $\frac{\partial C_Y}{\partial \xi}$ and $\frac{\partial C_n}{\partial \xi}$ respectively. Nevertheless it is considered that the order of these derivatives is established.

4 CONCLUSIONS

From results of wind tunnel tests at supersonic Mach numbers on a 1/24 scale model of the Fairey Delta 2 aircraft the main conclusions are as follows.

(1) Pitching moment curves are linear and have stable slopes over the test incidence range at all Mach numbers. There is virtually no change in slope $-\frac{\partial C_m}{\partial C_L}$ with Mach number or elevator setting, thus the aerodynamic centre position remains constant at 0·510 $\bar{\bar{c}}$ (i.e. 0·67 centre-line chord).

(2) Directional stability falls with increase in Mach number above M = 1·6 as a result of decreasing fin effectiveness.

(3) Directional stability falls with increase of incidence at constant Mach number, resulting from an increasing body sideforce acting ahead of the moment centre and from decreasing fin effectiveness.

(4) There is a large non-linear variation of directional stability with elevator setting ($0° \geq \eta \geq -10°$) particularly between Mach numbers of 1·4 and 1·8.

(5) The airbrakes produce:-

(a) a rearward movement of the aerodynamic centre of 0·02 $\bar{\bar{c}}$ at all Mach numbers;

(b) an increase in directional stability (at low lift) of about 25% at M = 1·42 and 40% at M ≥ 1·6.

(6) The ventral fuel tank has little effect on the longitudinal stability but causes a decrease in directional stability (at low lift) of about 25% at all Mach numbers.

LIST OF SYMBOLS

A_{en} area of intakes

A_{∞} cross sectional area of stream tube entering intakes

C_D drag coefficient (drag/q S)

ΔC_{Do} incremental drag coefficient at zero lift

C_L lift coefficient (lift/q S)

C_ℓ rolling moment coefficient (rolling moment/q Sb)

C_m pitching moment coefficient (pitching moment/q S $\bar{\bar{c}}$)

C_n yawing moment coefficient (yawing moment/q Sb)

C_Y sideforce coefficient (sideforce/q S)

b gross wing span

$\bar{\bar{c}}$ aerodynamic mean chord

M Mach number

P_o free stream total pressure

q dynamic pressure

Q mass flow of air (lb/sec)

S gross wing area

T free stream stagnation temperature (°F)

α angle of incidence of fuselage datum (degrees)

β angle of sideslip (degrees)

η elevator angle (degrees)

ξ aileron angle (degrees)

$\frac{\partial C_L}{\partial \alpha}$ and $\frac{dC_L}{d\alpha}$ untrimmed and trimmed lift curve slopes (per radian)

$\frac{\partial C_L}{\partial \eta}$ lift due to elevator (per radian)

$\frac{\partial C_m}{\partial \eta}$ elevator effectiveness (per radian)

$\frac{\partial C_\ell}{\partial \xi}$ aileron effectiveness (per radian)

LIST OF SYMBOLS (Contd.)

$\frac{\partial C_Y}{\partial \xi}$ and $\frac{\partial C_n}{\partial \xi}$ aileron derivatives (both per radian)

$\frac{\partial C_\ell}{\partial \beta}$, $\frac{\partial C_n}{\partial \beta}$ and $\frac{\partial C_Y}{\partial \beta}$ sideslip derivatives (all per radian)

Relationships of terms used in stability analysis (Not used in this note):-

$$y_v = \frac{1}{2}\frac{\partial C_Y}{\partial \beta}$$

$$n_v = \frac{\partial C_n}{\partial \beta}$$

$$\ell_v = \frac{\partial C_\ell}{\partial \beta}$$

$$y_\xi = \frac{1}{2}\frac{\partial C_Y}{\partial \xi}$$

$$n_\xi = \frac{\partial C_n}{\partial \xi}$$

$$\ell_\xi = \frac{\partial C_\ell}{\partial \xi}$$

LIST OF REFERENCES

No.	Author(s)	Title, etc.
1	Andrews, D.R.	Measurements in flight of the longitudinal stability derivatives of a 60° delta wing aircraft (Fairey E.R.103) A.R.C. C.P. 639 April, 1959.
2	Rose, R.	Flight measurements of the Dutch Roll characteristics of a 60° delta wing aircraft (Fairey Delta 2) at Mach numbers from 0·4 to 1·5 with stability derivatives extracted by vector analysis. A.R.C. C.P. 653 March, 1961.

LIST OF REFERENCES (Contd.)

No.	Author	Title, etc.
3	Seddon, J. Nicholson, L.F.	The representation of engine airflow in wind tunnel model testing. A.R.C. R. & M. 3079 May, 1955.
4	Morris, D.E.	Calibration of the flow in the working section of the 3 ft × 3 ft tunnel, National Aeronautical Establishment. A.R.C. C.P. 261 September, 1954.

TABLE 1

Principal dimensions of models

Scale	1 : 24
Test moment centre	0·317 $\bar{\bar{c}}$ (= 0·544 centre-line chord)
Fuselage	
length	22·16 in.
maximum width	2·00 in.
maximum depth	2·275 in.
Wing	
gross span	13·417 in.
gross area	90 sq in.
centre-line chord	12·50 in.
tip chord	0·92 in.
aerodynamic mean chord	8·34 in.
aspect ratio	2·0
angle of sweepback of L.-E.	59·92°
aerofoil section	4% symmetrical maximum thickness at 0·295 chord
wing chord line to fuselage angle	$1\frac{1}{2}^{\circ}$
Fin	
exposed height	2·69 in.
exposed area	8·98 in.
aspect ratio $\left[\frac{(\text{exposed height})^2}{\text{exposed area}}\right]$	0·80
angle of sweepback of L.-E.	60°
aerofoil section	6% symmetrical
Controls	
Elevator	
hingeline length (per flap)	2·8 in.
total area (two flaps)	4·97 sq in.
Aileron (horn balance)	
hingeline length (per flap)	2·93 in.
total area (two flaps)	4·05 sq in.

DS 82977 Wt 59 K4 11/63 XL/CL/P

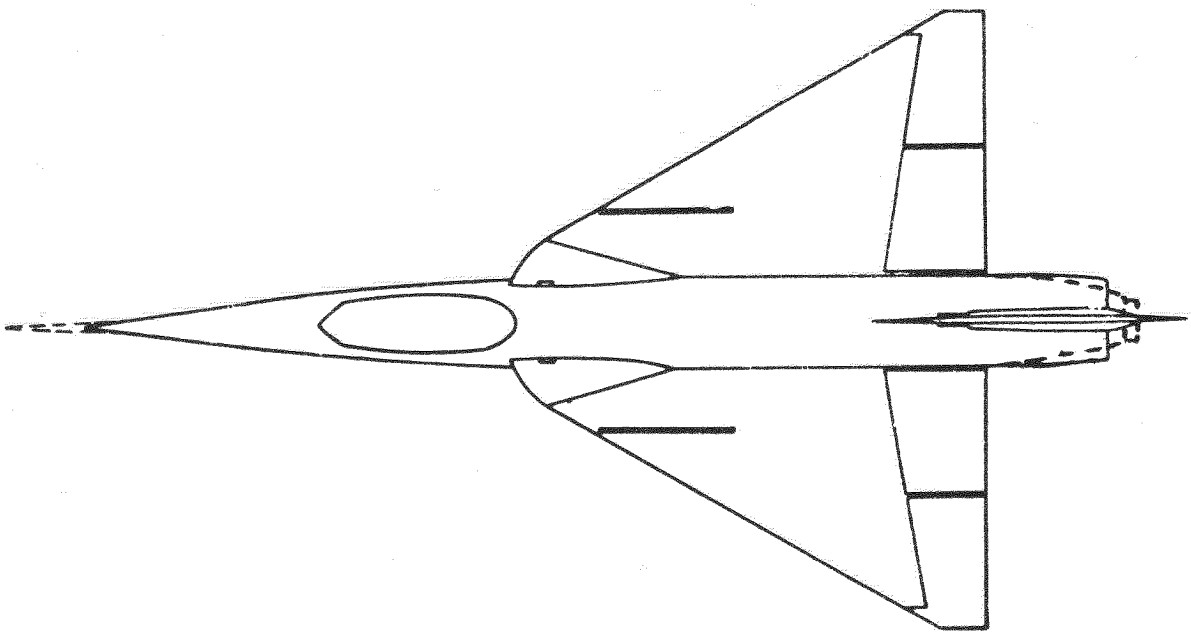

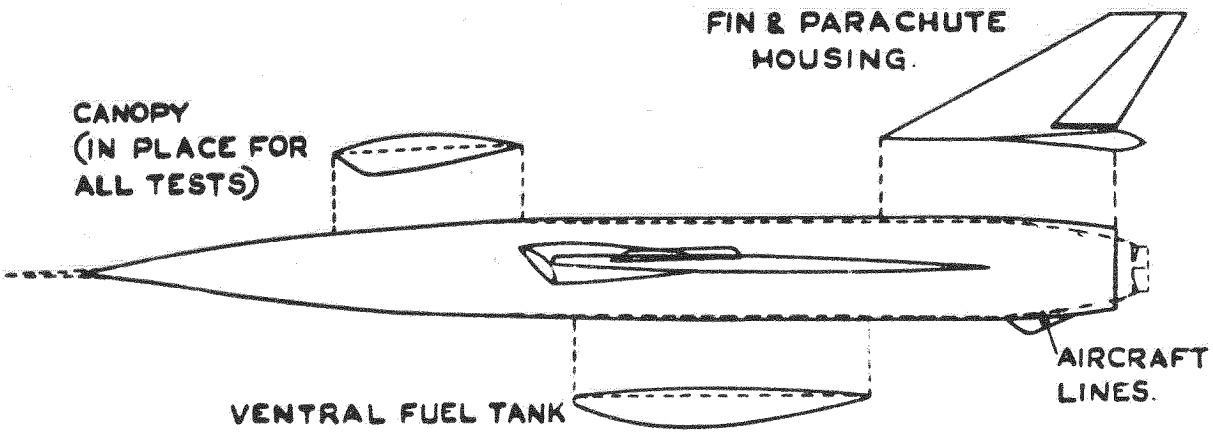

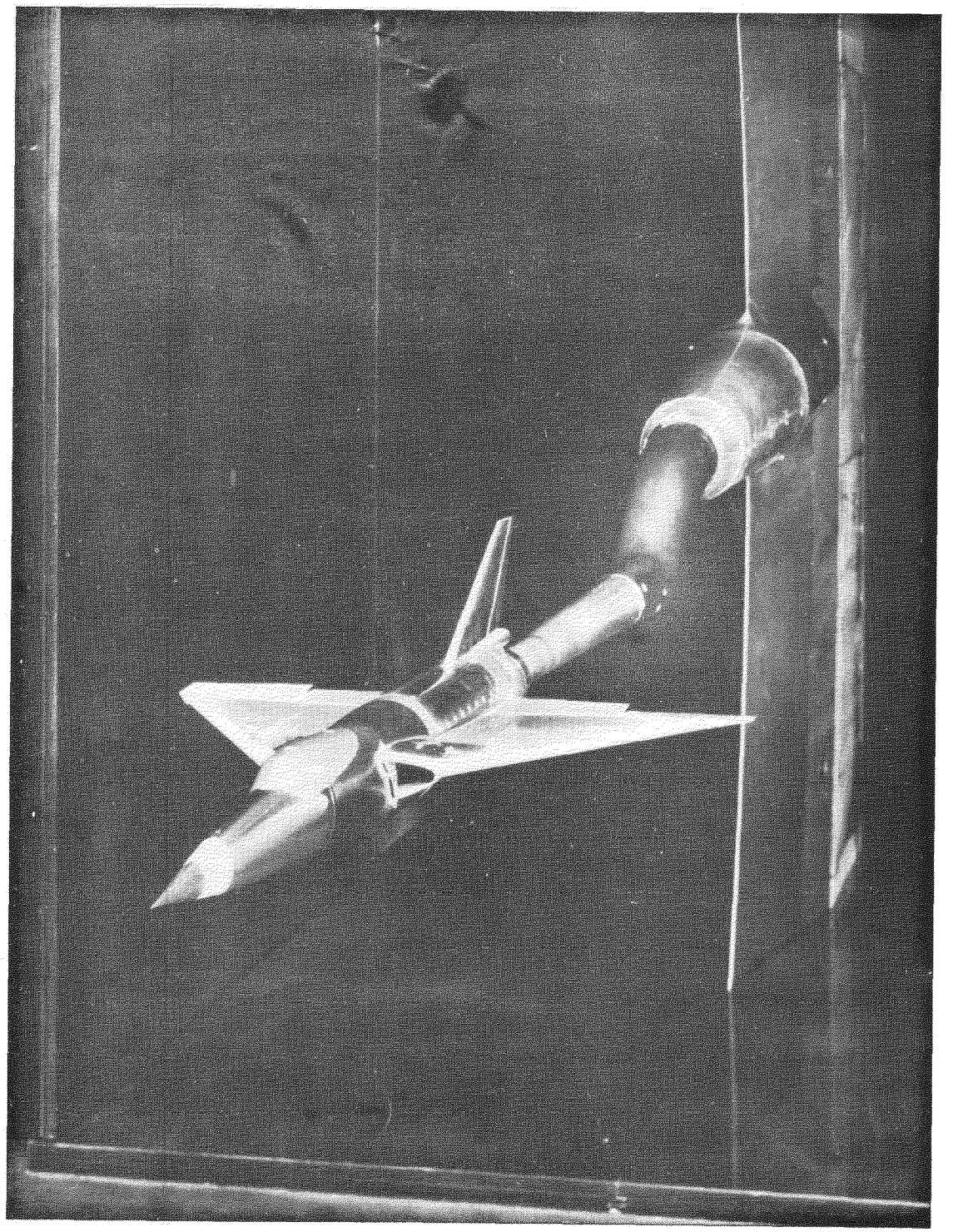

FIG.2. MODEL IN TUNNEL

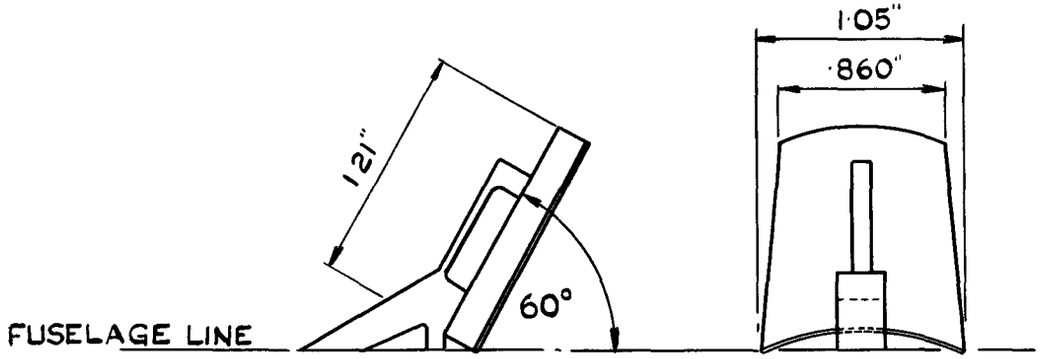

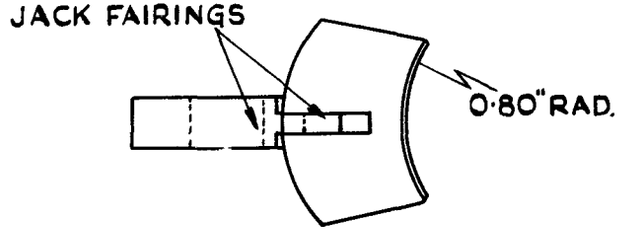

TOTAL PROJECTED AREA (4 FLAPS) 3·92 SQ.IN.

FLAP DETAILS.

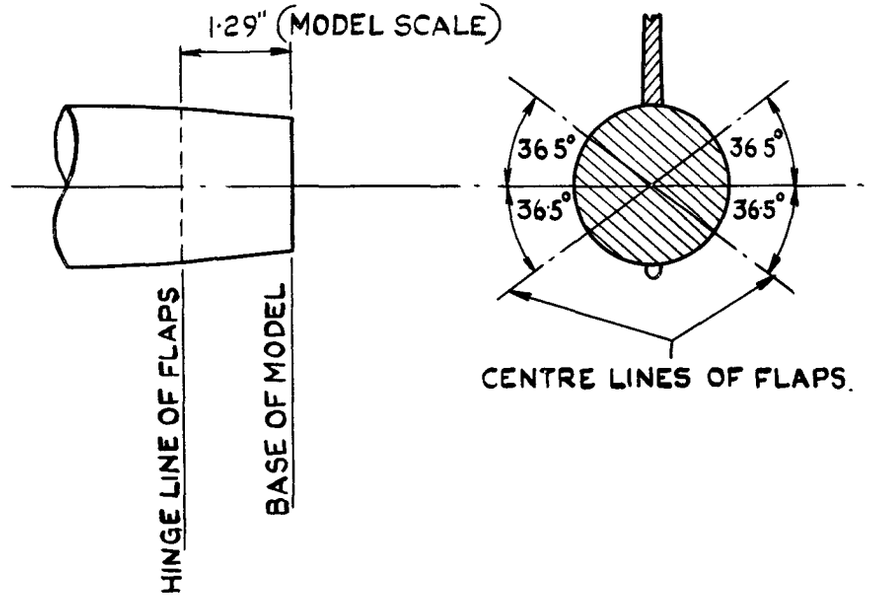

FLAP POSITIONS.

FIG. 3. DETAILS OF AIRBRAKES.

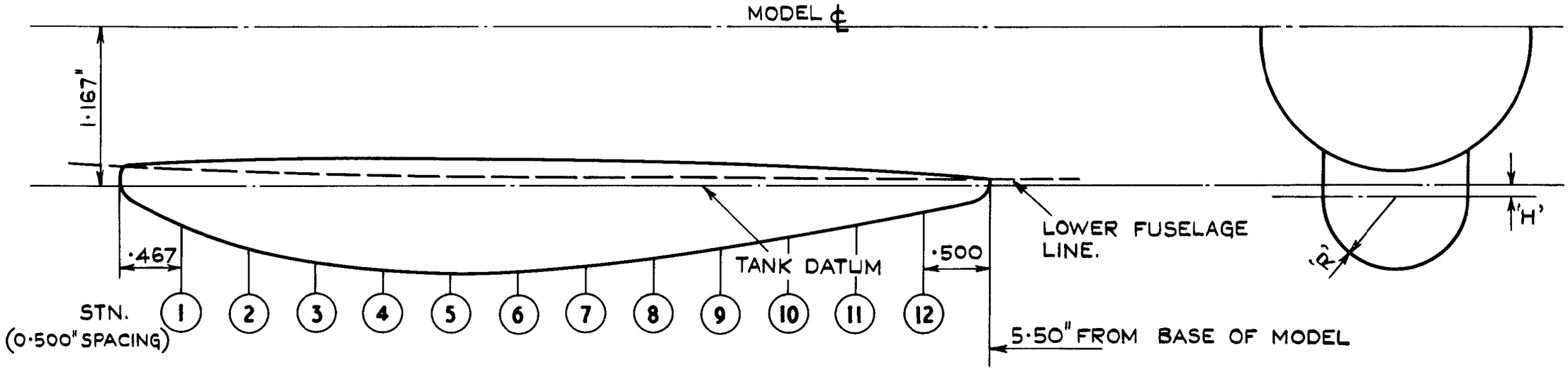

STATION	1	2	3	4	5	6	7	8	9	10	11	12
DIM. 'R'	·248	·375	·450	·493	·507	·500	·478	·442	·395	·333	·260	·172
DIM. 'H'	·027	·063	·095	·115	·128	·130	·125	·110	·087	·060	·036	·017

FIG. 4. DETAILS OF VENTRAL TANK.

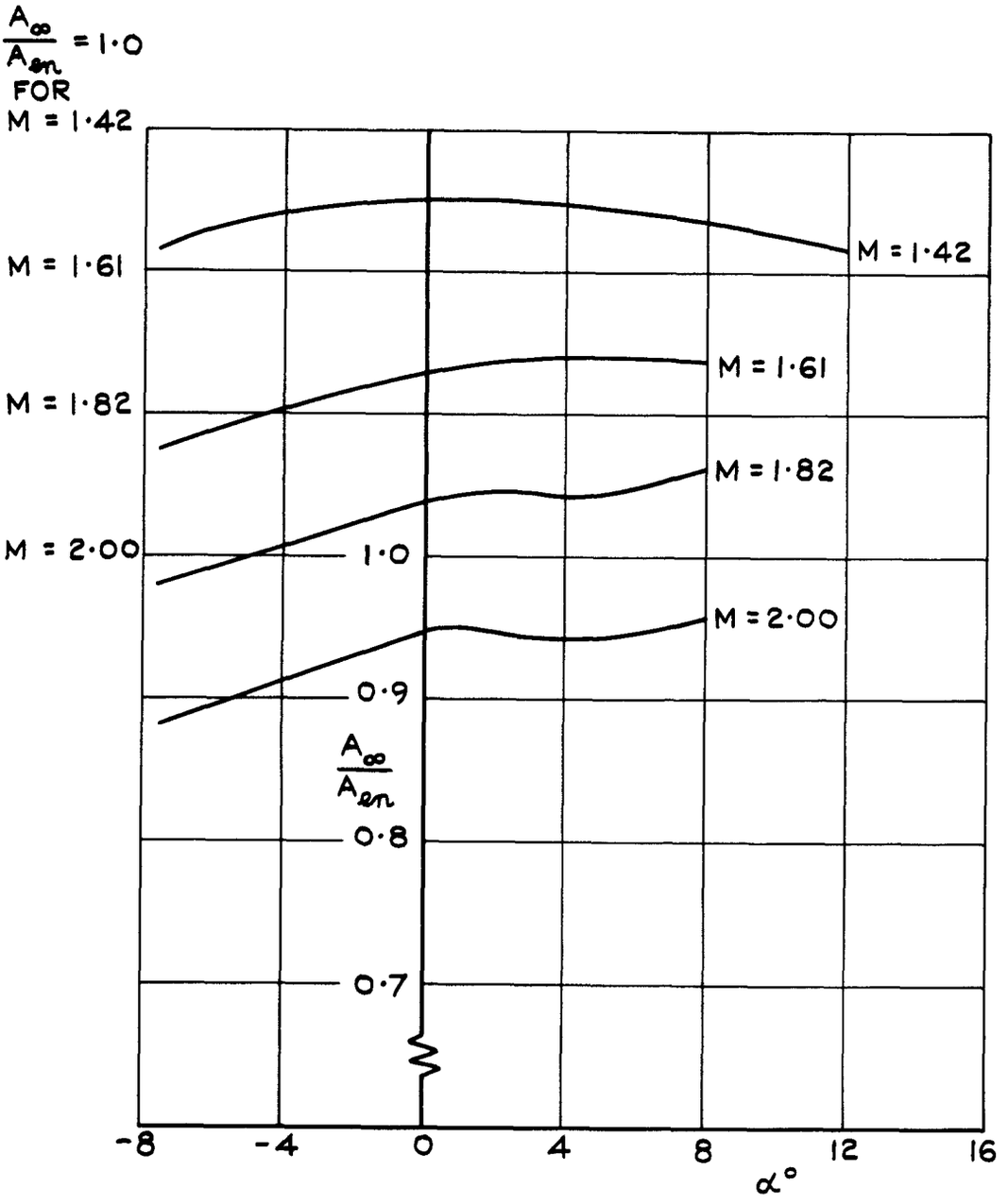

FIG. 5. MASS FLOW RATIO - VARIATION WITH MACH NUMBER AND INCIDENCE.

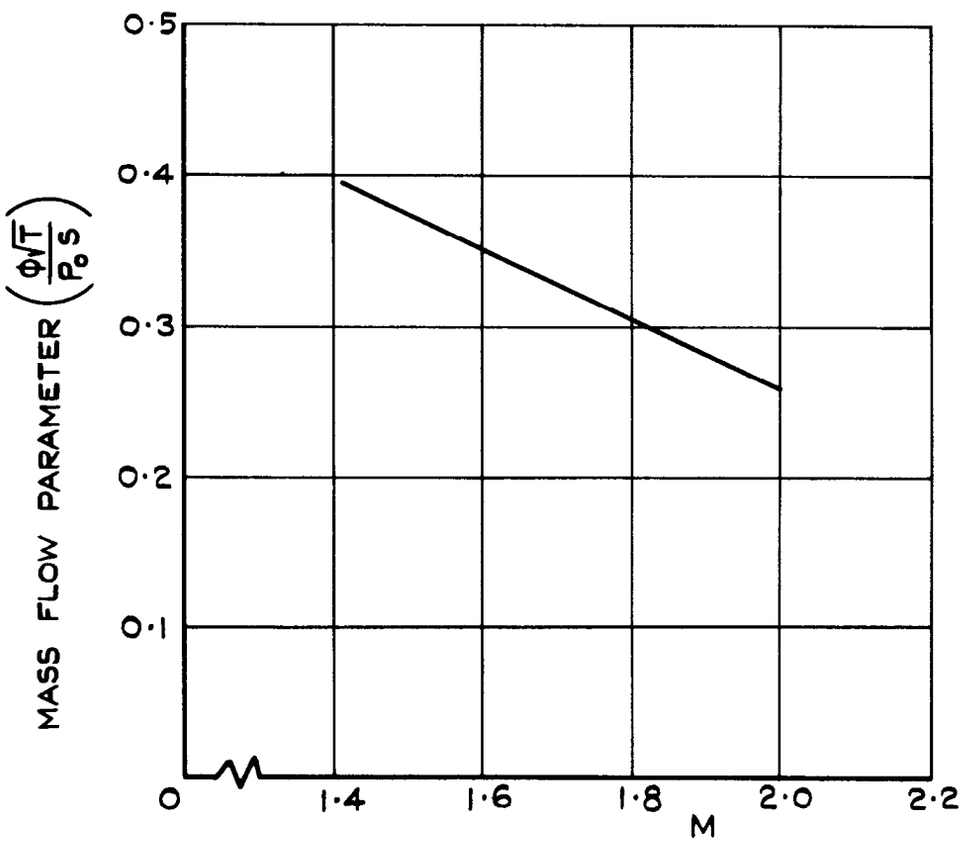

FIG. 6. MASS FLOW PARAMETER - VARIATION WITH MACH NUMBER, INCIDENCE = 0°.

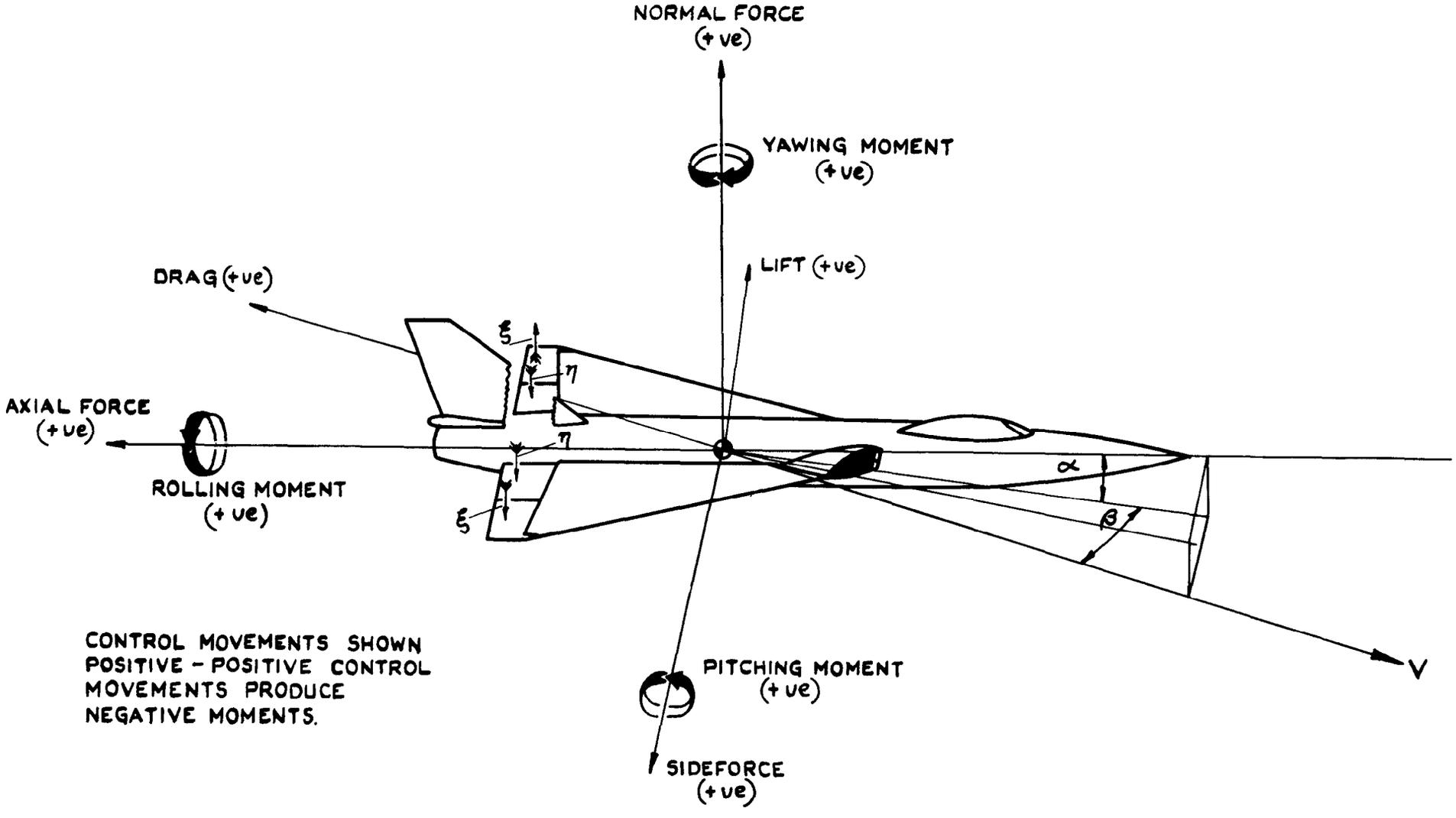

FIG. 7. SYSTEM OF AXES AND SIGN CONVENTION FOR FORCES, MOMENTS AND CONTROL SETTINGS.

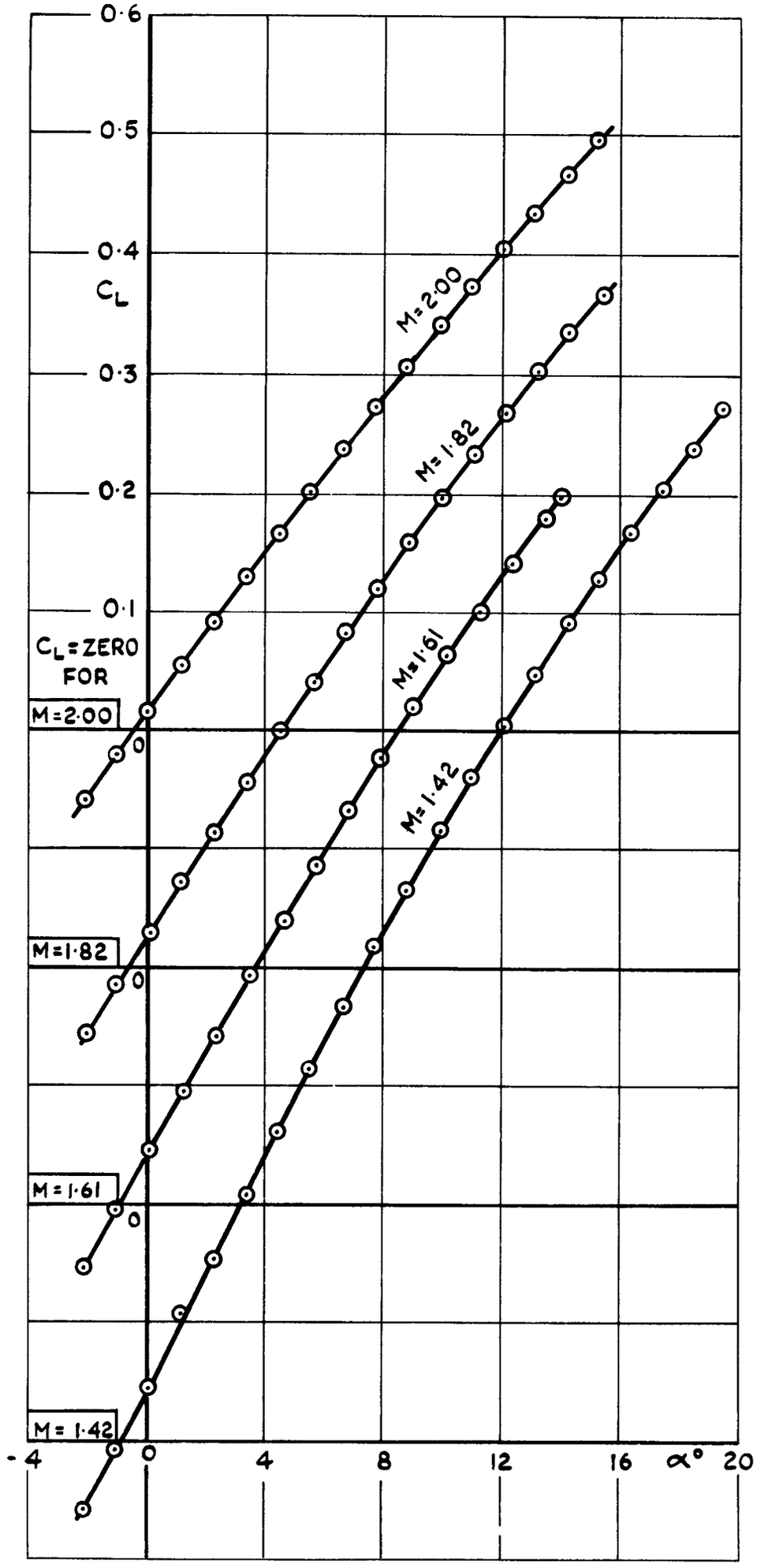

(a) $\eta = 0°$

FIG.8. LIFT–VARIATION WITH INCIDENCE, MACH NUMBER AND ELEVATOR SETTING.

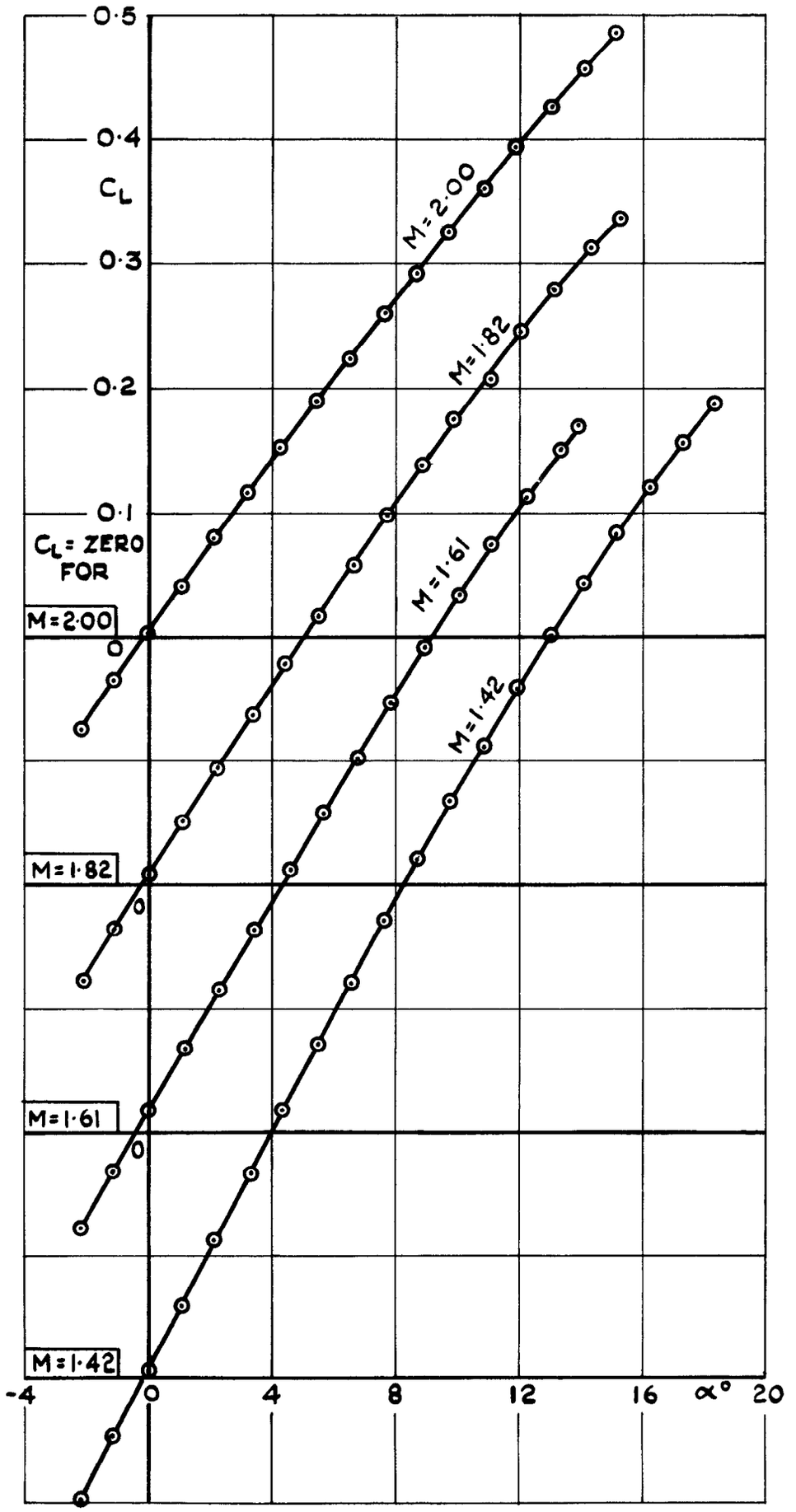

(b) $\eta = -4°$

FIG. 8. (CONTD)

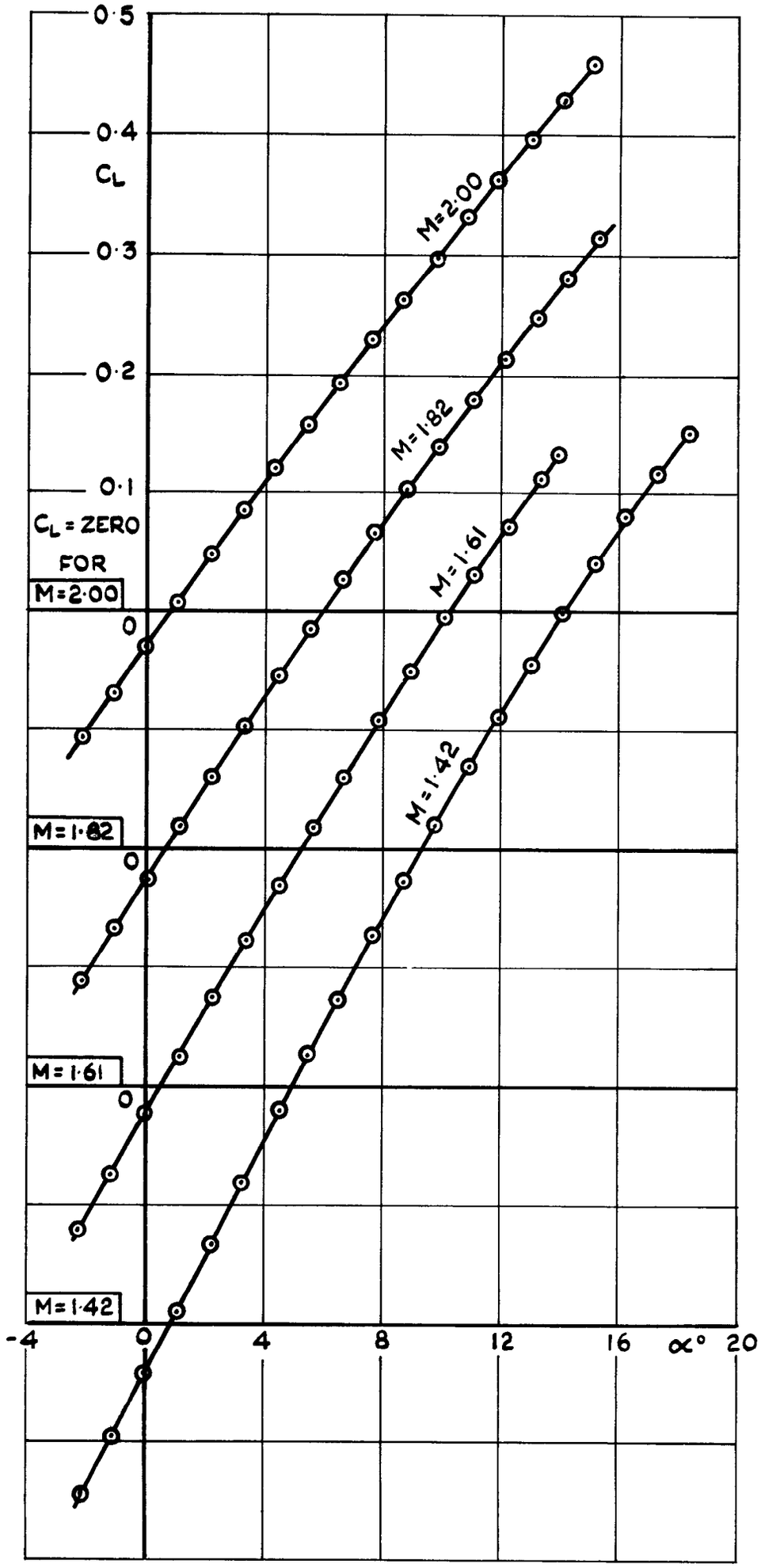

(c) $\eta = -10°$

FIG. 8.(CONCLD.)

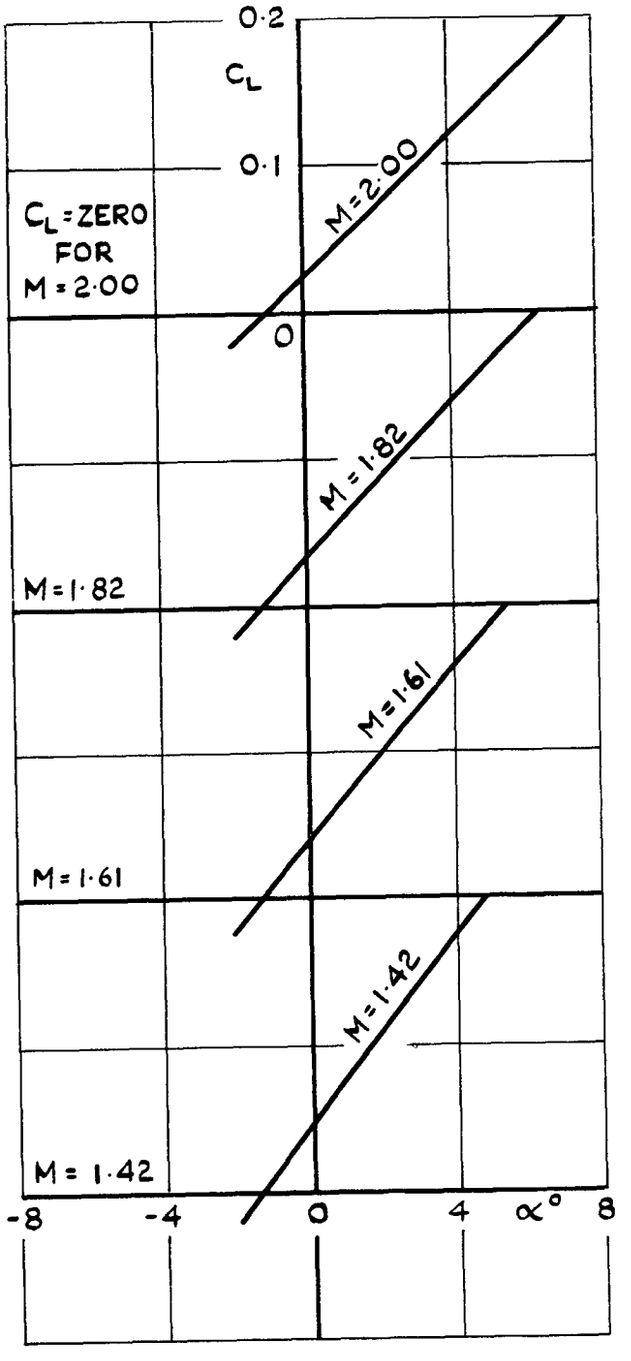

FIG. 9. LIFT – VARIATION WITH INCIDENCE AND MACH NUMBER, MODEL TRIMMED.

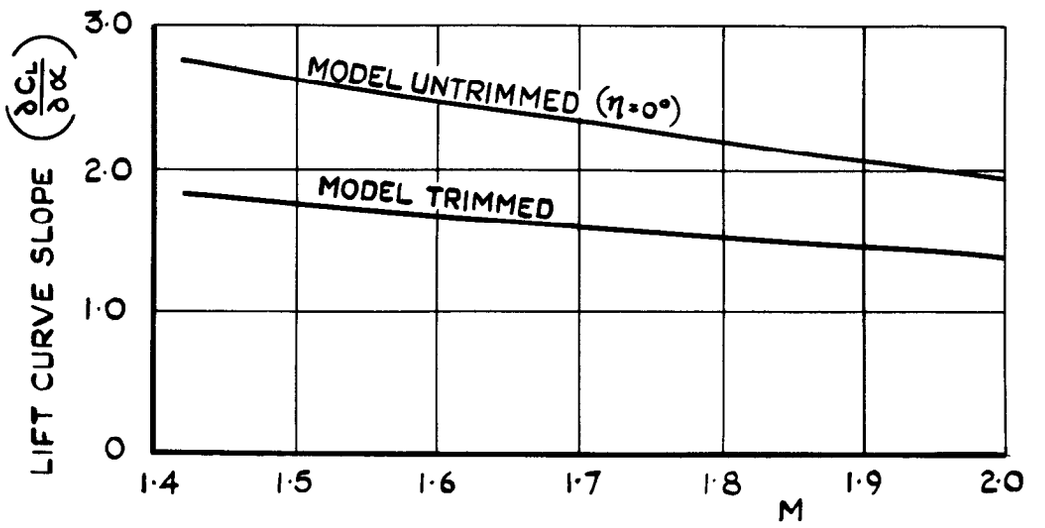

FIG. 10. LIFT CURVE SLOPE (MEASURED AT LOW LIFT) –VARIATION WITH MACH NUMBER.

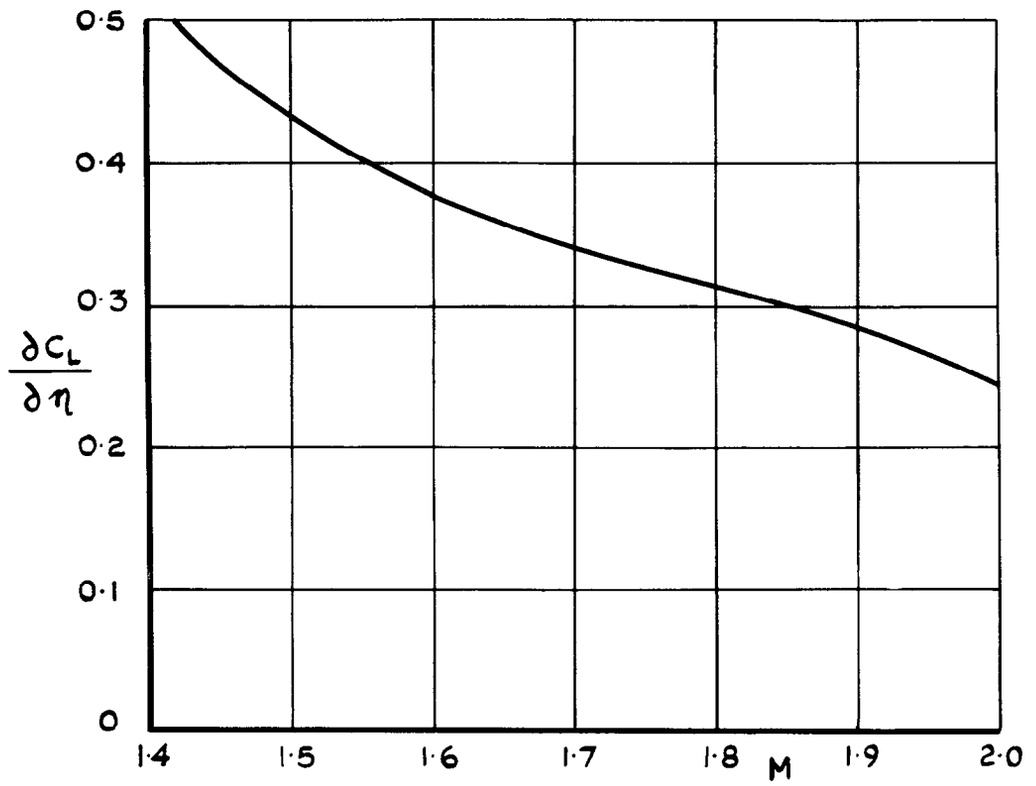

FIG. 11. LIFT DUE TO ELEVATOR –VARIATION WITH MACH NUMBER.

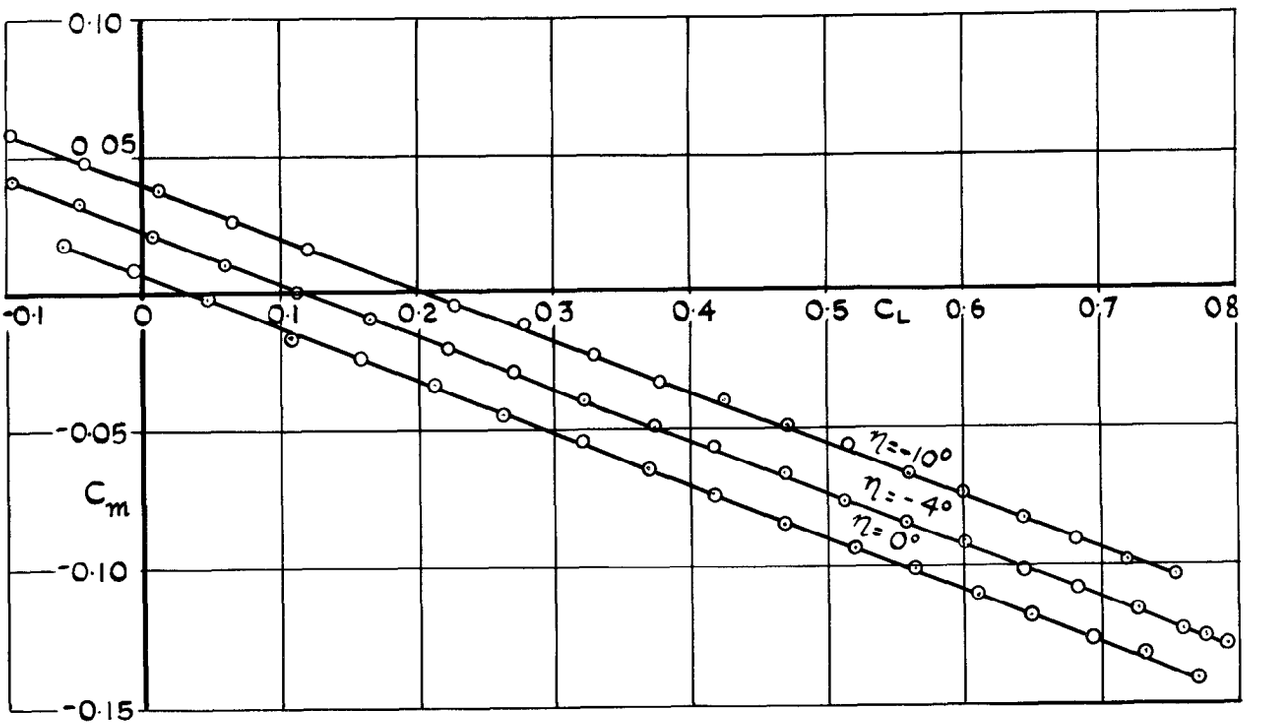

(a) M = 1·42

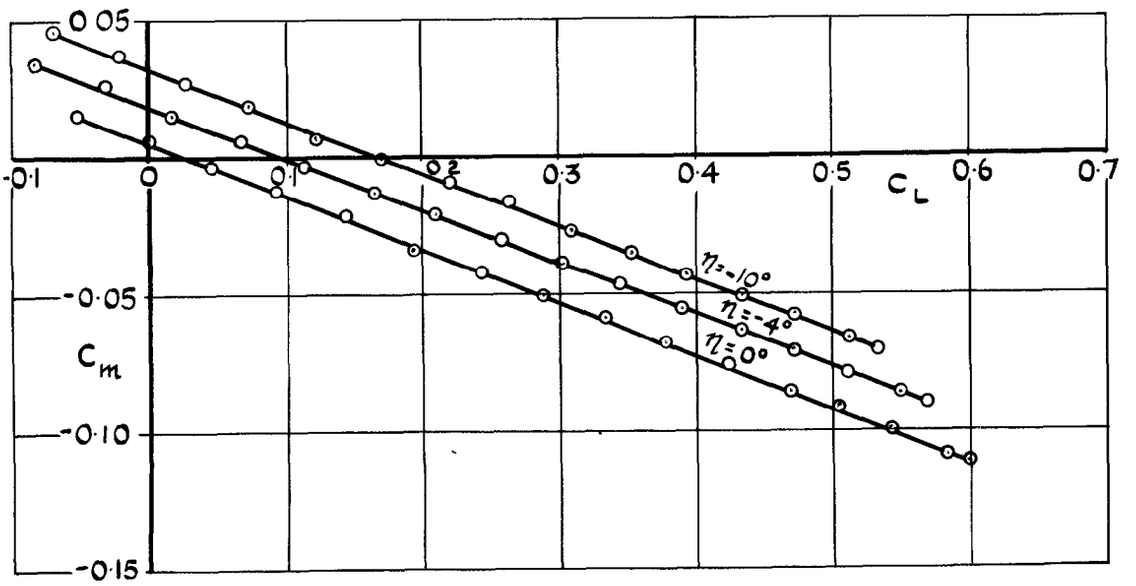

(b) M = 1·61

FIG. 12. PITCHING MOMENT-VARIATION WITH LIFT, ELEVATOR SETTING AND MACH NUMBER.

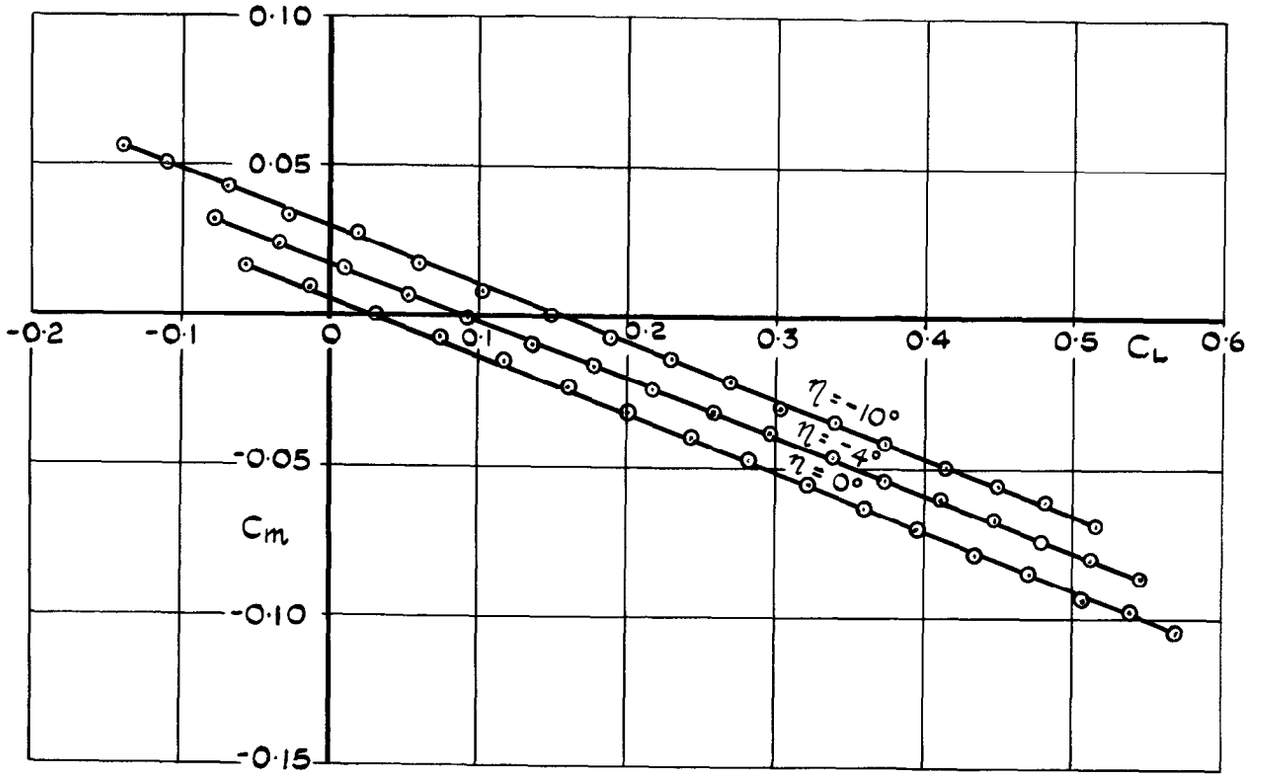

(c) M = 1·82

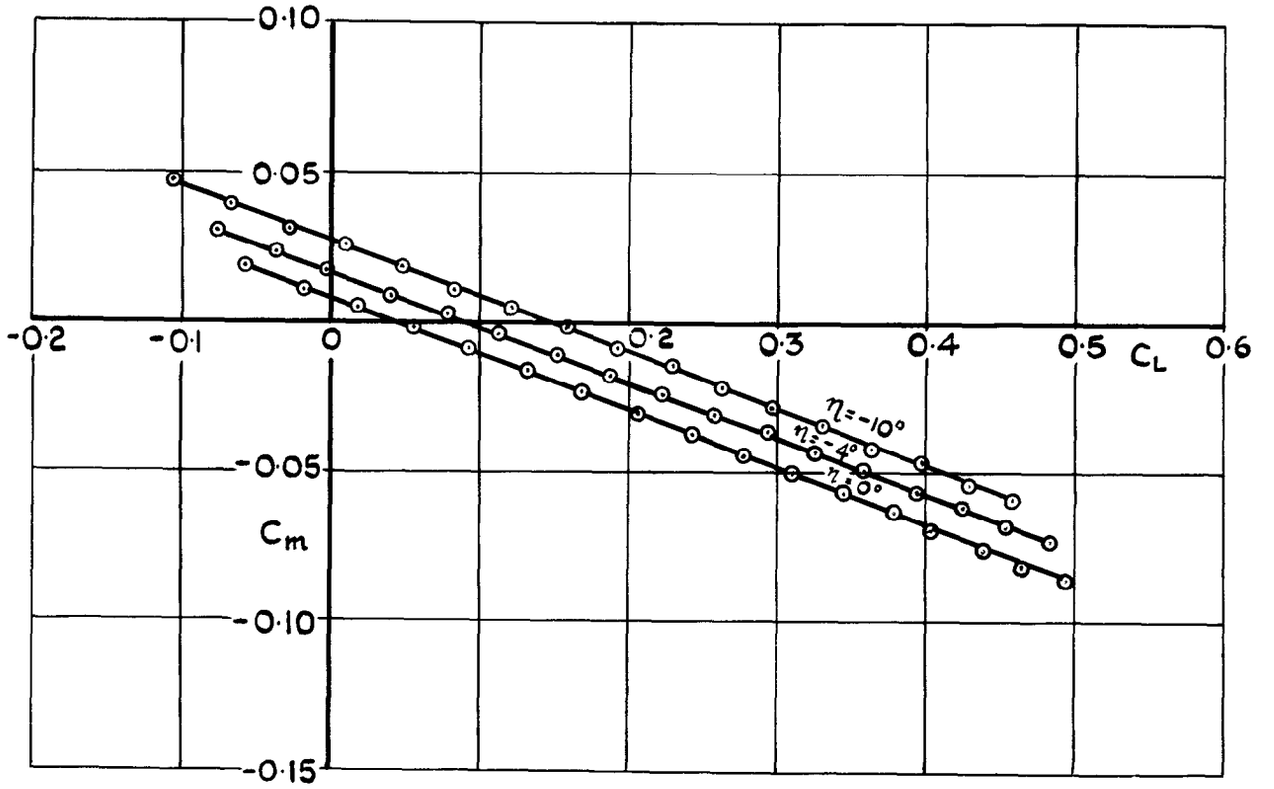

(d) M = 2·00

FIG. 12. (CONTD.)

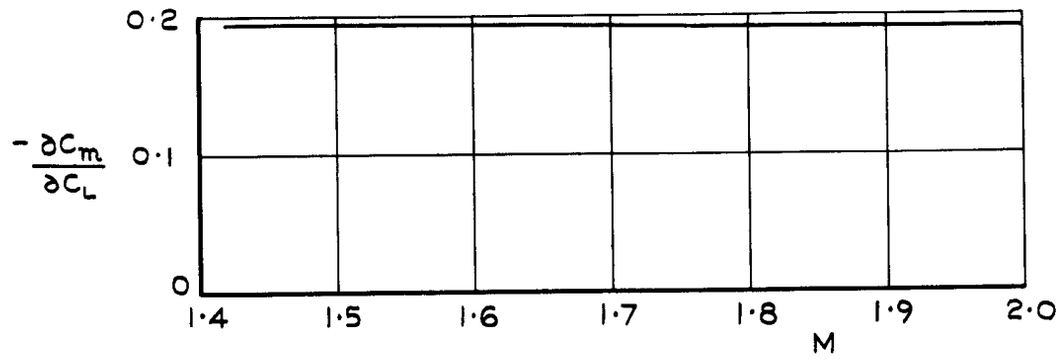

FIG. 13. $\left(\frac{-\partial C_m}{\partial C_L}\right)$ - VARIATION WITH MACH NUMBER.

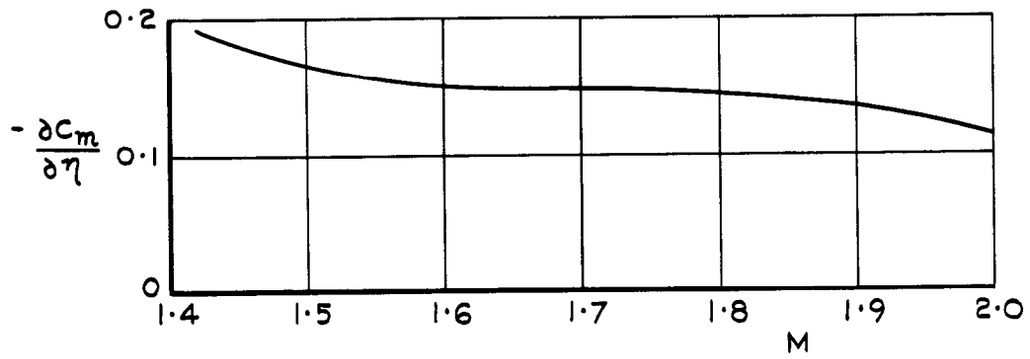

FIG. 14. ELEVATOR EFFECTIVENESS - VARIATION WITH MACH NUMBER.

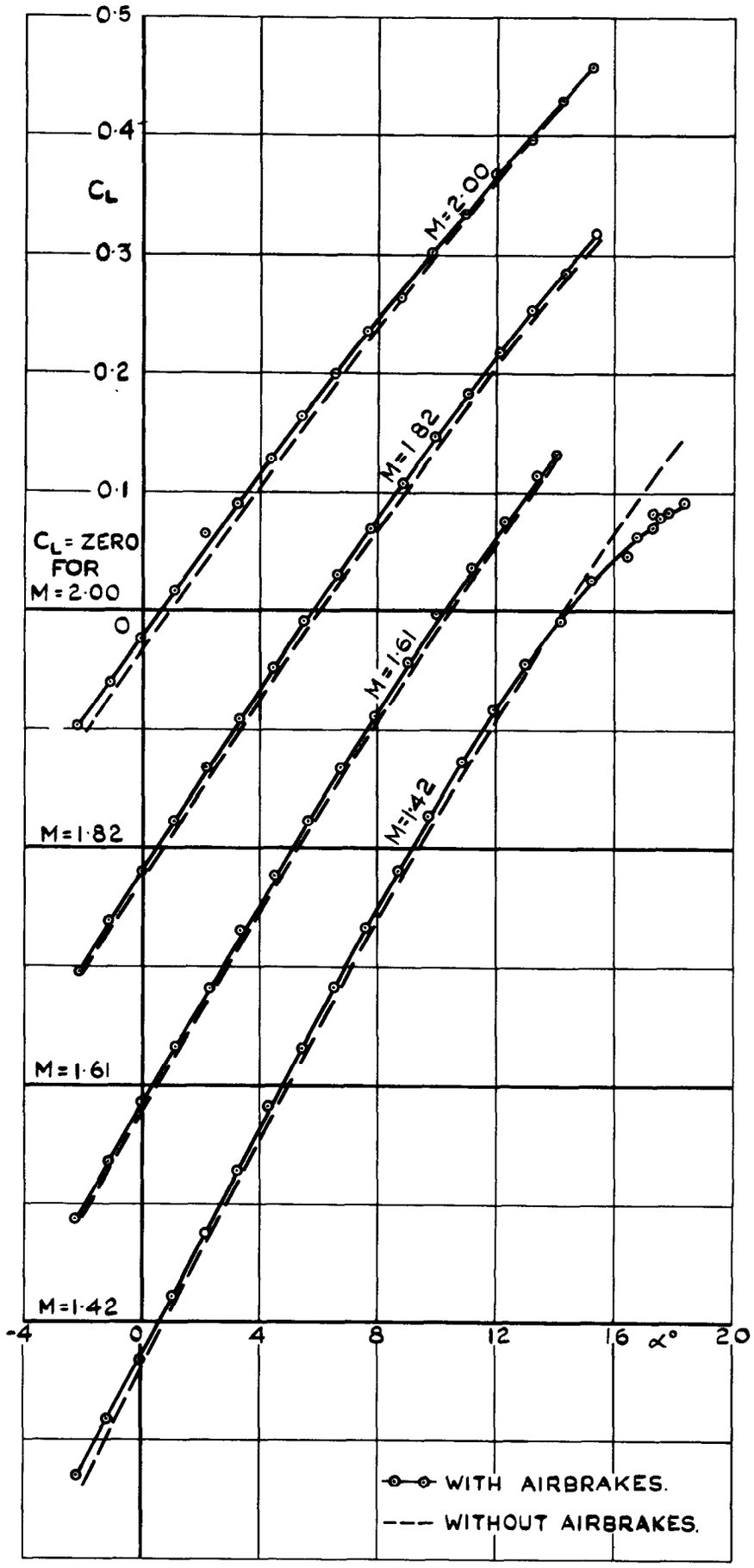

FIG. 15. AIRBRAKES - VARIATION OF LIFT WITH INCIDENCE AND MACH NUMBER, MODEL WITH $\eta = -10°$

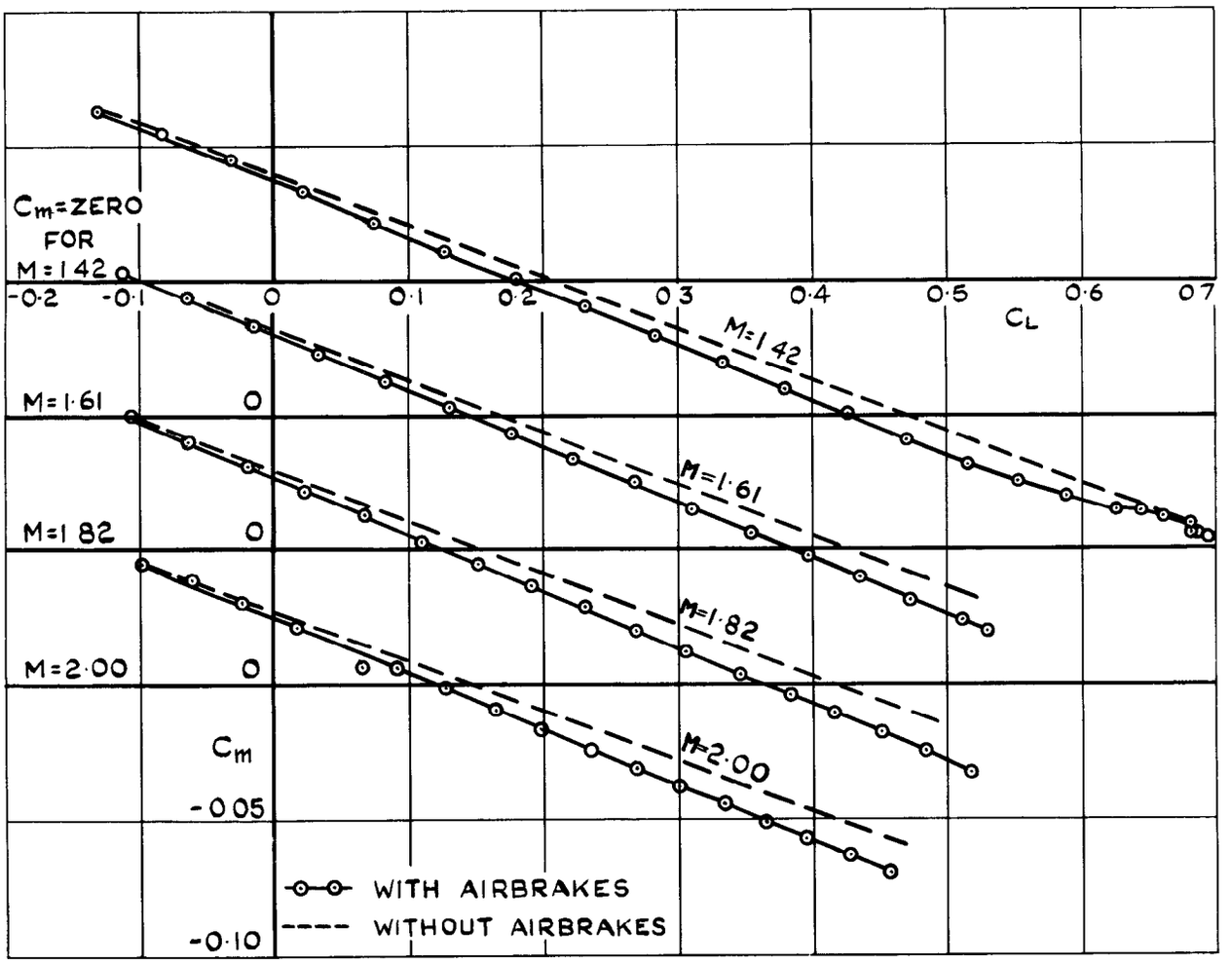

FIG. 16. AIRBRAKES - VARIATION OF PITCHING MOMENT WITH LIFT & MACH NUMBER, MODEL WITH $\eta = -10°$

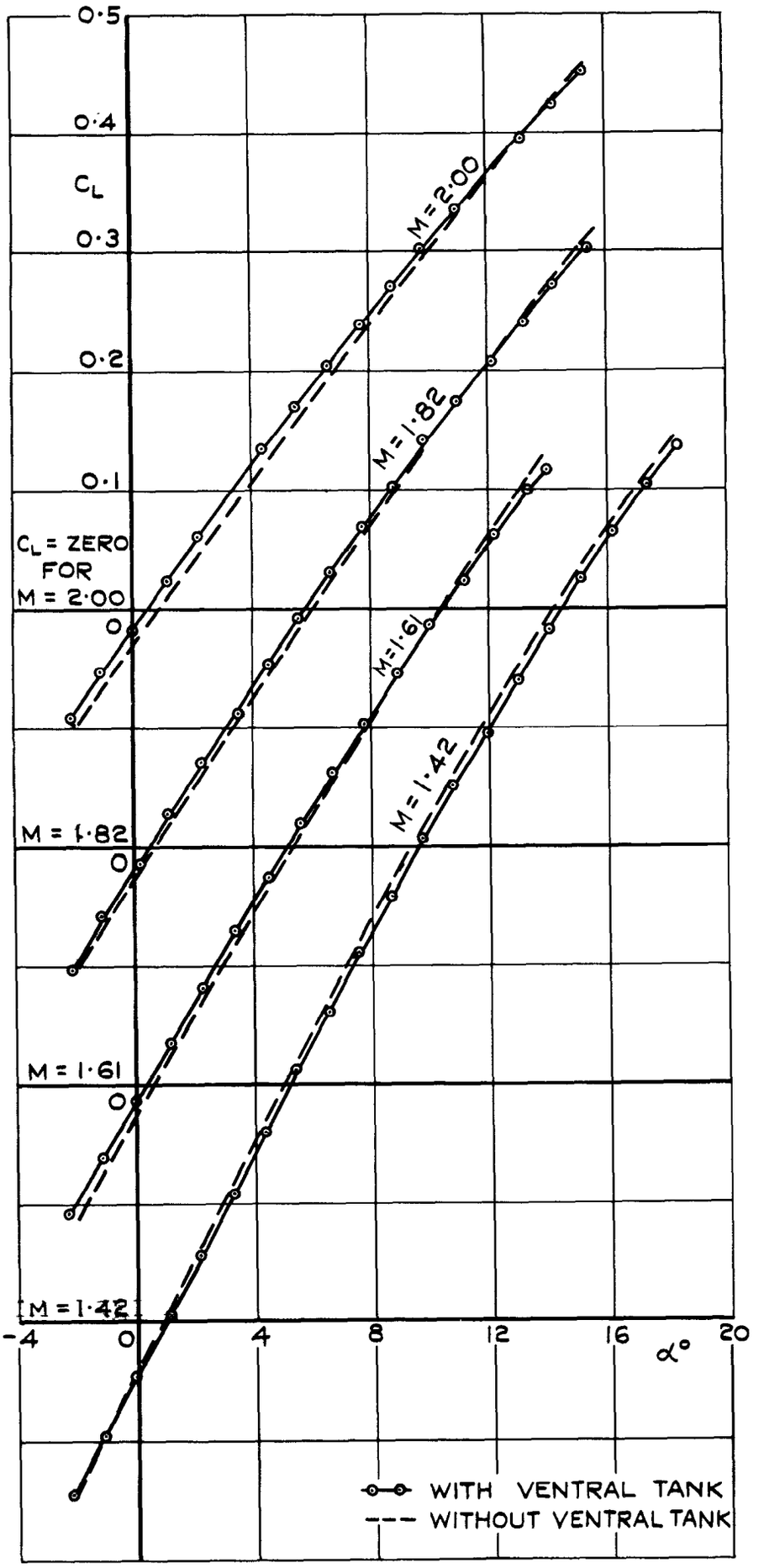

FIG. 17. VENTRAL FUEL TANK - VARIATION OF LIFT WITH INCIDENCE AND MACH NUMBER, MODEL WITH $\eta = -10°$

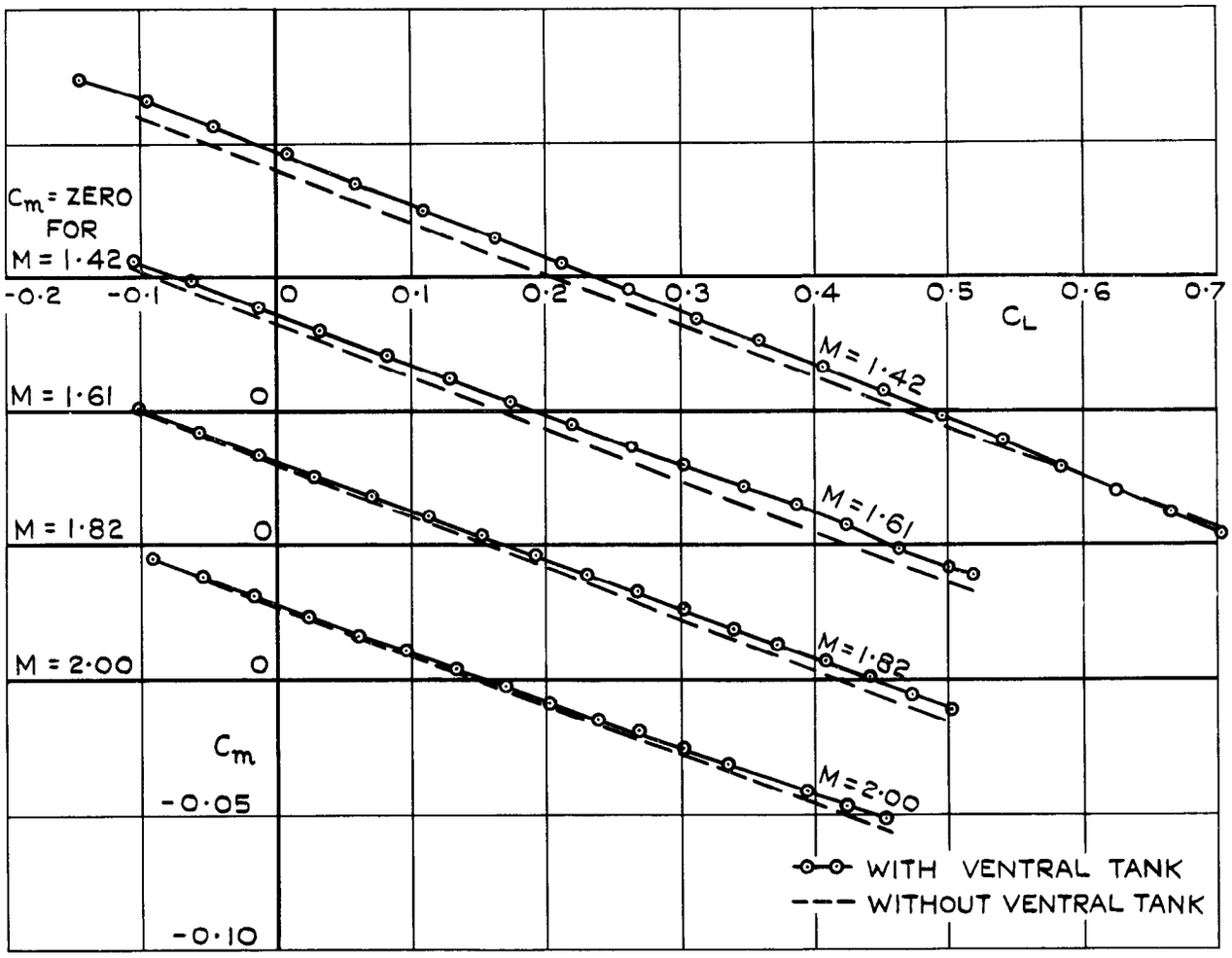

FIG. 18. VENTRAL FUEL TANK-VARIATION OF PITCHING MOMENT WITH LIFT AND MACH NUMBER, MODEL WITH $\eta = -10°$.

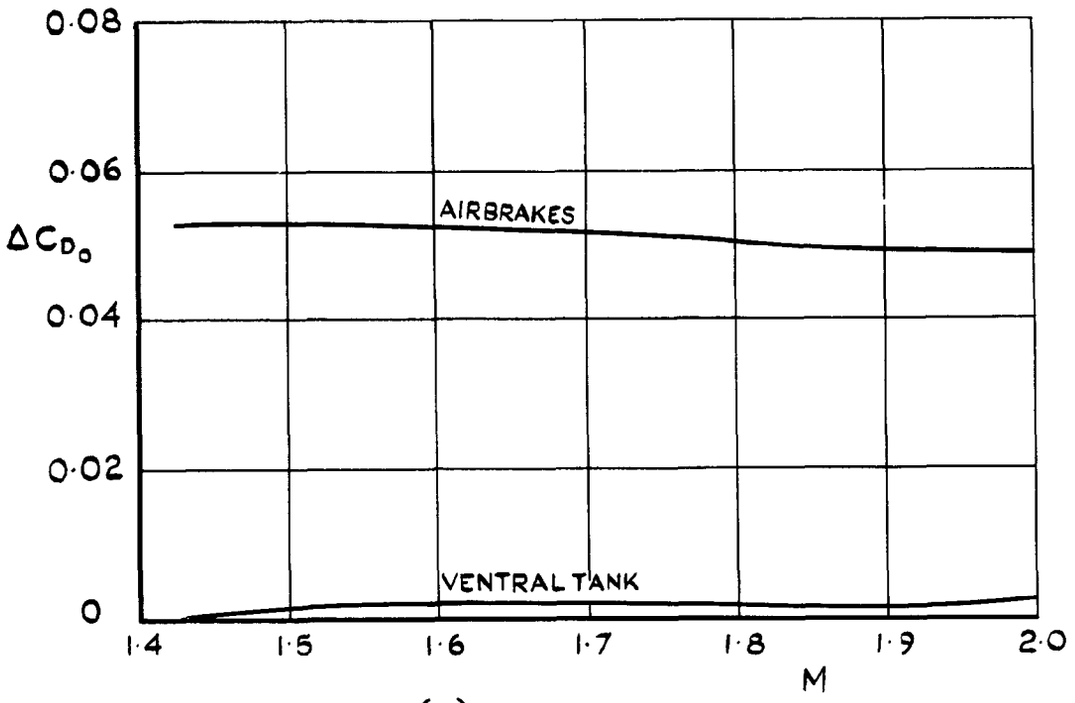

(a.) APPENDAGES

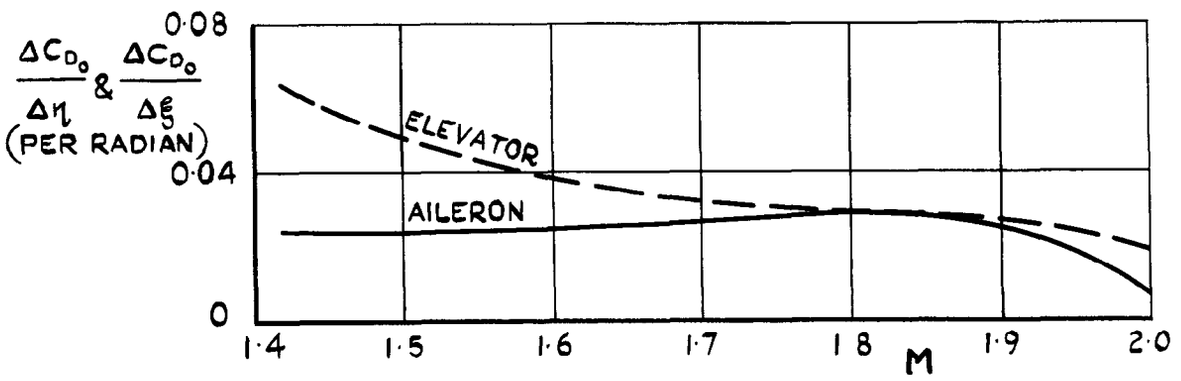

(b.) CONTROL DEFLECTION.

FIG. 19. DRAG INCREMENTS AT ZERO LIFT- VARIATION WITH MACH NUMBER.

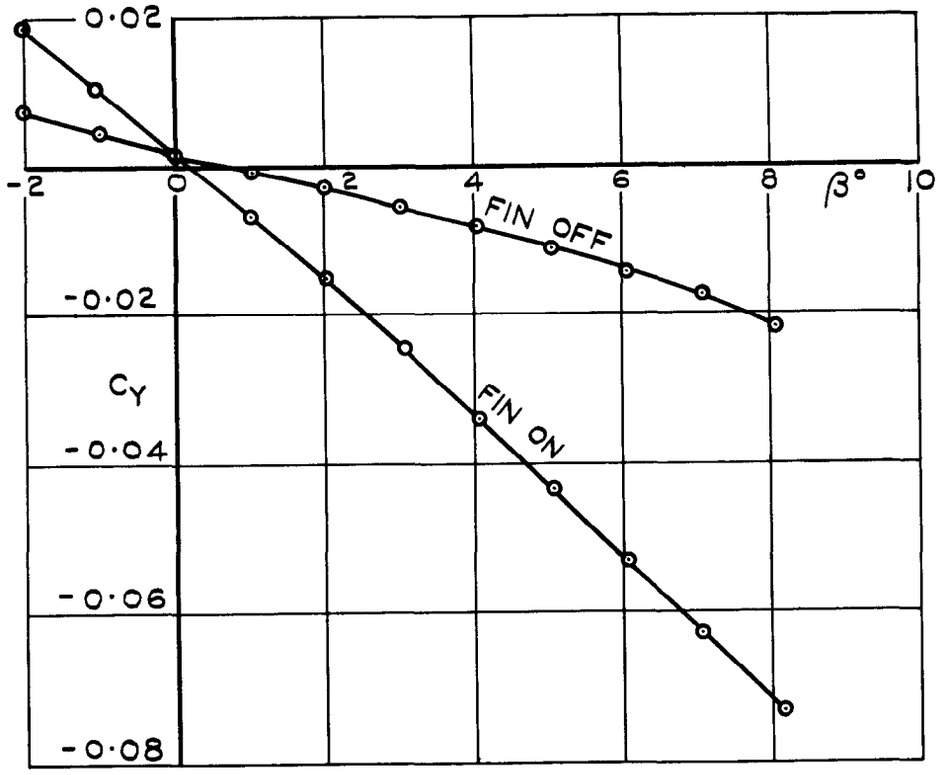

(a.) M = 1·42

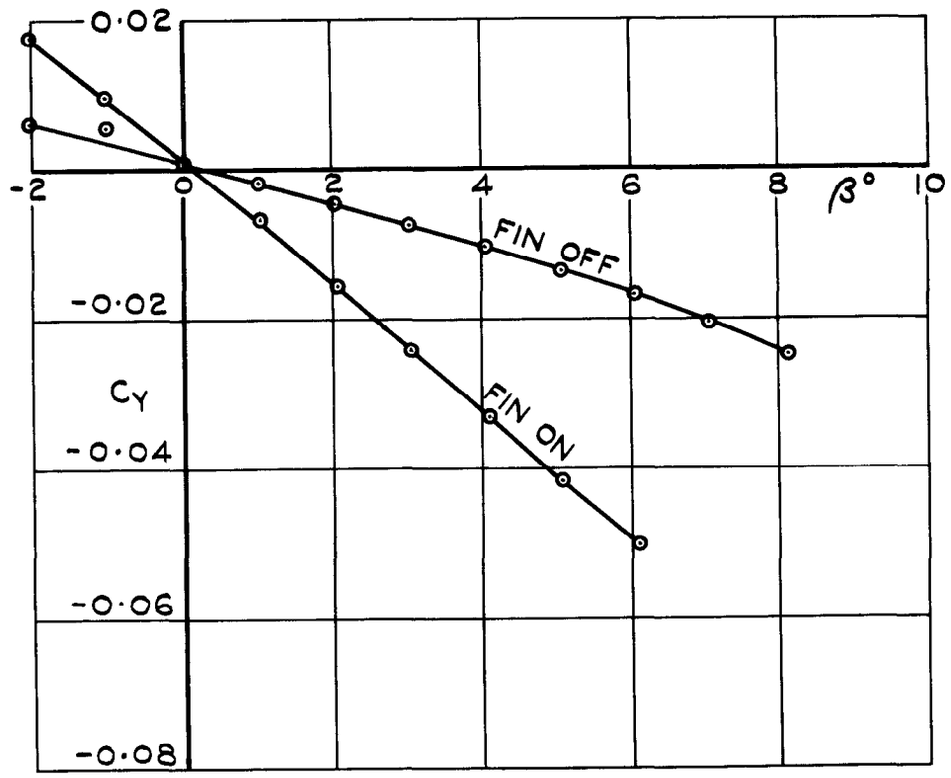

(b.) M = 1·61

FIG. 20. SIDEFORCE - VARIATION WITH SIDESLIP ANGLE AND MACH NUMBER, MODEL WITH $\eta = 0°$, AT $\alpha = 0°$.

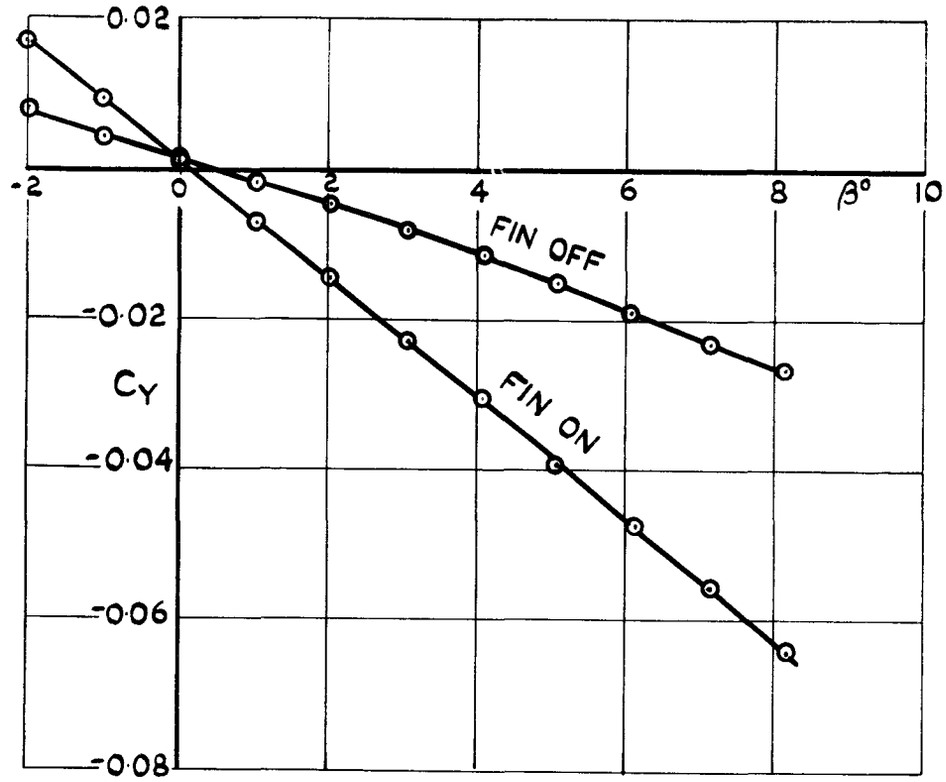

(c) M = 1·82

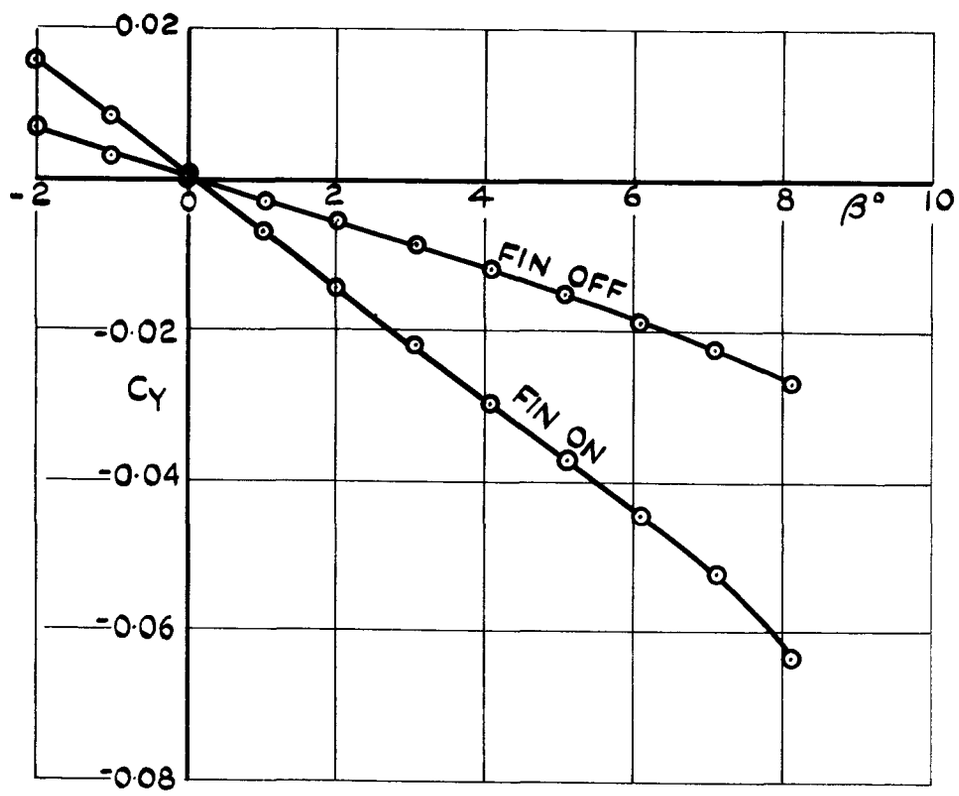

(d) M = 2·00

FIG. 20 (CONTD)

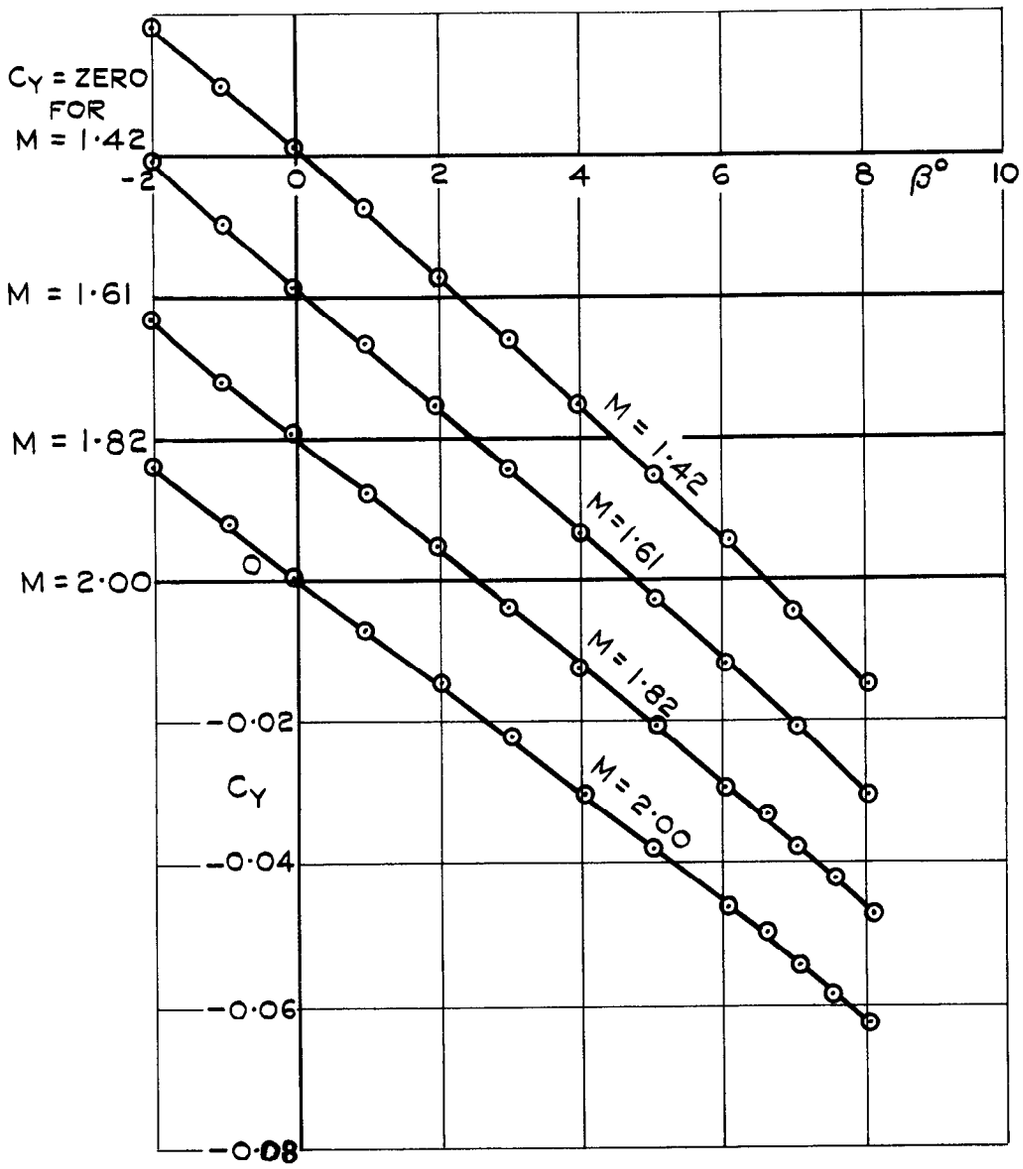

FIG.21. SIDEFORCE-VARIATION WITH SIDESLIP ANGLE AND MACH NUMBER, MODEL WITH FIN ON, $\eta = -4°$, AT $\alpha = 0°$.

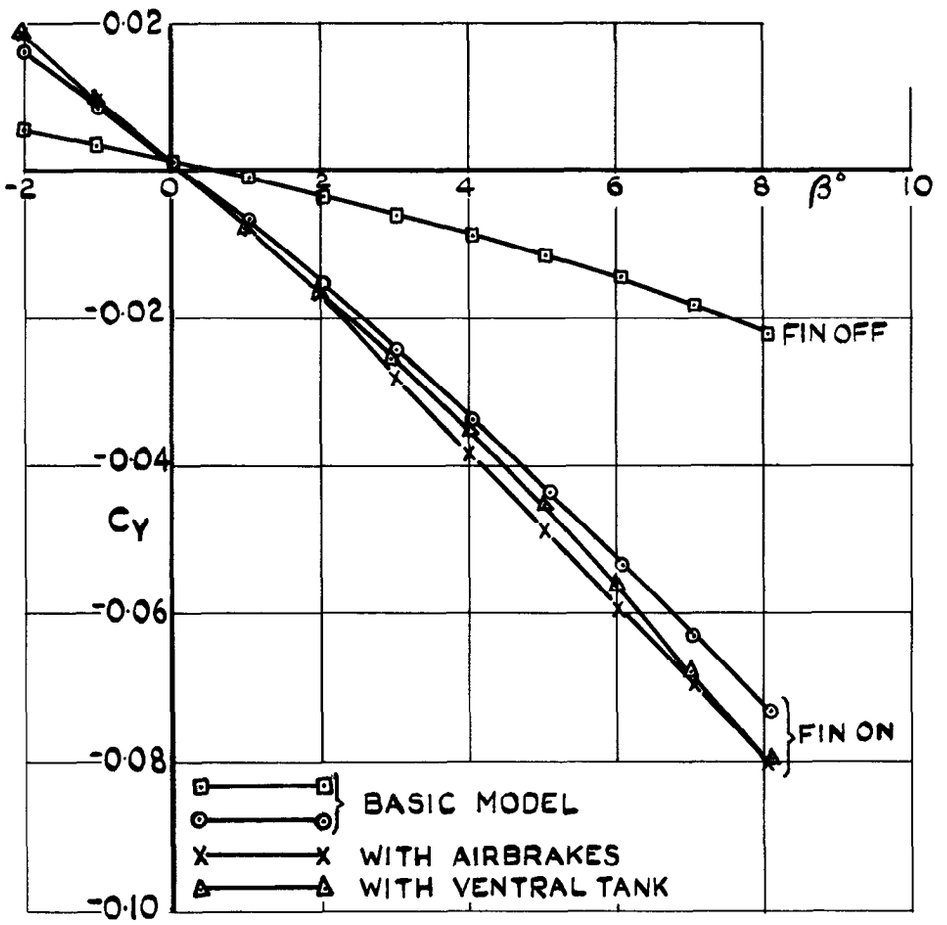

(a) M = 1·42.

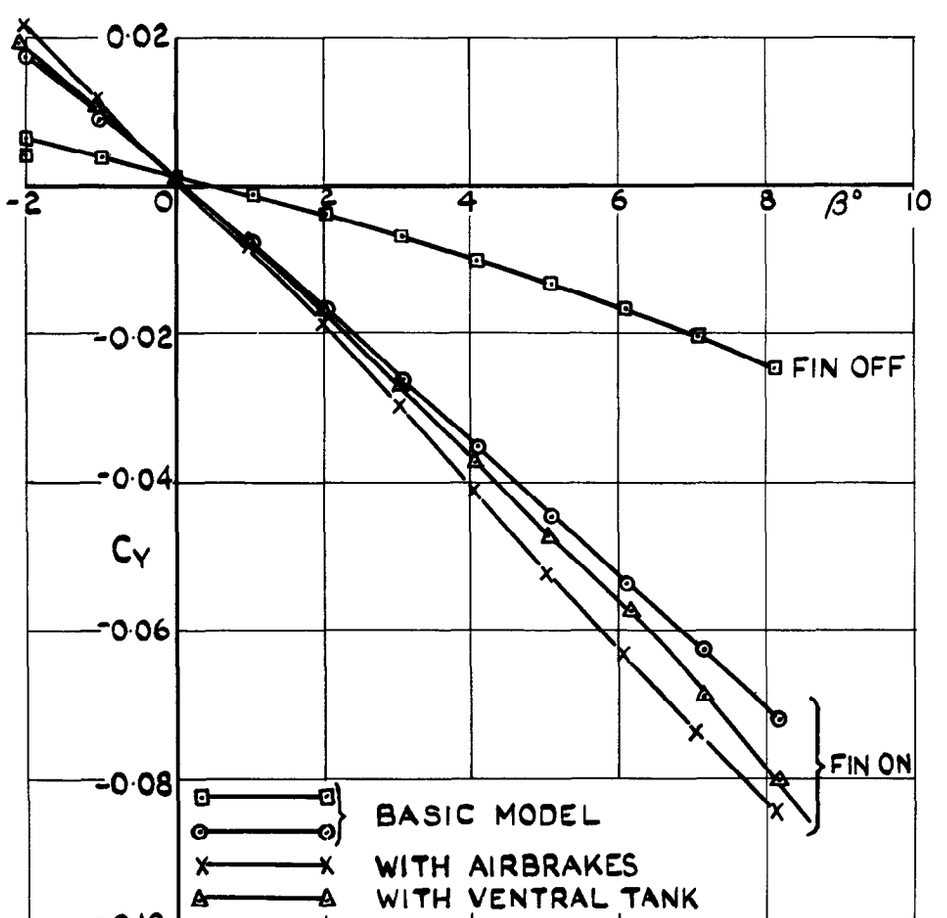

(b) M = 1·61.

FIG. 22. SIDEFORCE–VARIATION WITH SIDESLIP ANGLE AND MACH NUMBER, MODEL WITH $\eta = -10°$ AT $\alpha = 0°$.

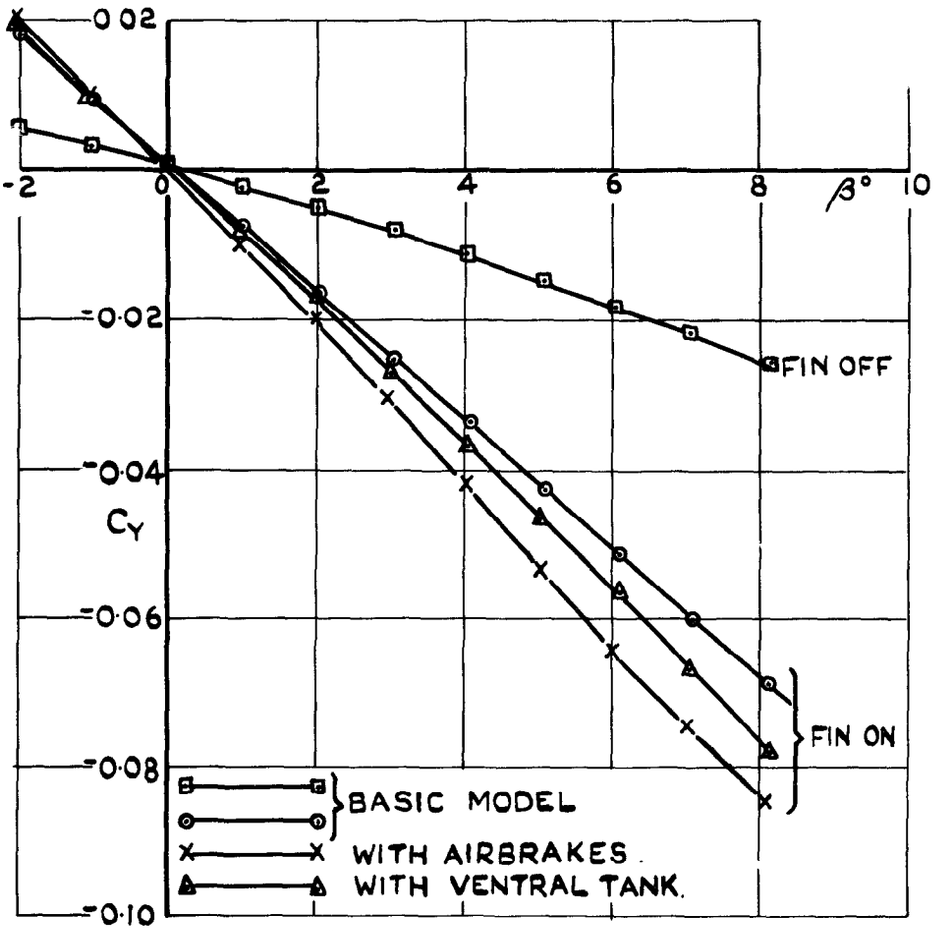

(C) M = 1·82

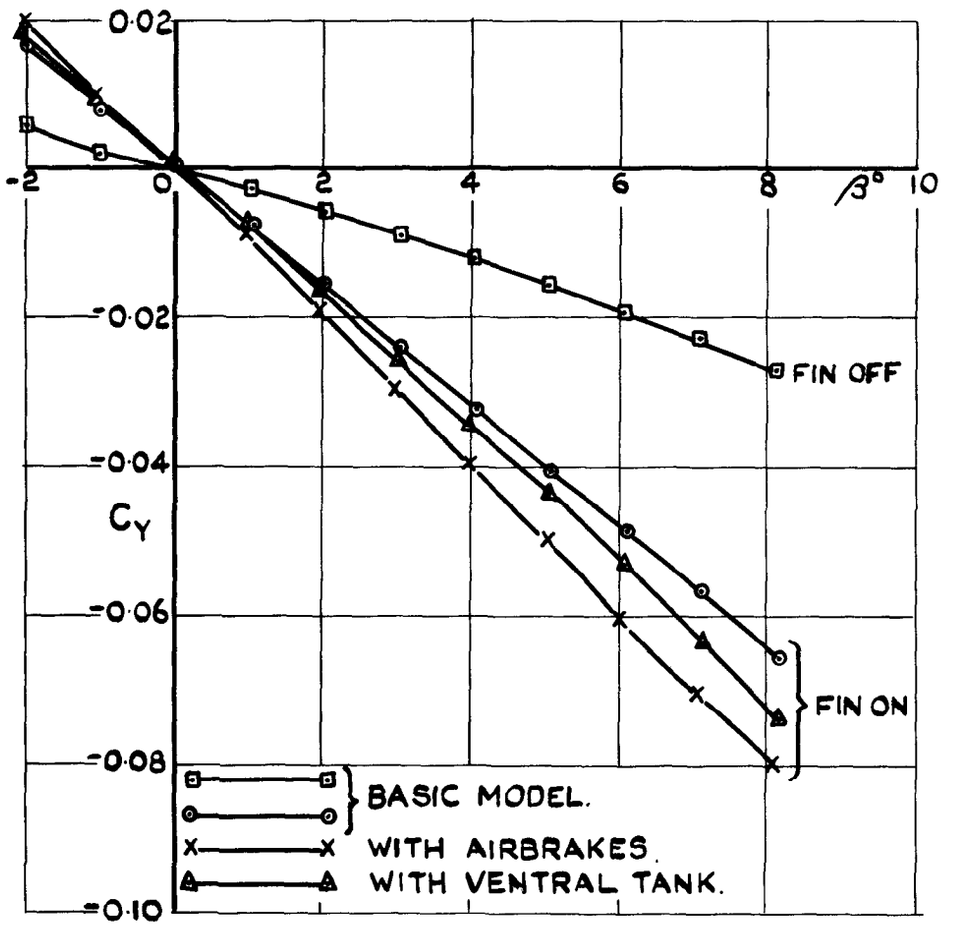

(d) M=2·00

FIG. 22. (CONTD)

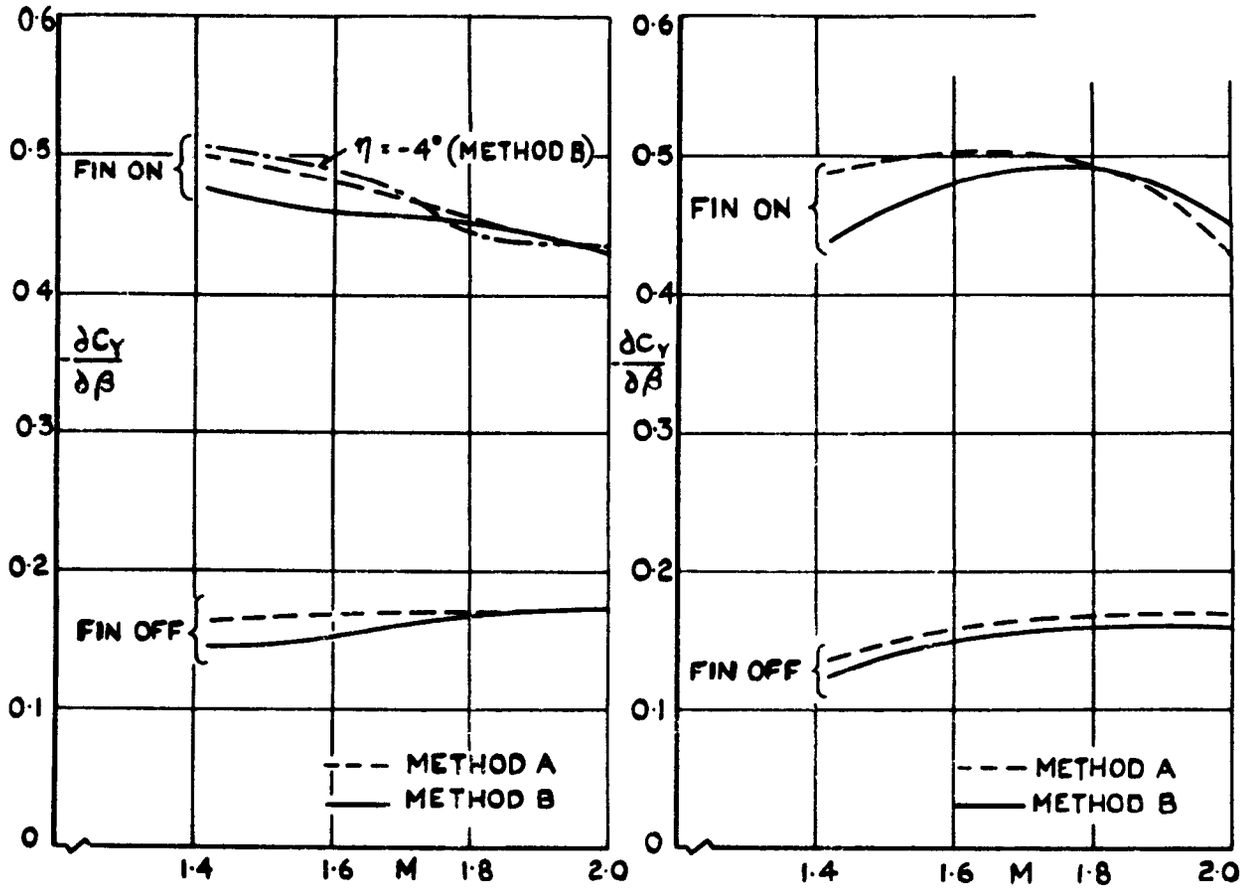

(a) WITH $\eta = 0°$ & $\eta = -4°$ (INDICATED)

(b) WITH $\eta = -10°$.

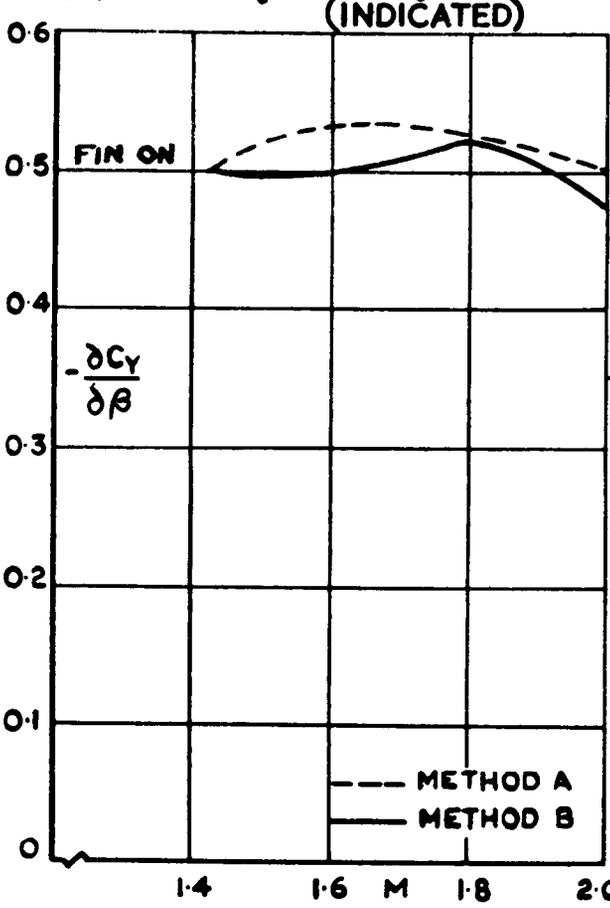

(c) WITH VENTRAL TANK ($\eta = -10°$)

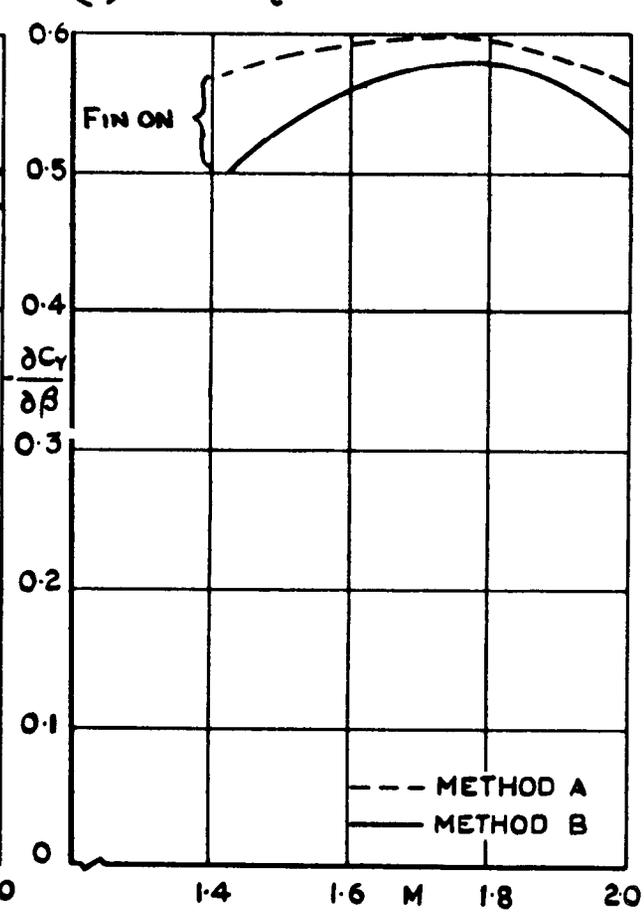

(d) WITH AIR BRAKES ($\eta = -10°$)

FIG. 23. SIDEFORCE DUE TO SIDESLIP (AT $\alpha = 0°$) —VARIATION WITH MACH NUMBER.

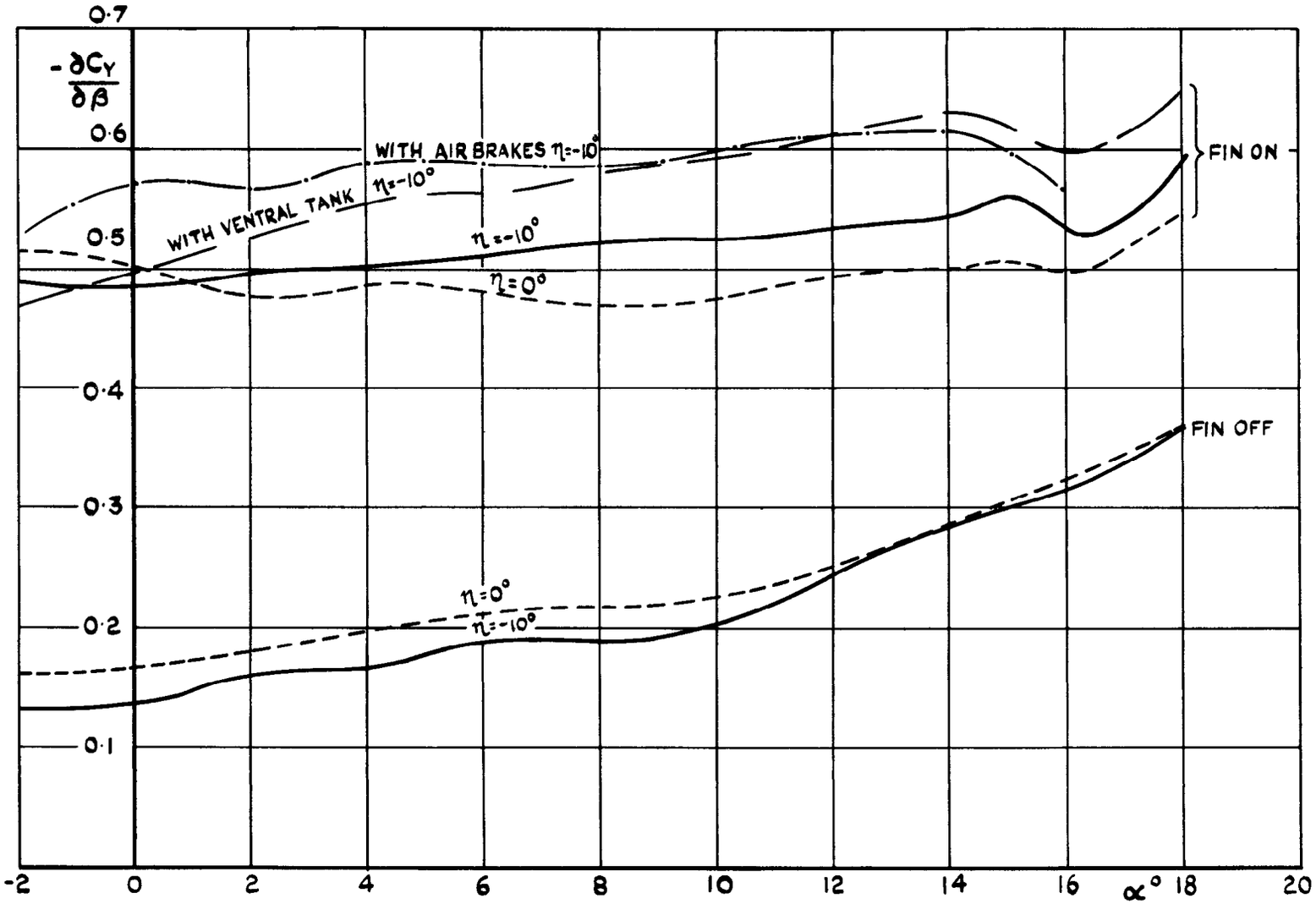

(a) M = 1·42

FIG. 24. SIDEFORCE DUE TO SIDESLIP—VARIATION WITH INCIDENCE AND MACH NUMBER.

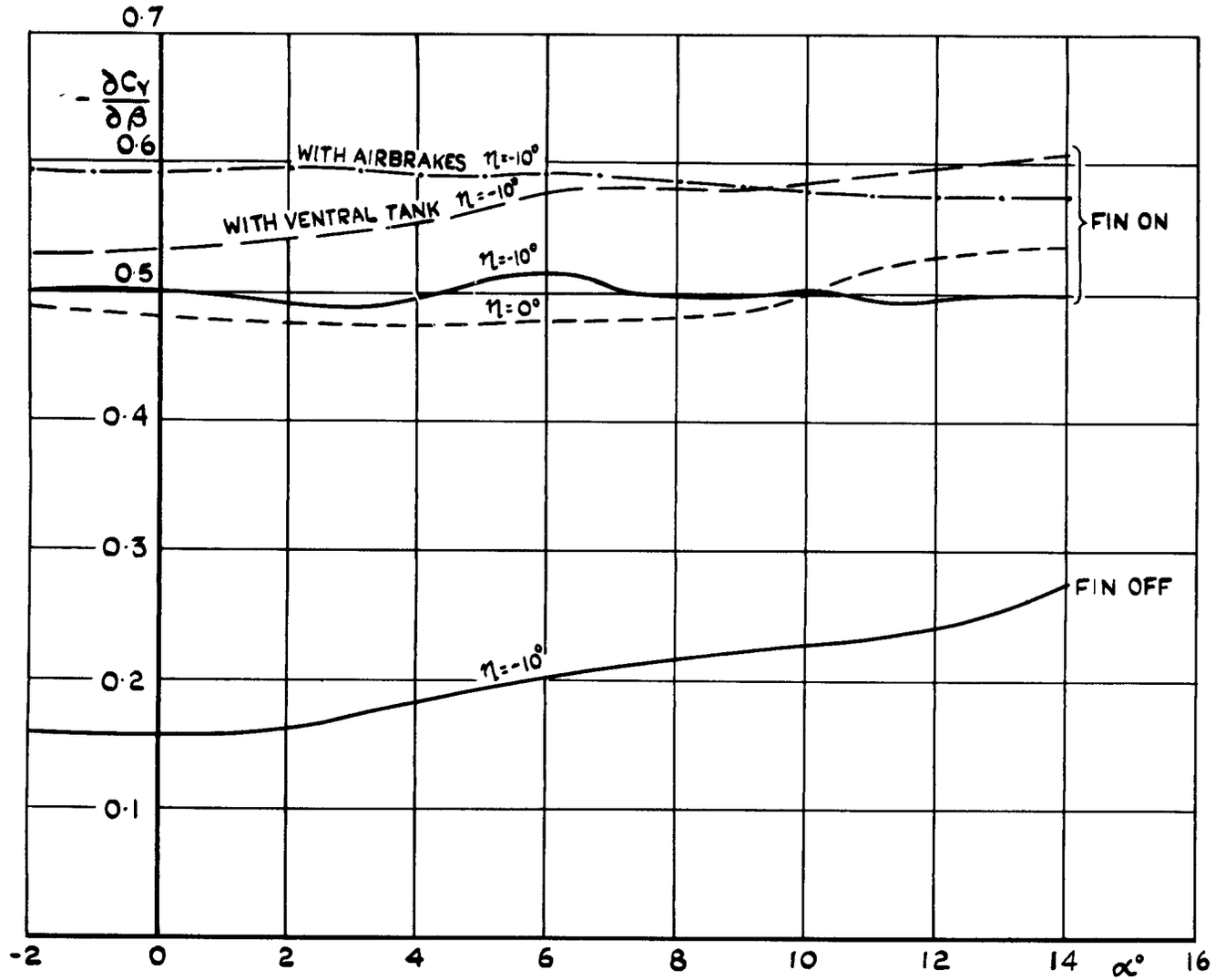

(b) M = 1·61.

FIG. 24. (CONTD.)

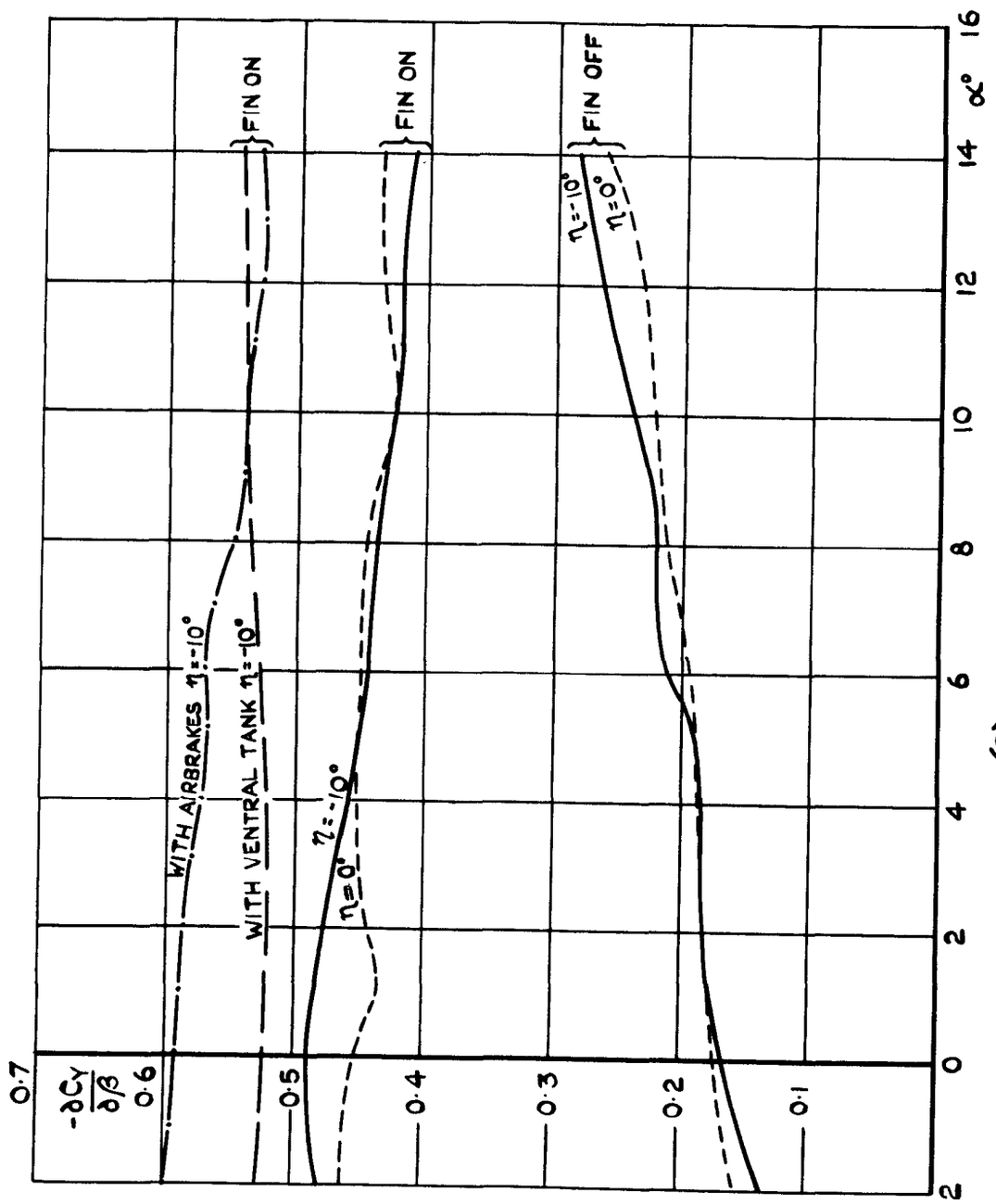

(C) M=1·82

FIG. 24. (CONTD.)

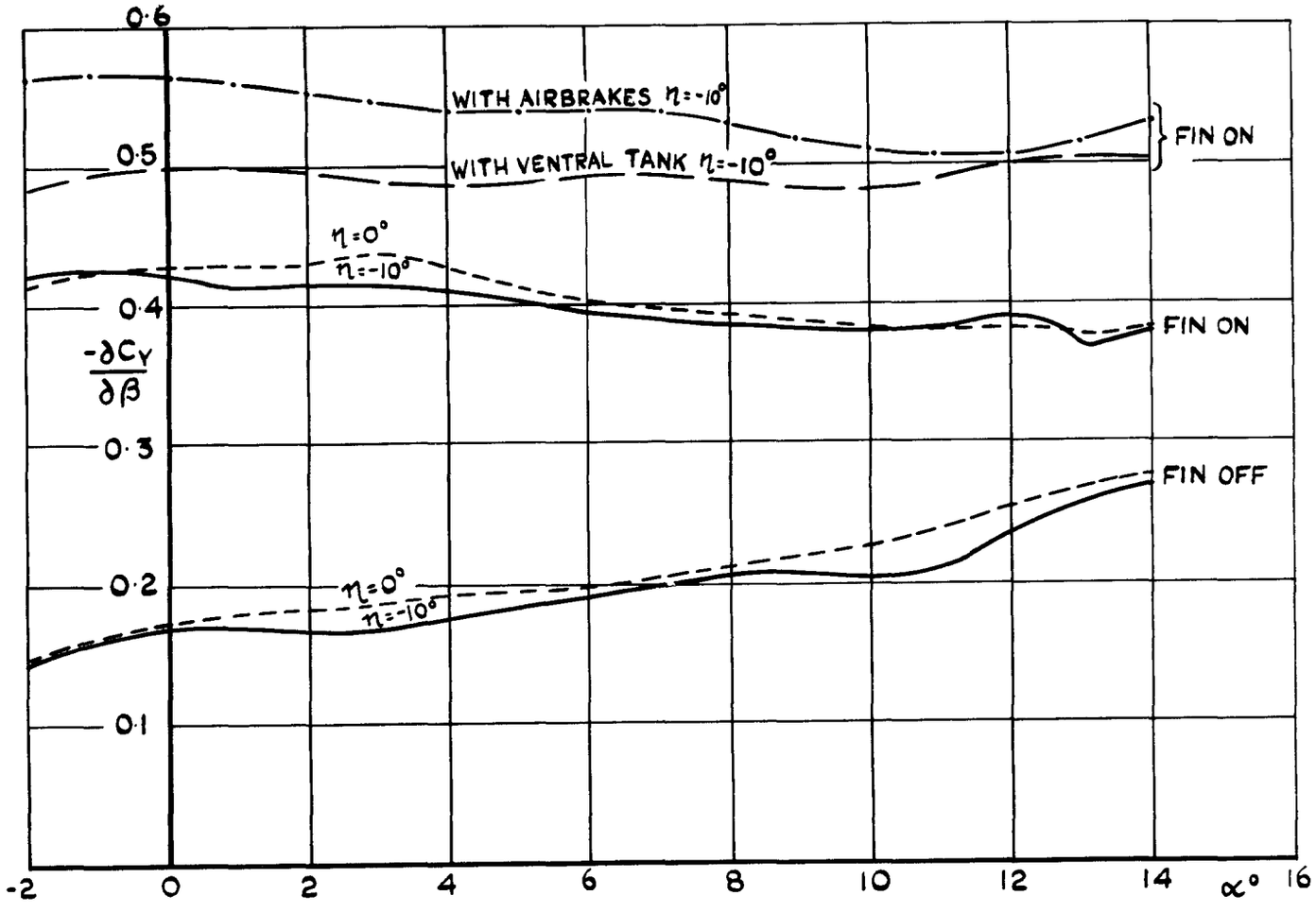

(d) M=2·00.

FIG. 24. (CONCLD.)

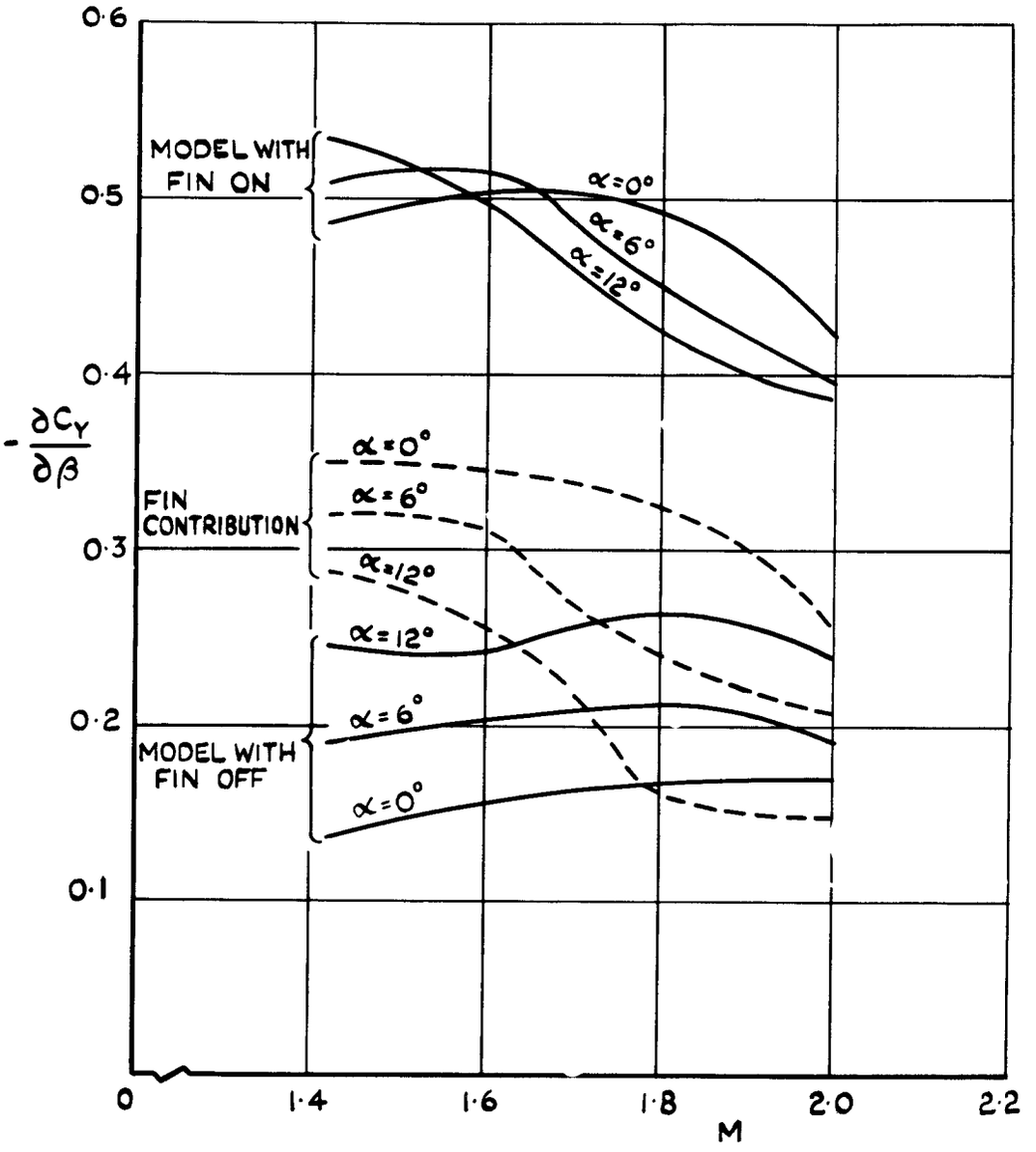

FIG. 25. SIDEFORCE DUE TO SIDESLIP—VARIATION WITH MACH NUMBER AT CONSTANT INCIDENCE, MODEL WITH η=-10° (METHOD A).

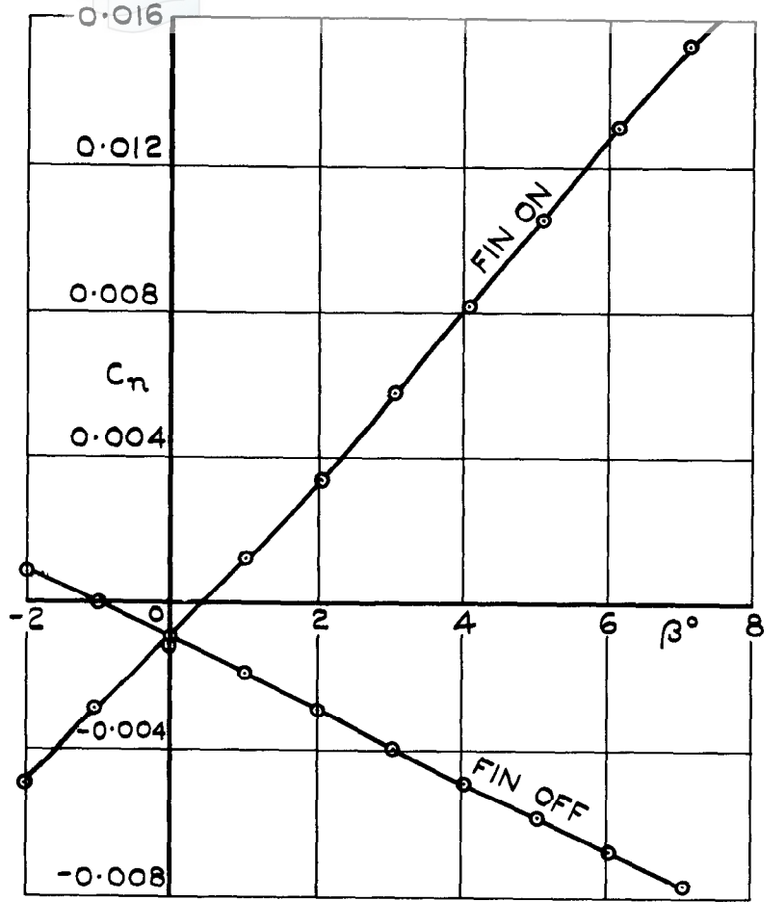

(a) M = 1·42

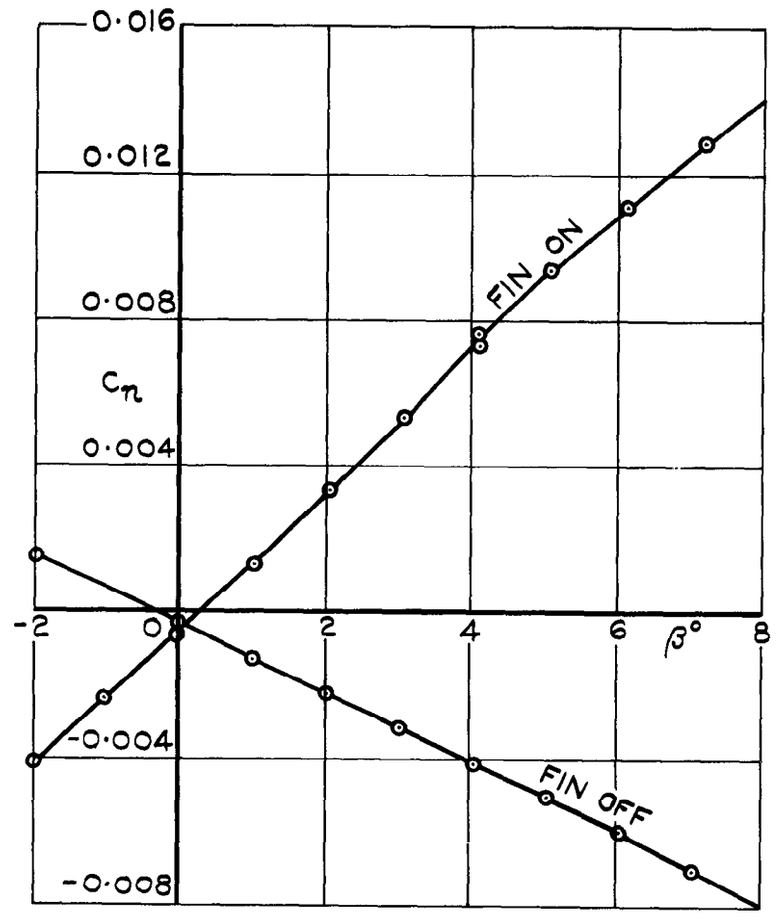

(b) M = 1·61

FIG. 26. YAWING MOMENT-VARIATION WITH SIDESLIP ANGLE AND MACH NUMBER, MODEL WITH $\eta = 0°$, AT $\alpha = 0°$

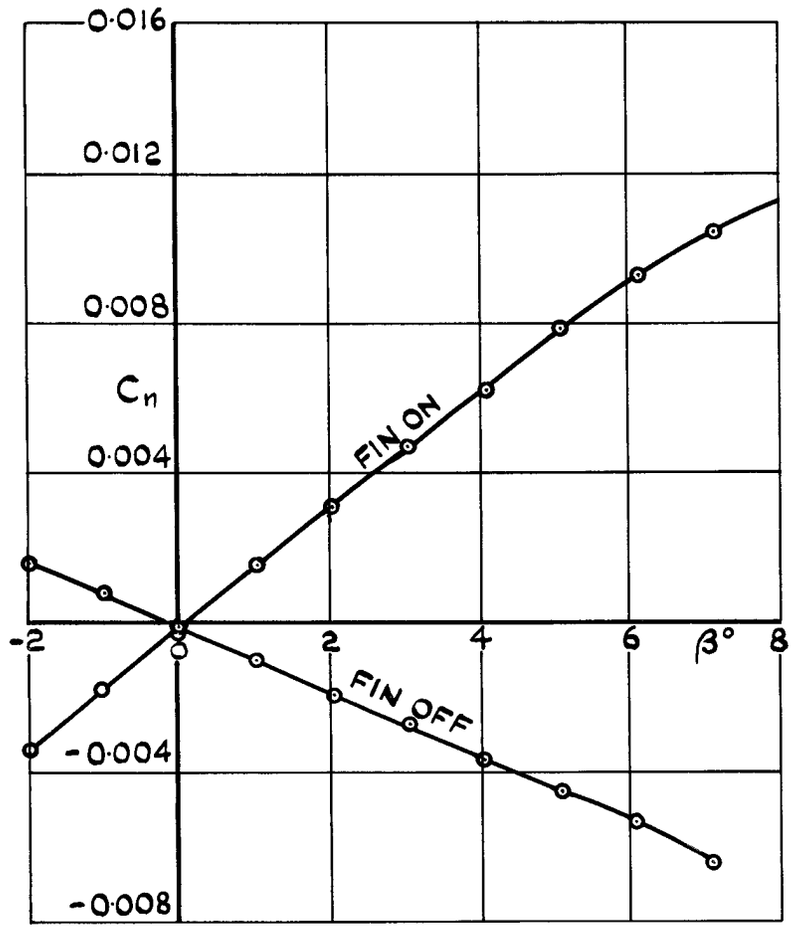

(C.) M = 1·82

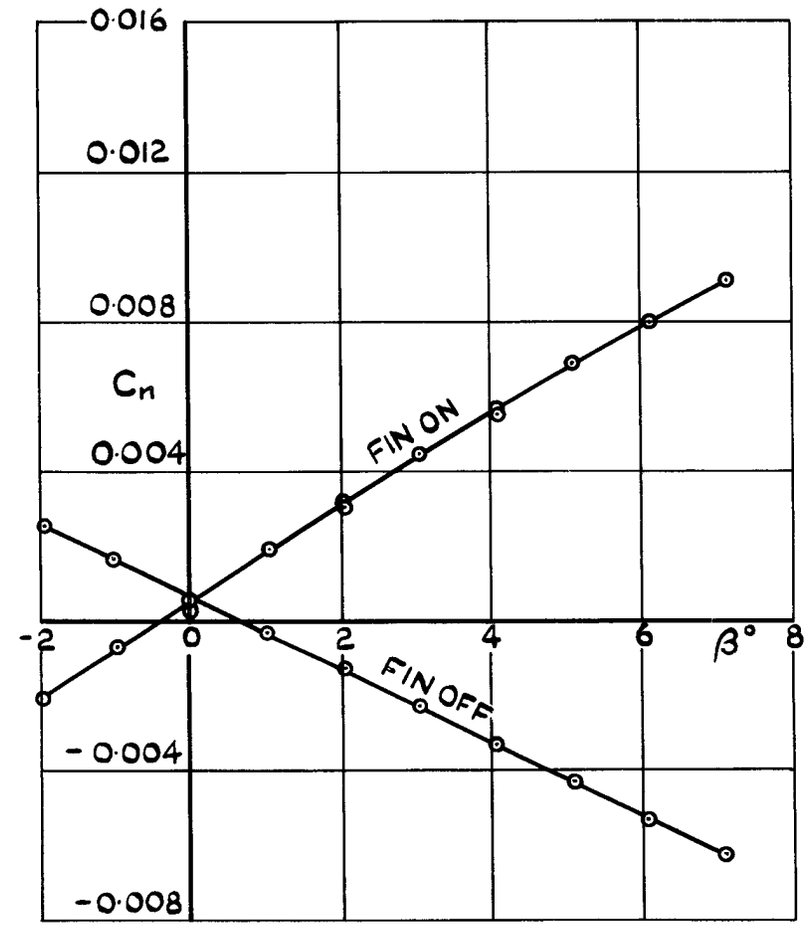

(d.) M = 2·00

FIG. 26. (CONTD.)

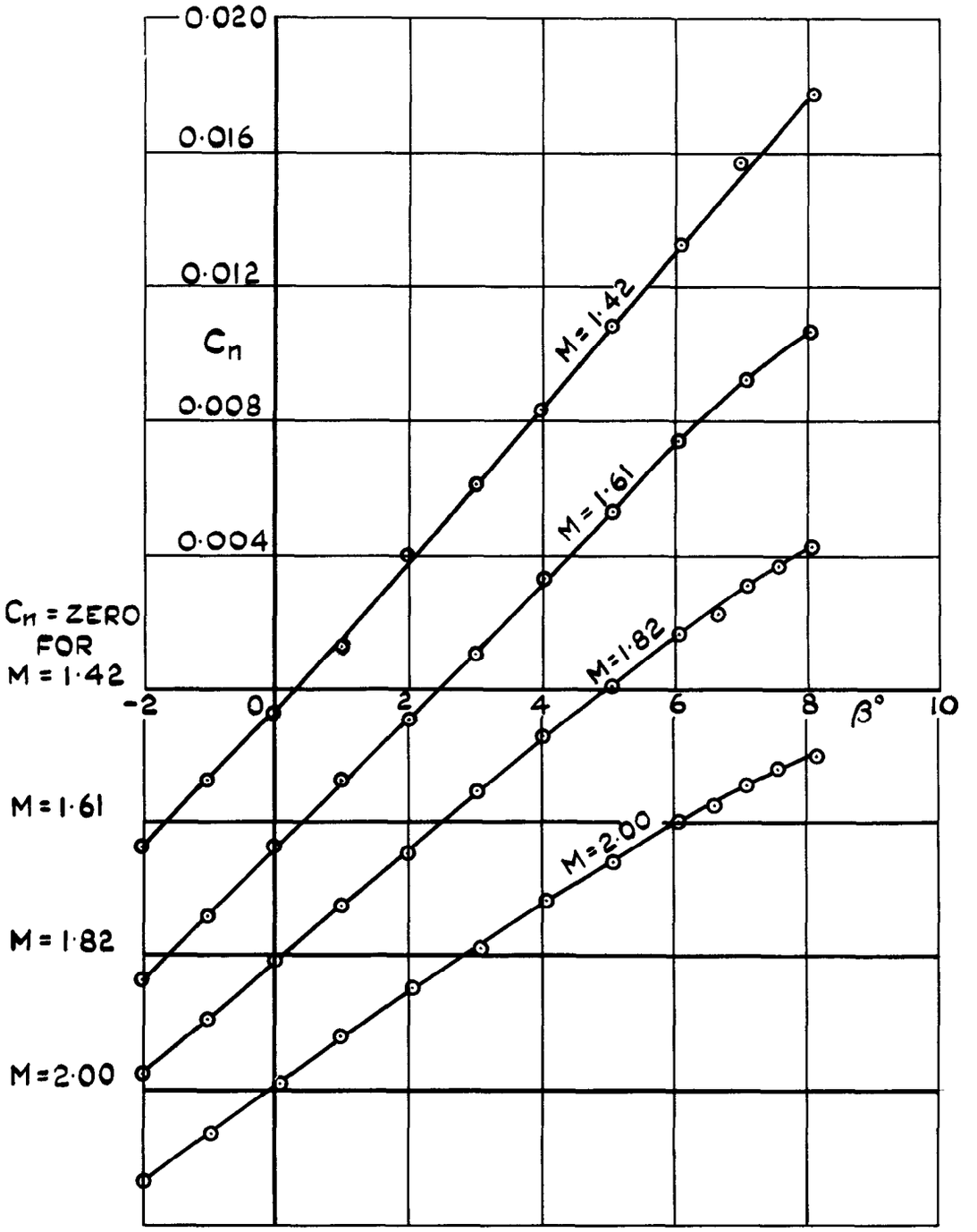

FIG. 27. YAWING MOMENT - VARIATION WITH SIDESLIP ANGLE AND MACH NUMBER, MODEL WITH FIN ON, $\eta = -4°$ AT $\alpha = 0°$

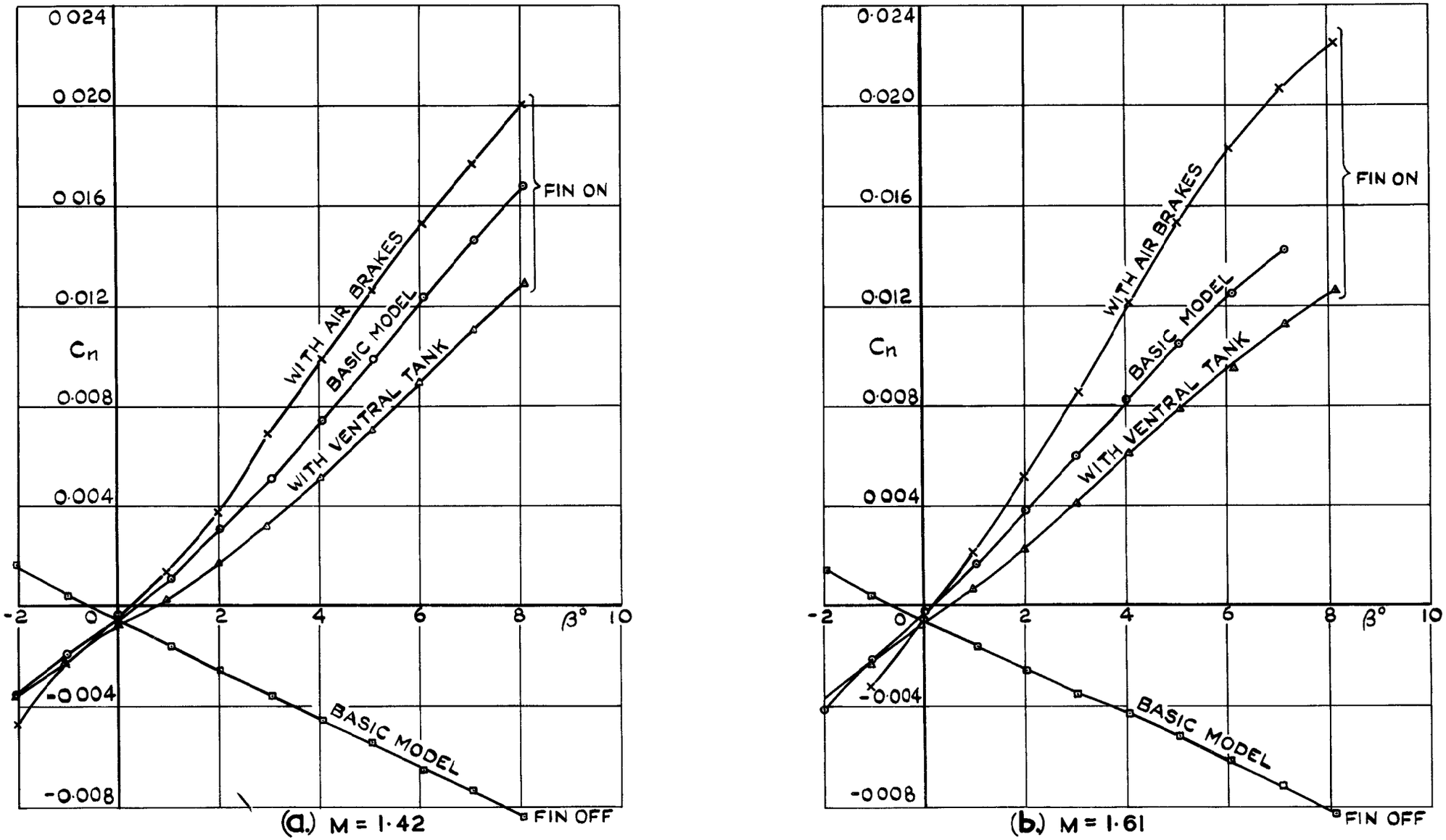

FIG. 28. YAWING MOMENT-VARIATION WITH SIDESLIP ANGLE AND MACH NUMBER, MODEL WITH $\eta = -10^{\circ}$ AT $\alpha = 0^{\circ}$

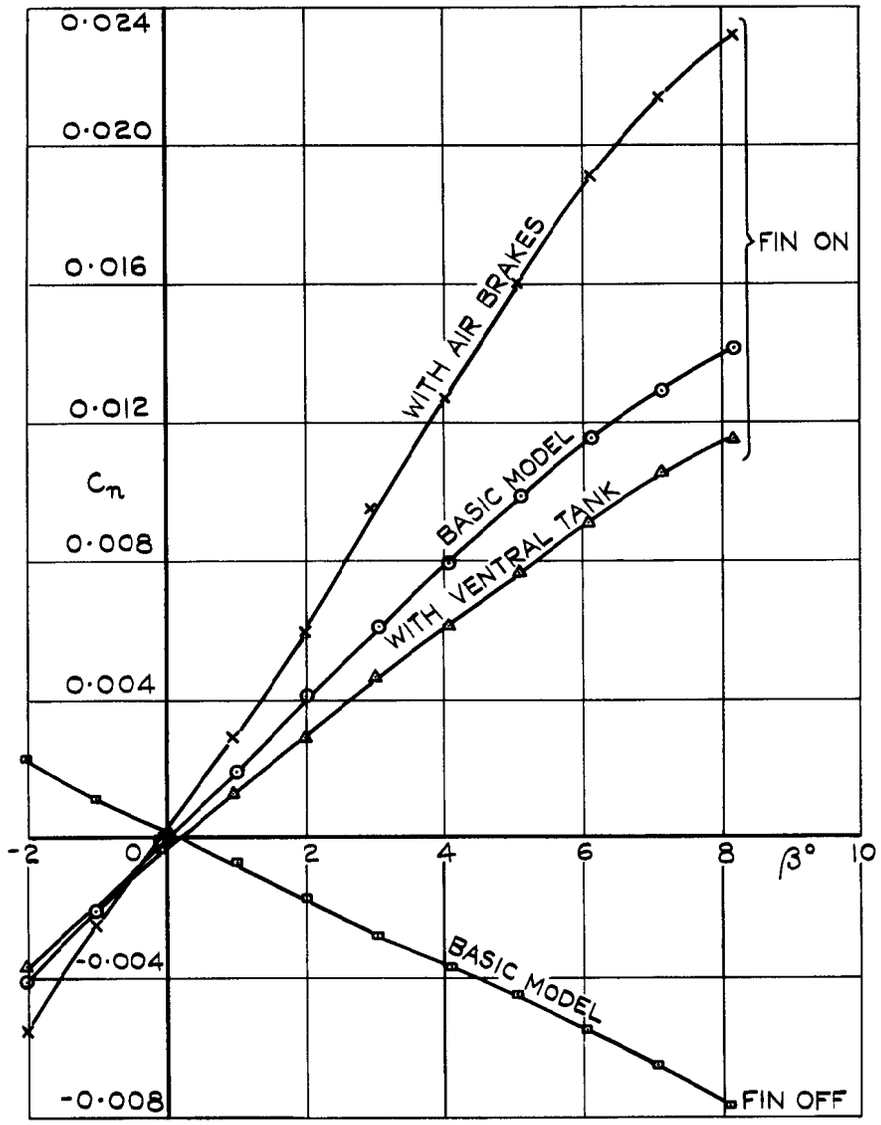

(c) M = 1·82

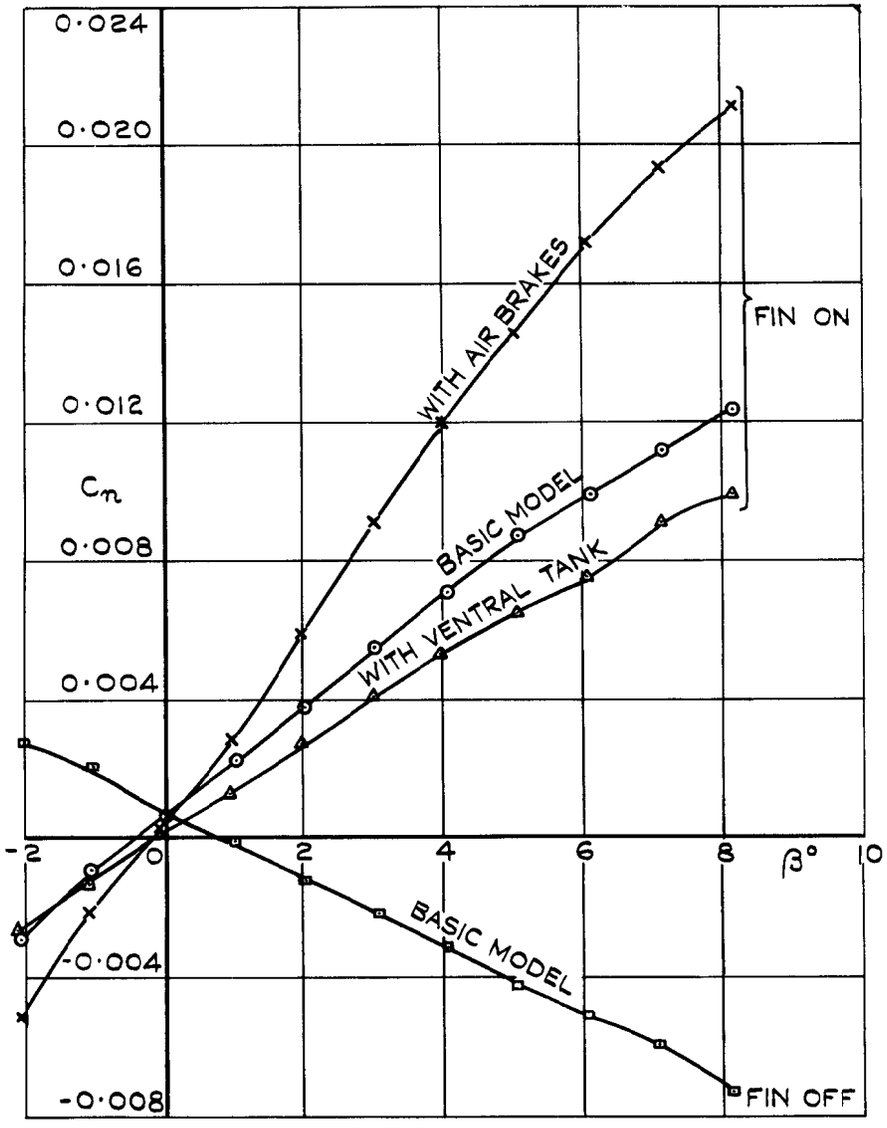

(d) M = 2·00

FIG. 28. (CONTD.)

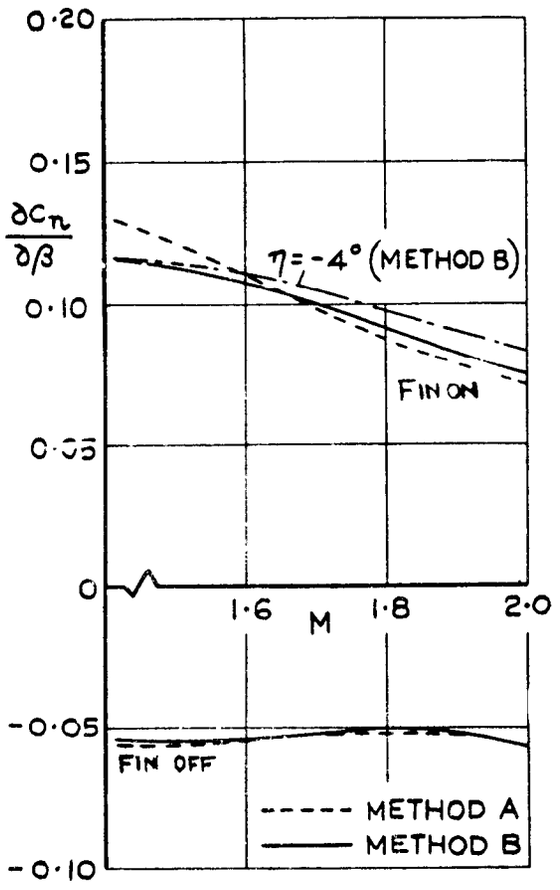

(a) WITH $\eta = 0°$ & $\eta = -4°$ (INDICATED).

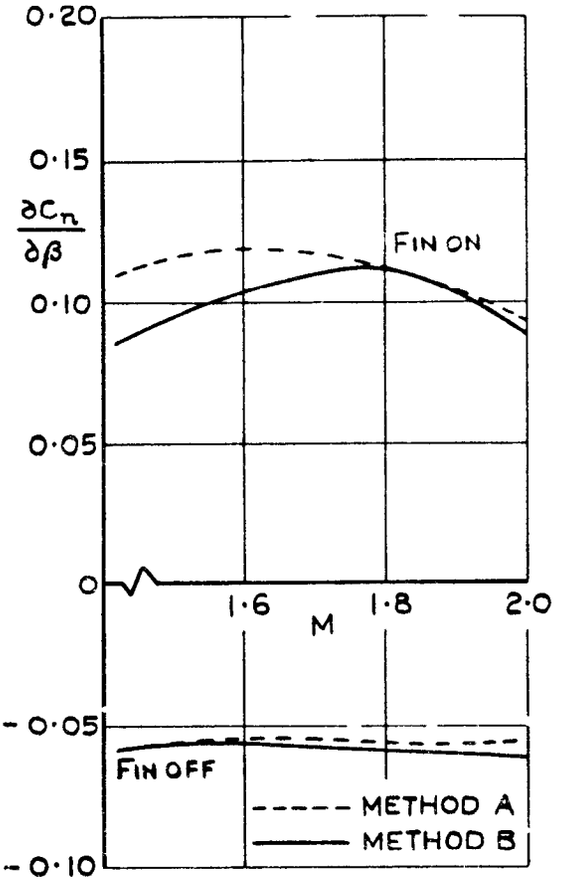

(b) WITH $\eta = -10°$.

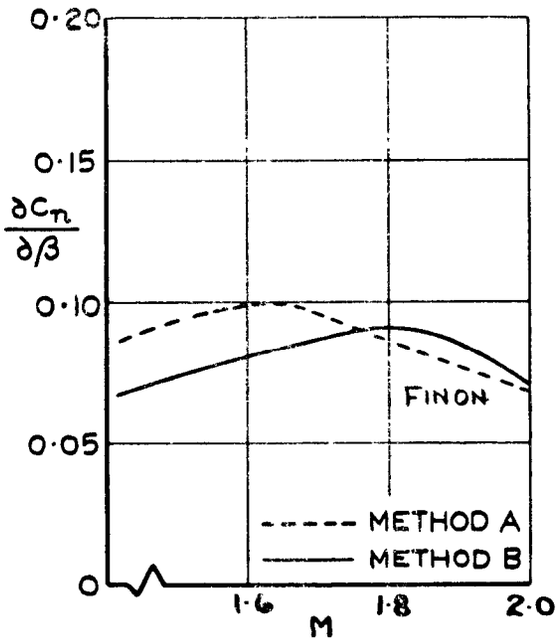

(c) WITH VENTRAL TANK ($\eta = -10°$).

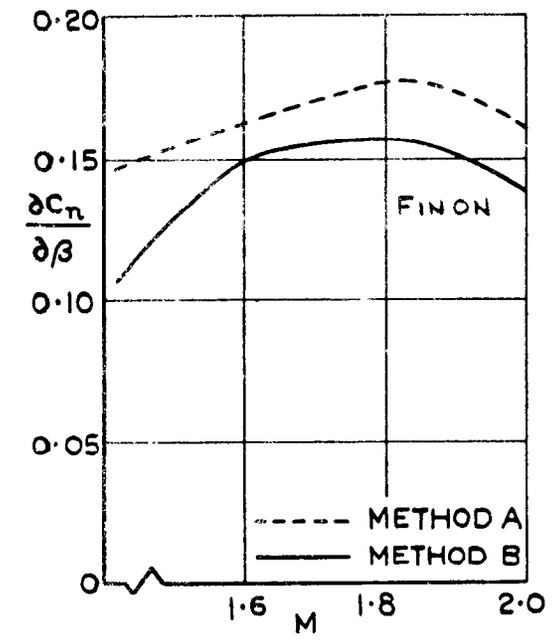

(d) WITH AIRBRAKES ($\eta = -10°$).

FIG. 29. YAWING MOMENT DUE TO SIDESLIP (AT $\alpha = 0°$) —VARIATION WITH MACH NUMBER.

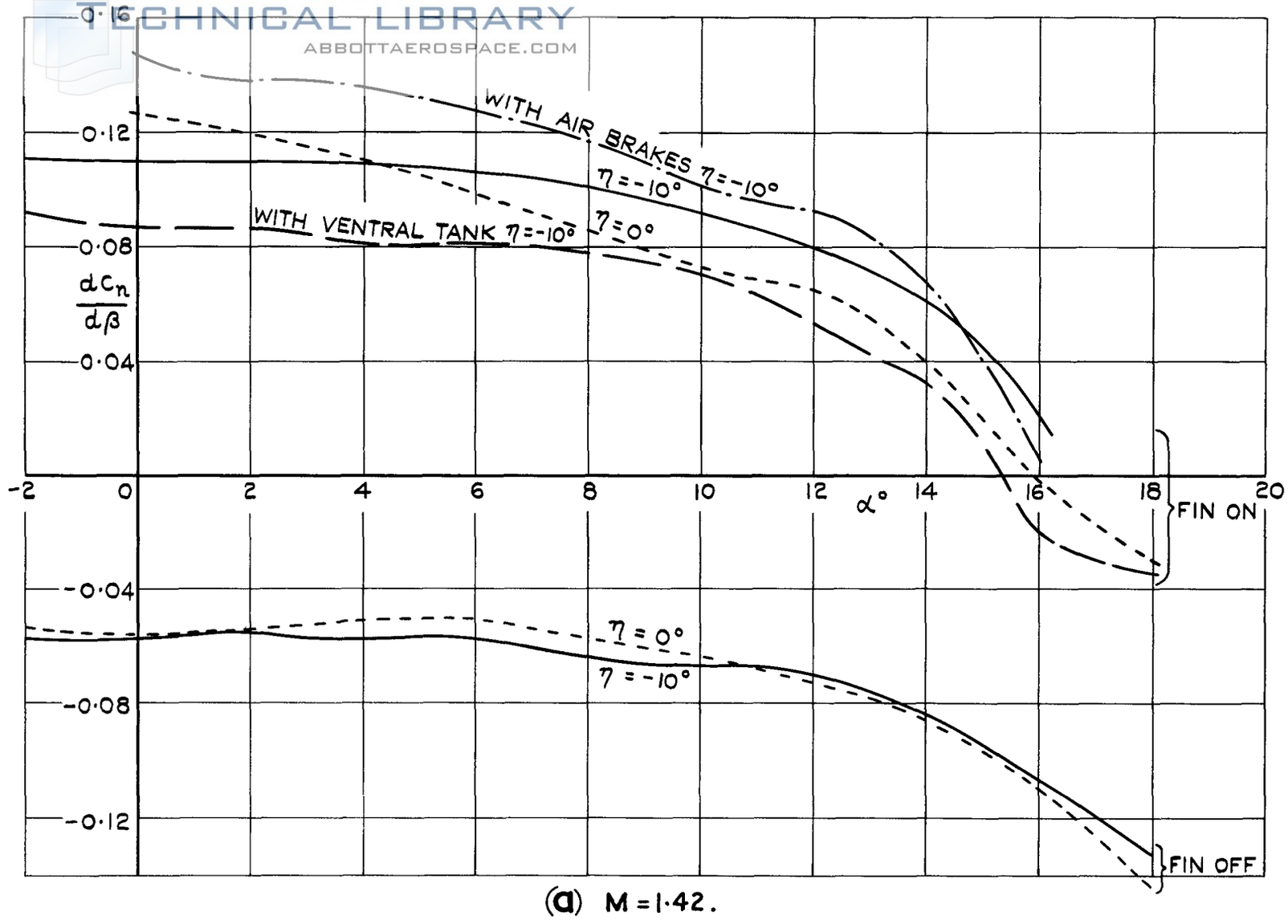

(a) M=1·42.

FIG. 30. YAWING MOMENT DUE TO SIDESLIP — VARIATION WITH INCIDENCE AND MACH NUMBER.

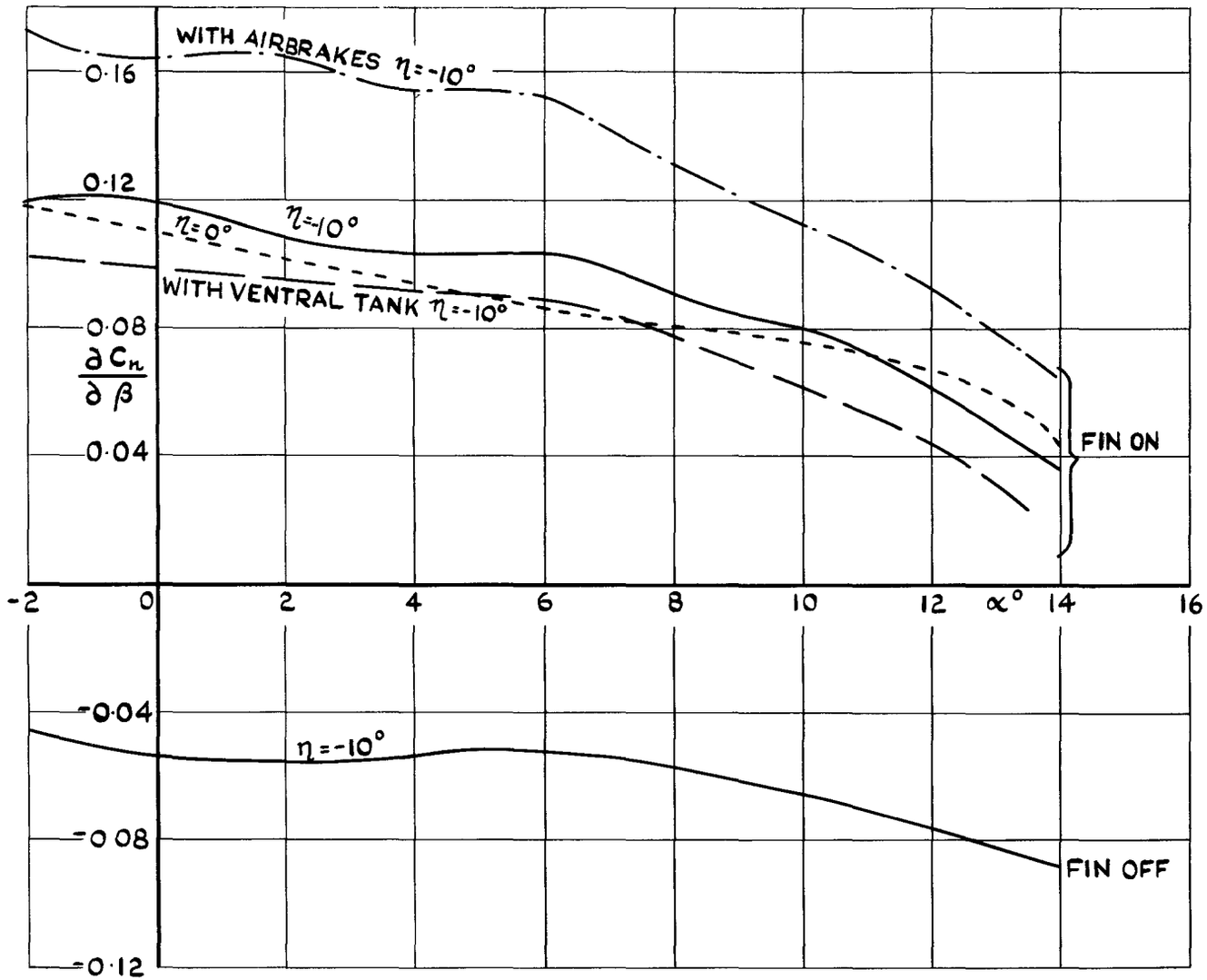

(b) M=1·61.

FIG. 30 (CONTD.)

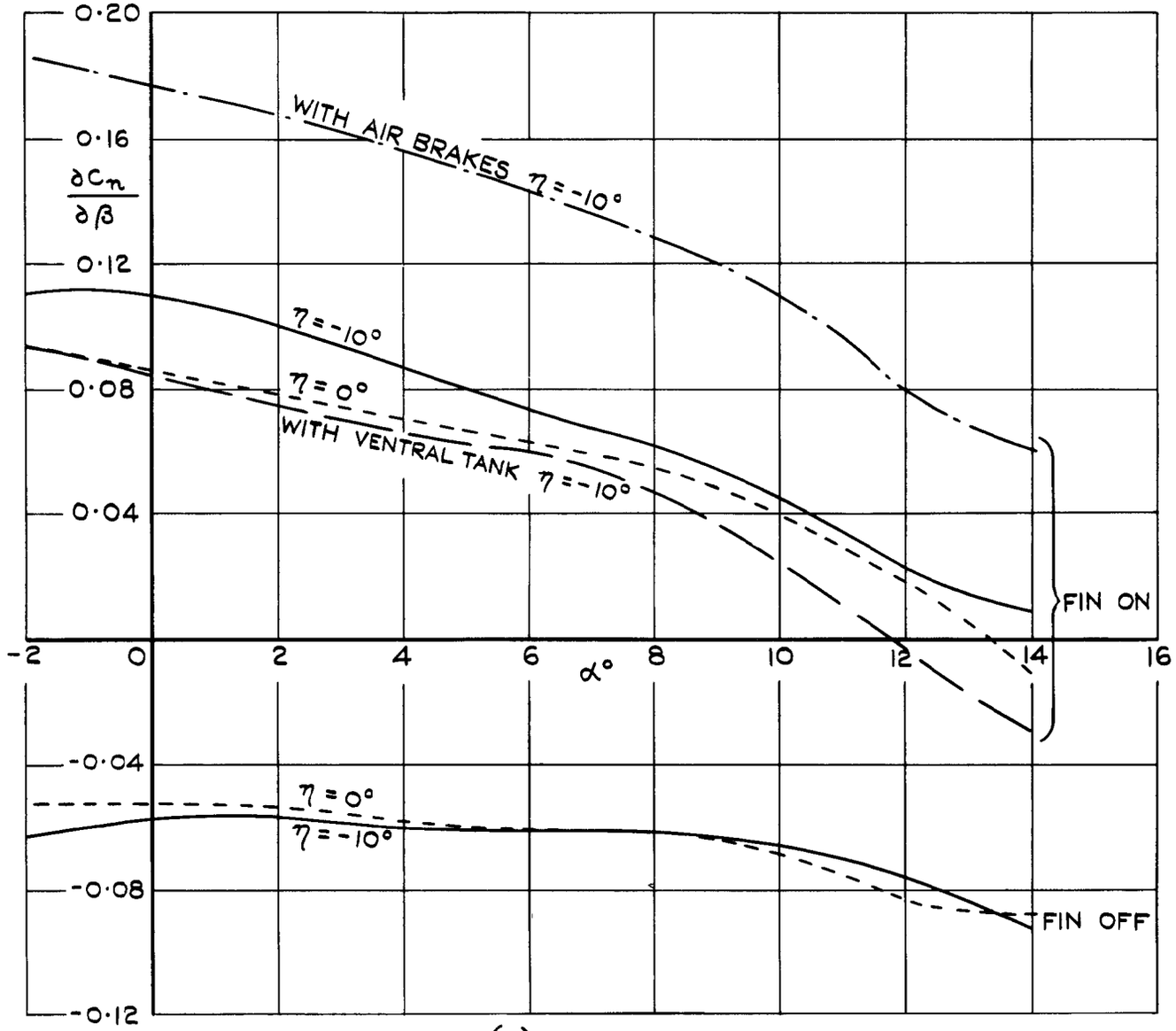

(c) M=1·82.

FIG. 30 (CONTD.).

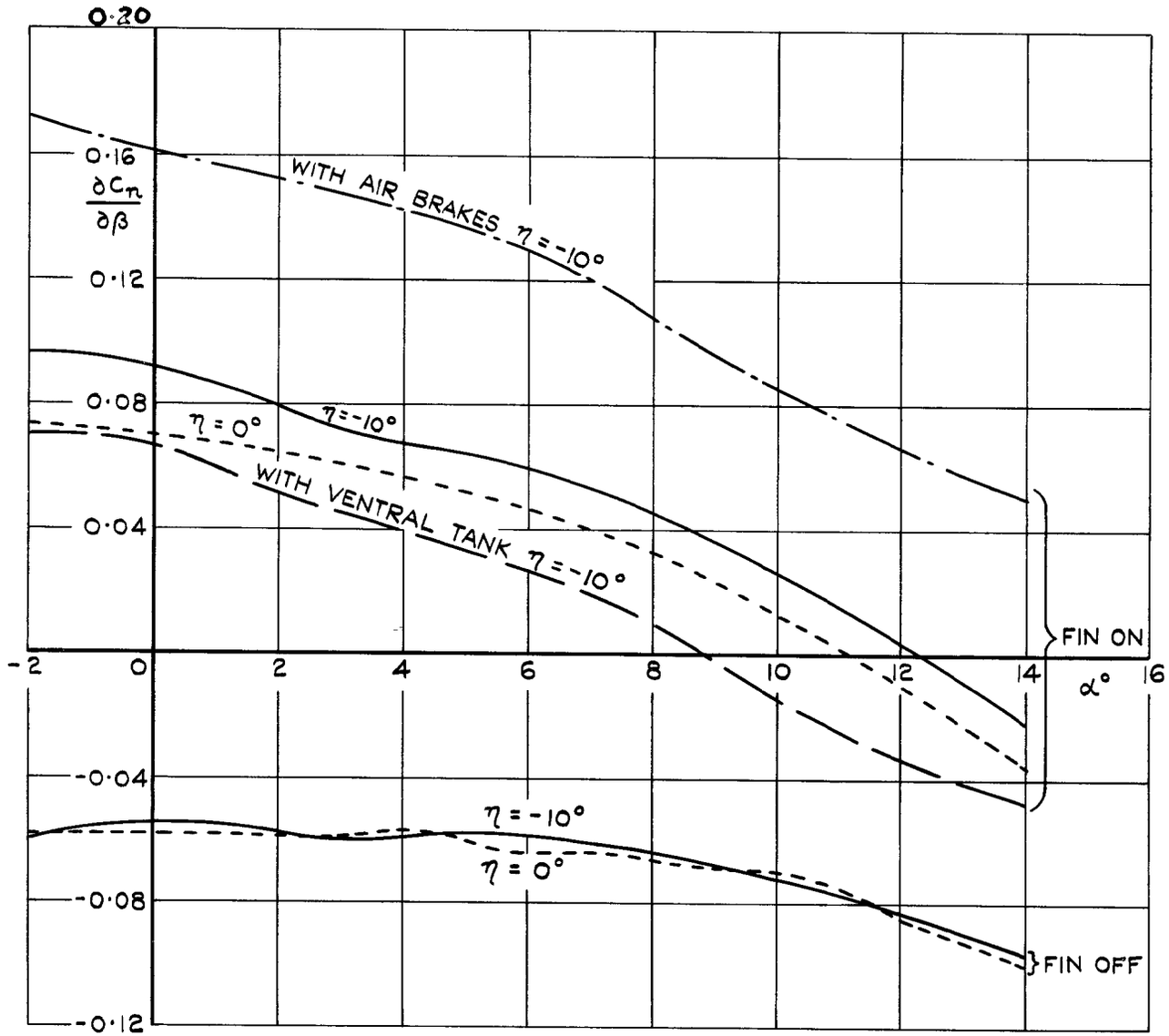

(d) M=2·00.

FIG. 30 (CONCLD.).

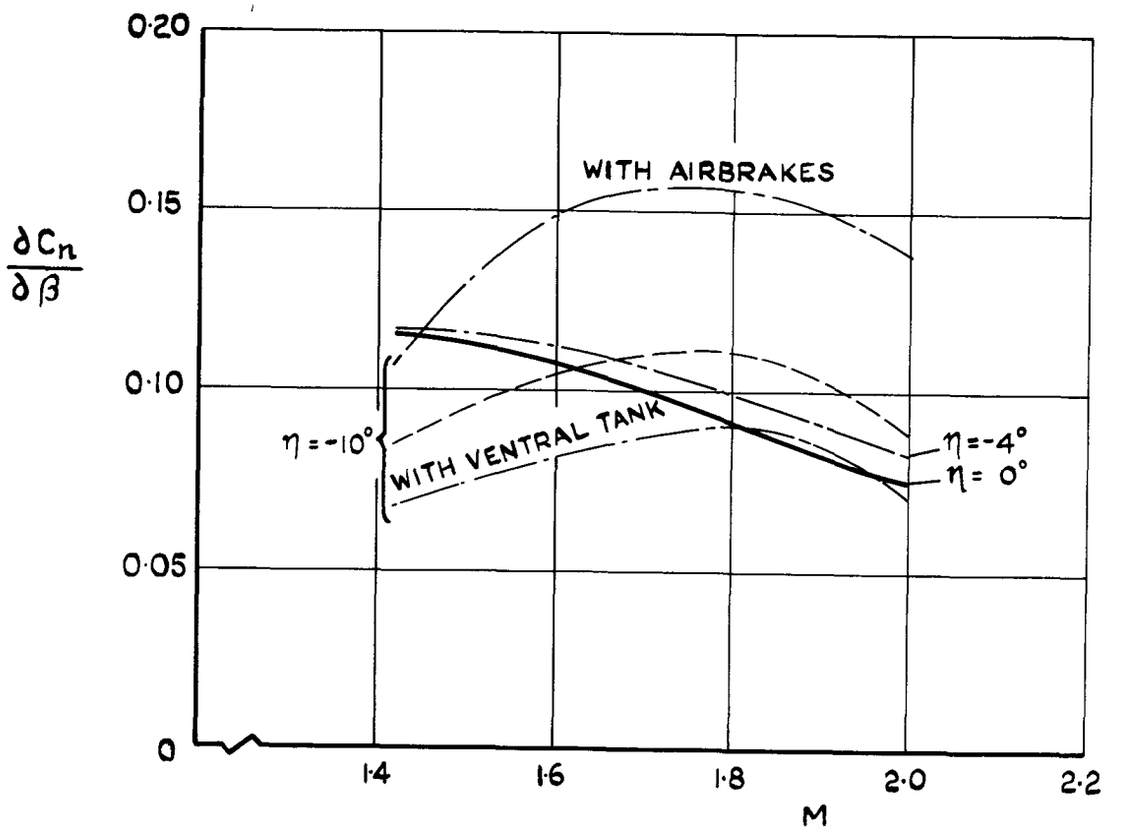

FIG.31. YAWING MOMENT DUE TO SIDESLIP — VARIATION WITH MACH NUMBER, (α=0, METHOD B).

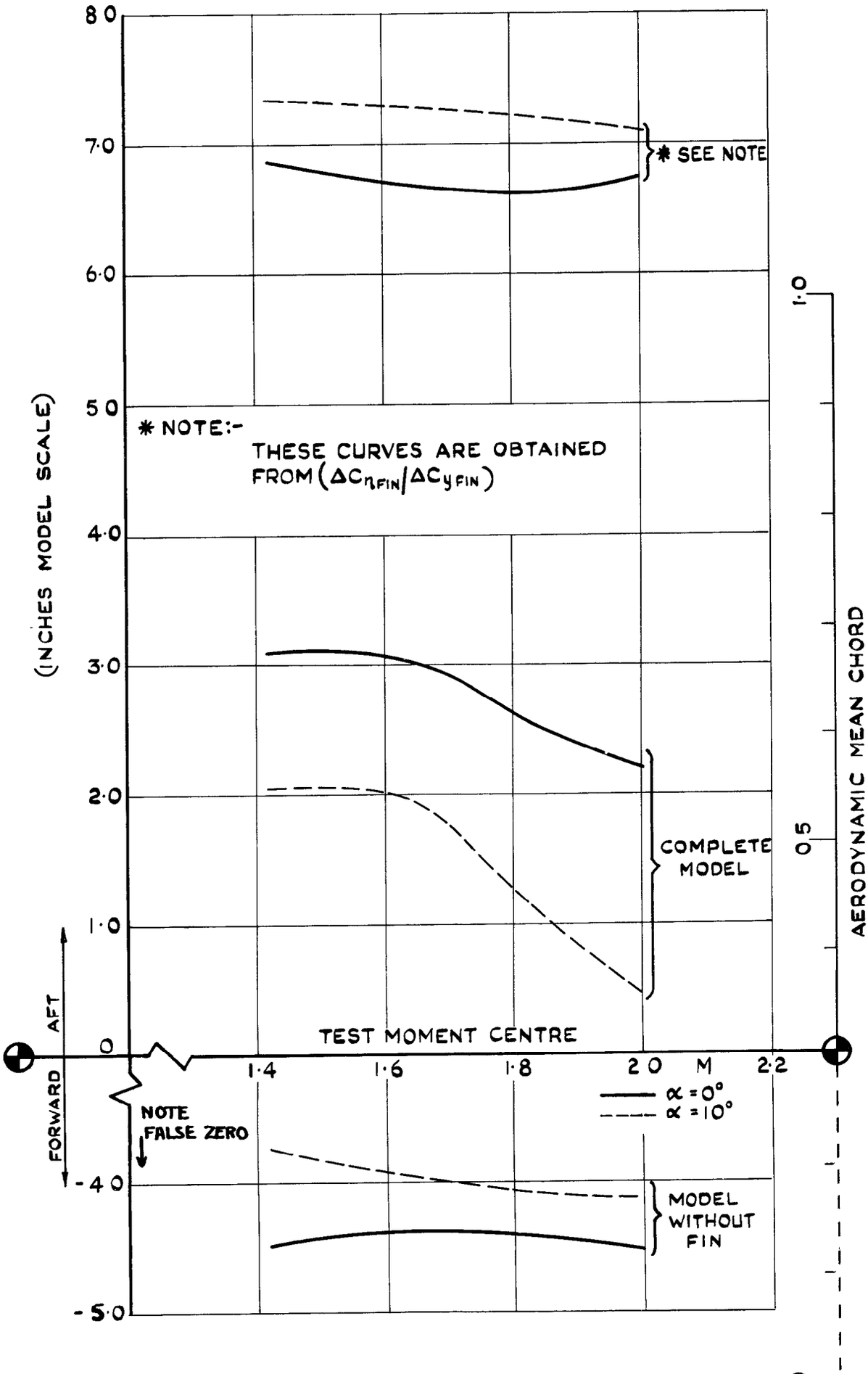

FIG. 32. C_n/C_Y – VARIATION WITH MACH NUMBER AT CONSTANT INCIDENCE, (MODEL WITH $\eta = 0°$).

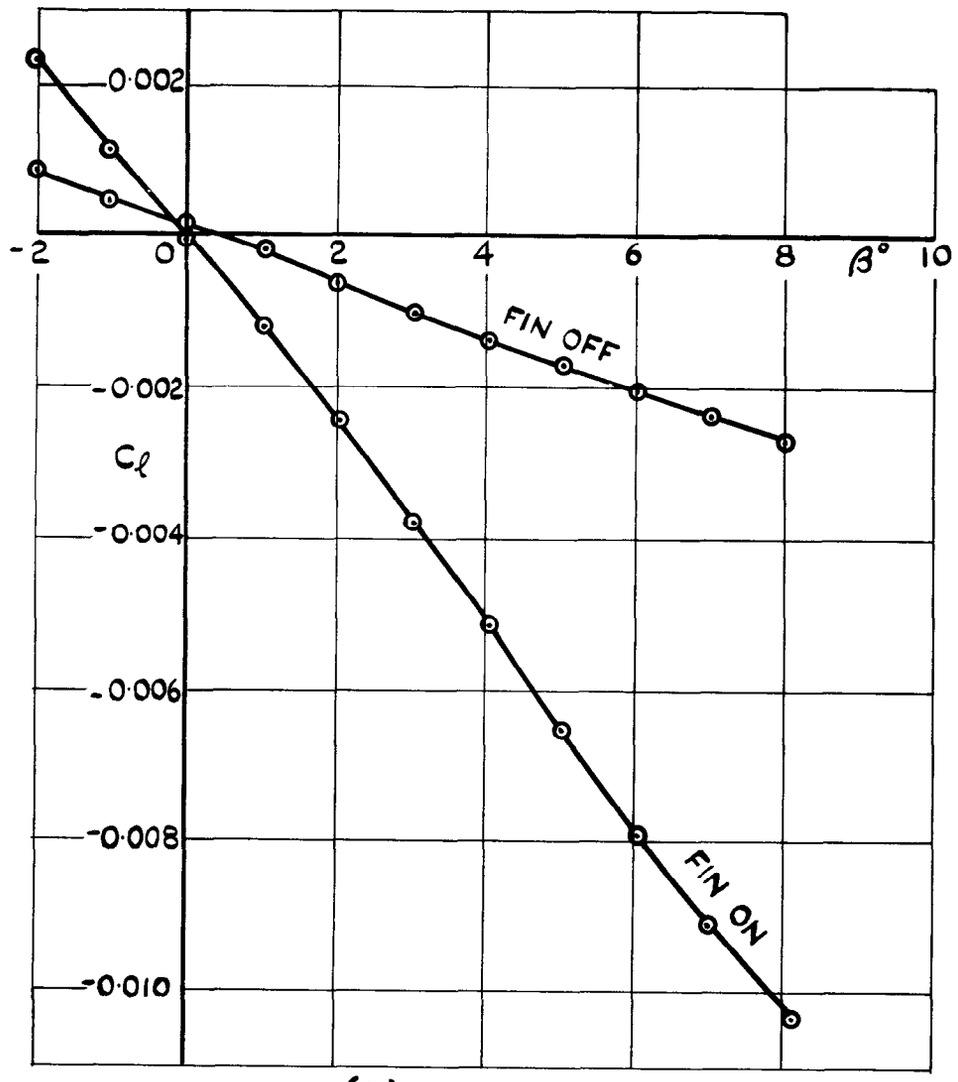

(a) M = 1·42

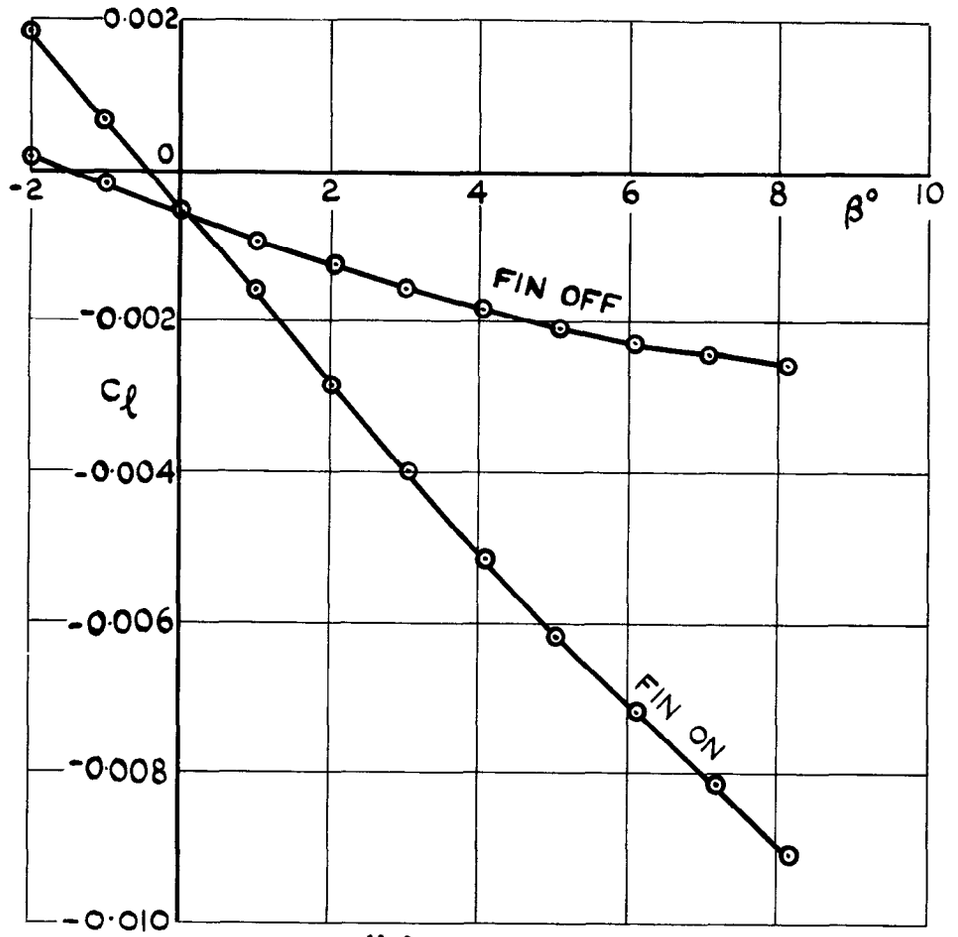

(b) M = 1·61

FIG.33. ROLLING MOMENT—VARIATION WITH SIDESLIP ANGLE AND MACH NUMBER, MODEL WITH $\eta = 0°$, AT $\alpha = 0°$.

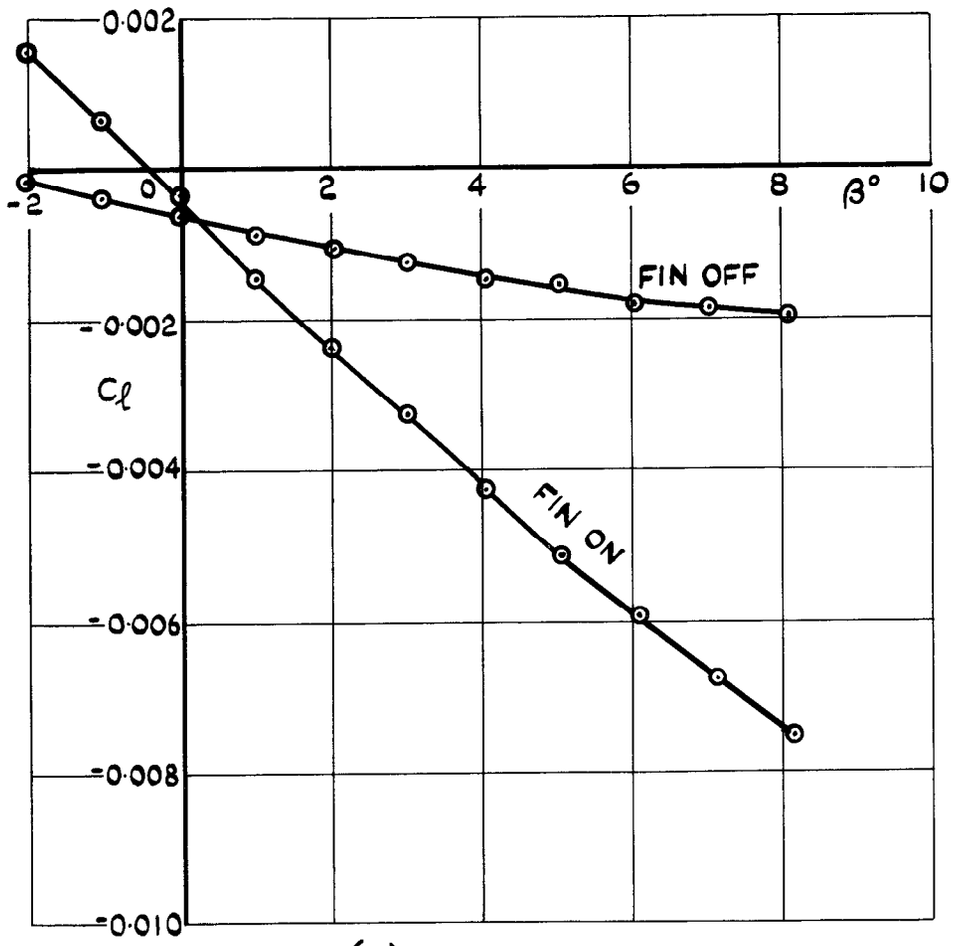

(c) M = 1·82

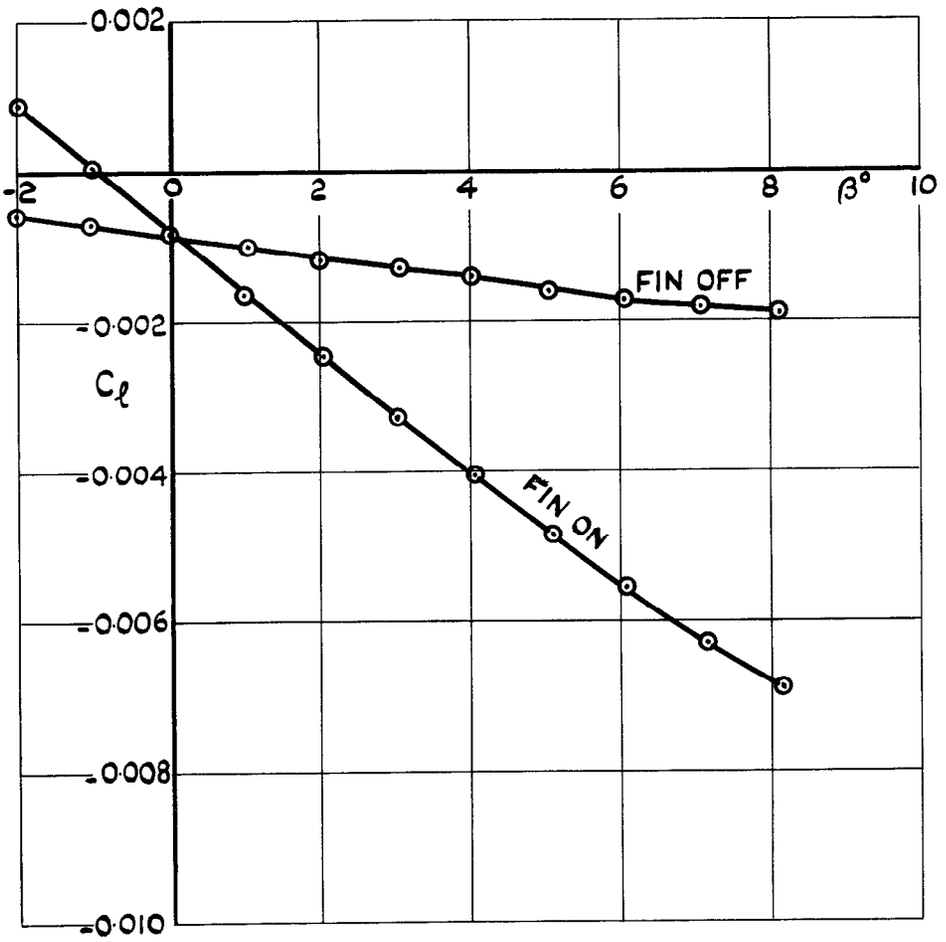

(d) M = 2·00

FIG. 33. (CONTD)

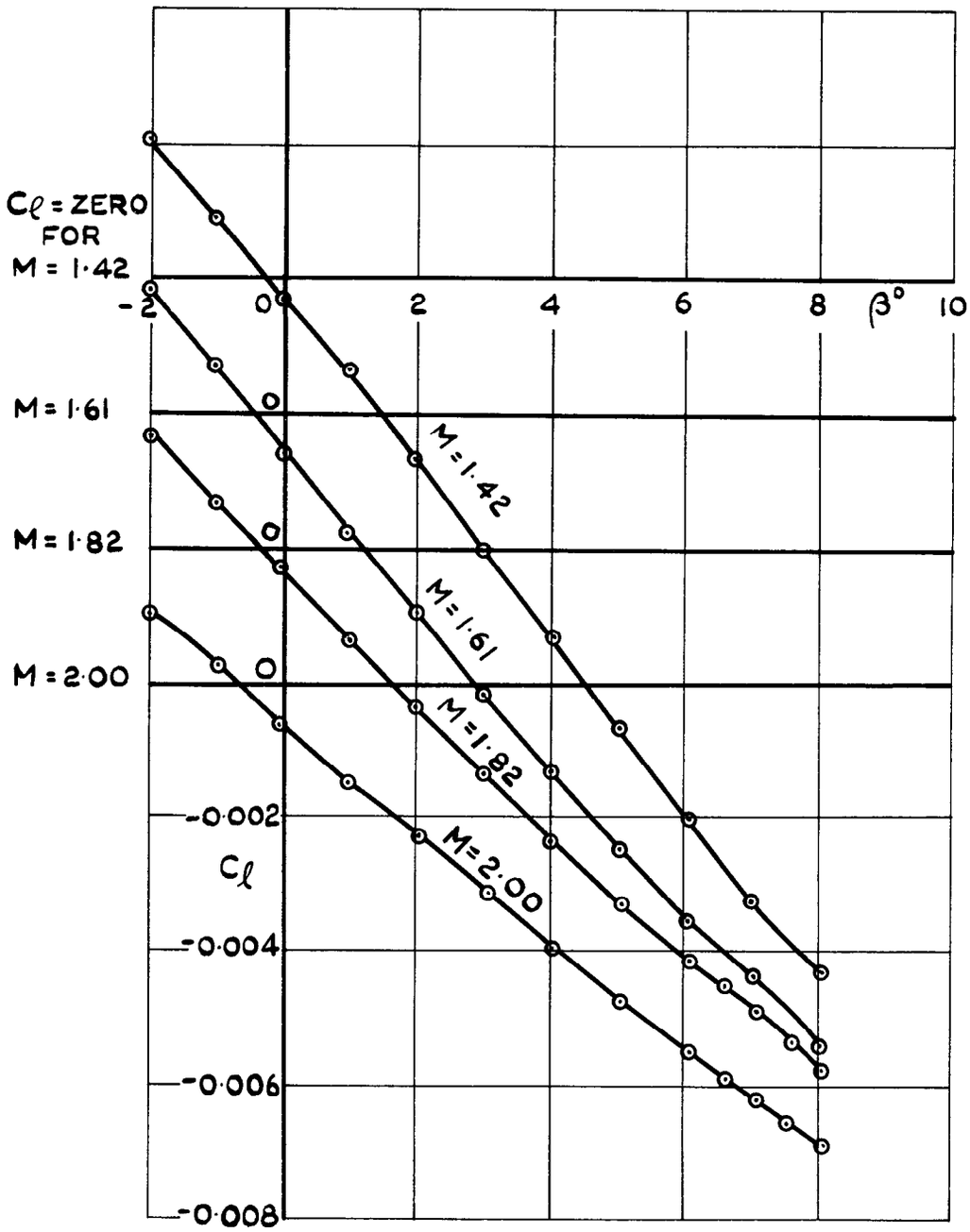

FIG. 34. ROLLING MOMENT—VARIATION WITH SIDESLIP ANGLE AND MACH NUMBER, MODEL WITH FIN ON, $\eta = -4^{\circ}$. AT $\alpha = 0^{\circ}$.

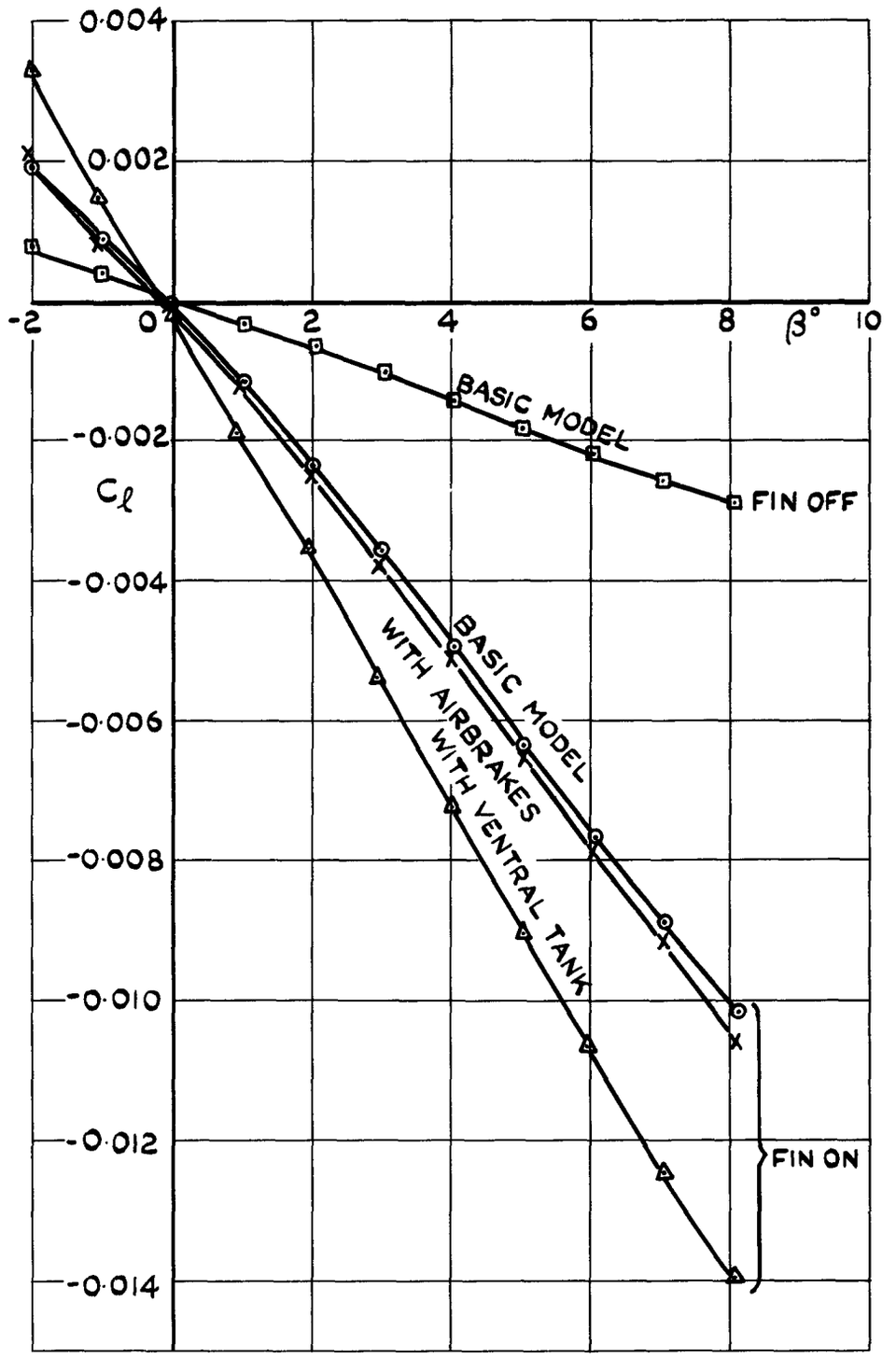

(a) M = 1·42

FIG 35. ROLLING MOMENT—VARIATION WITH SIDESLIP ANGLE AND MACH NUMBER, MODEL WITH $\eta = -10°$, AT $\alpha = 0°$.

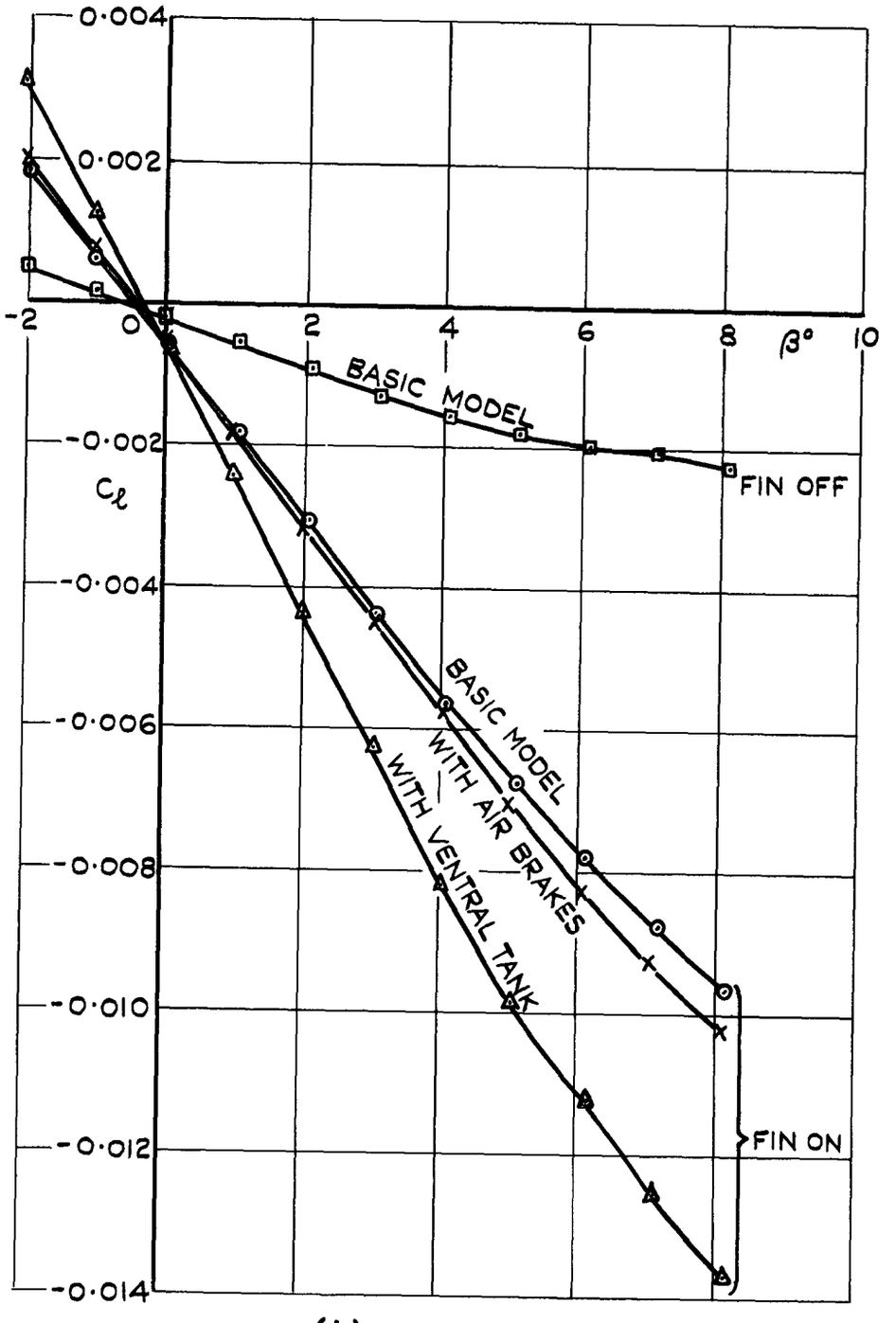

(b) M = 1·61

FIG. 35. (CONTD)

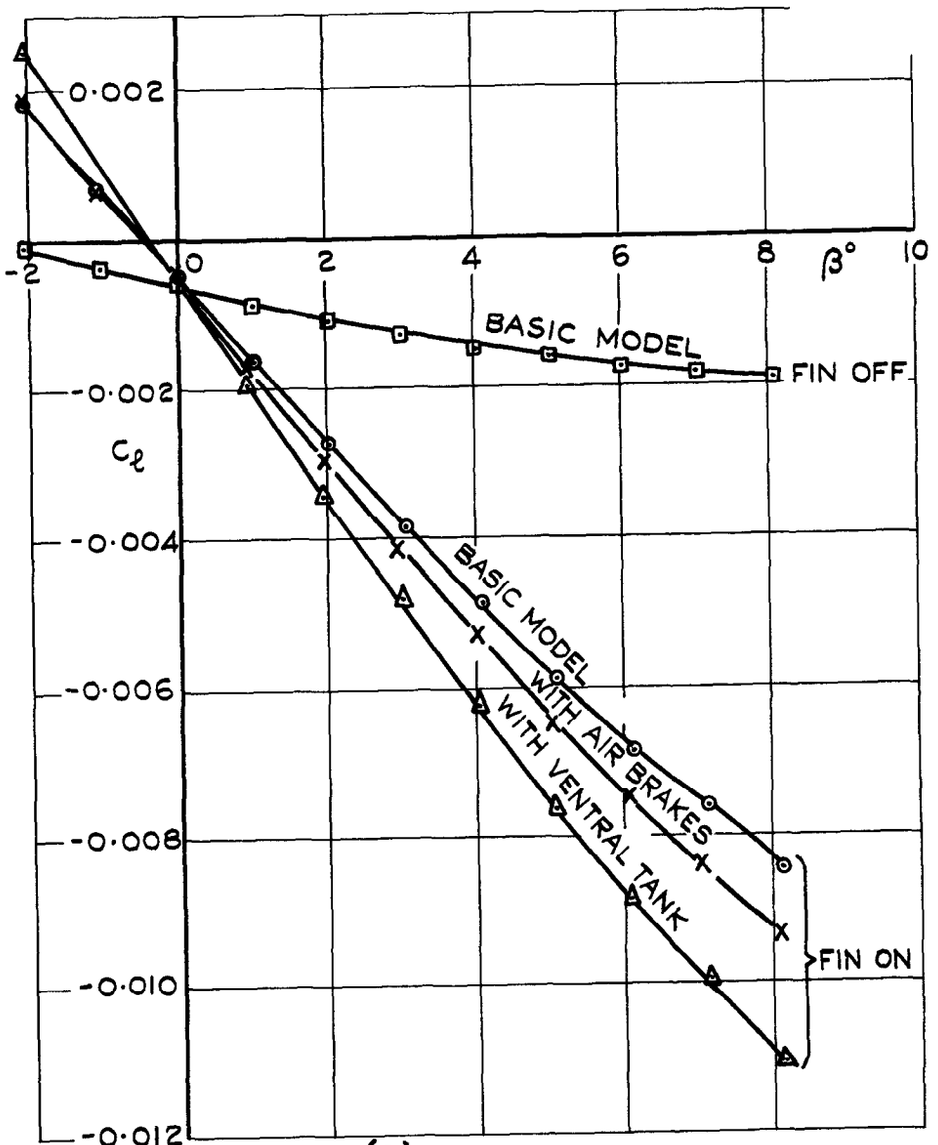

(c) M = 1·82

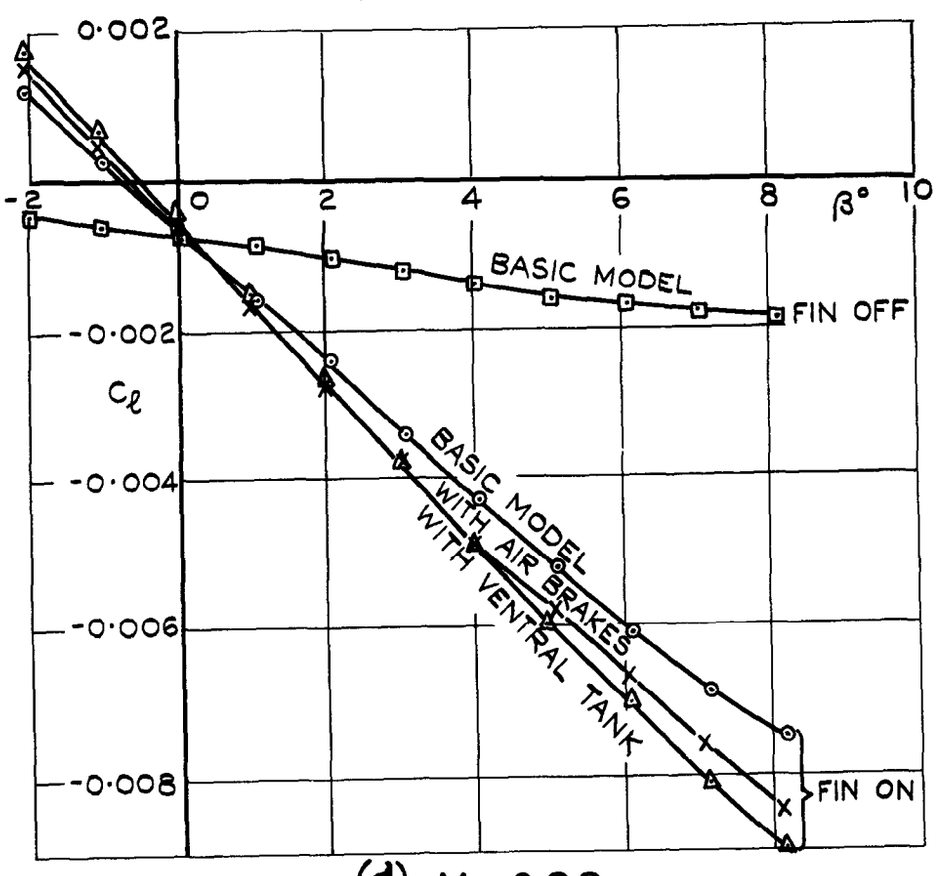

(d) M = 2·00

FIG. 35. (CONCLD)

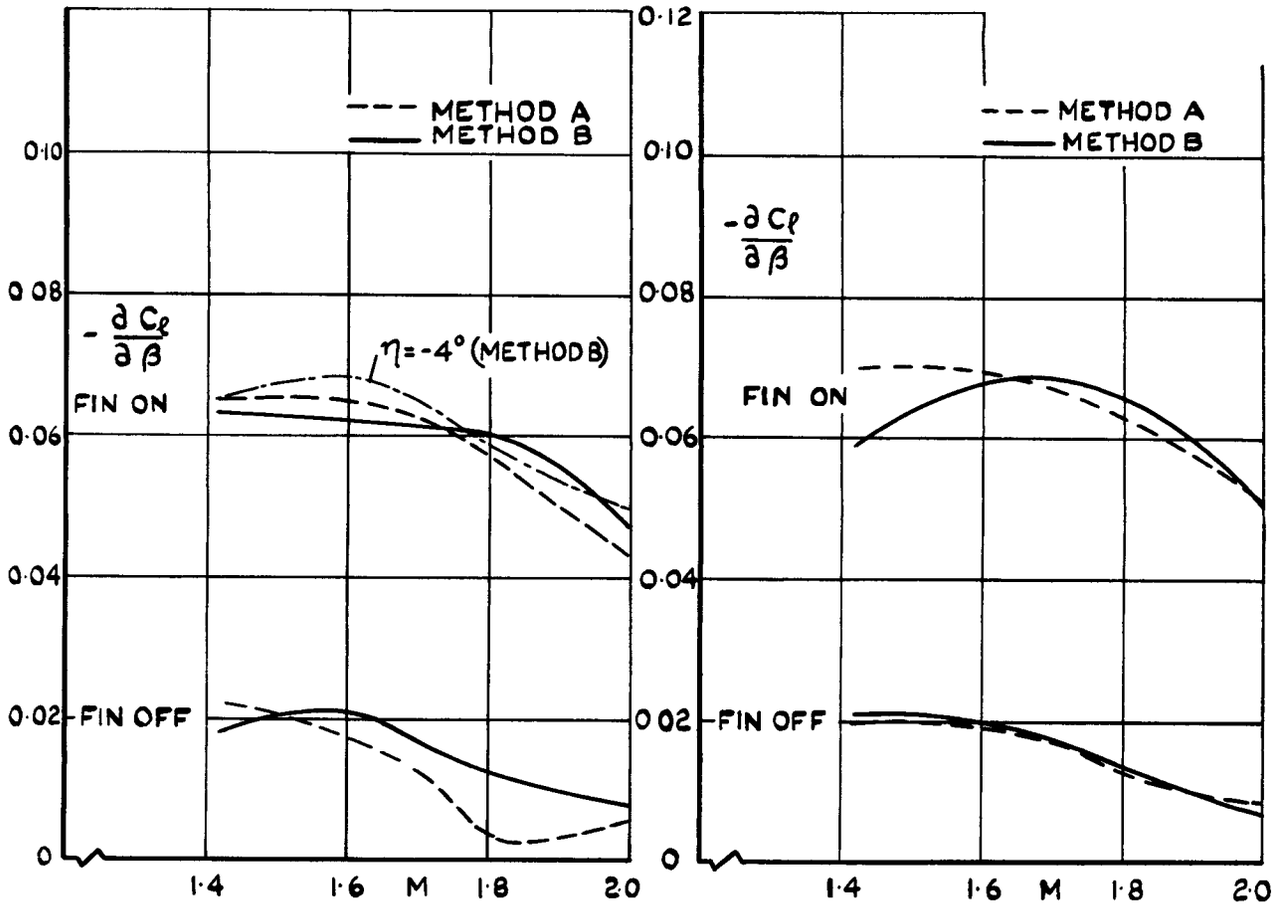

(a) WITH $\eta=0°$ & $\eta=-4°$ (INDICATED) (b) WITH ($\eta=-10°$)

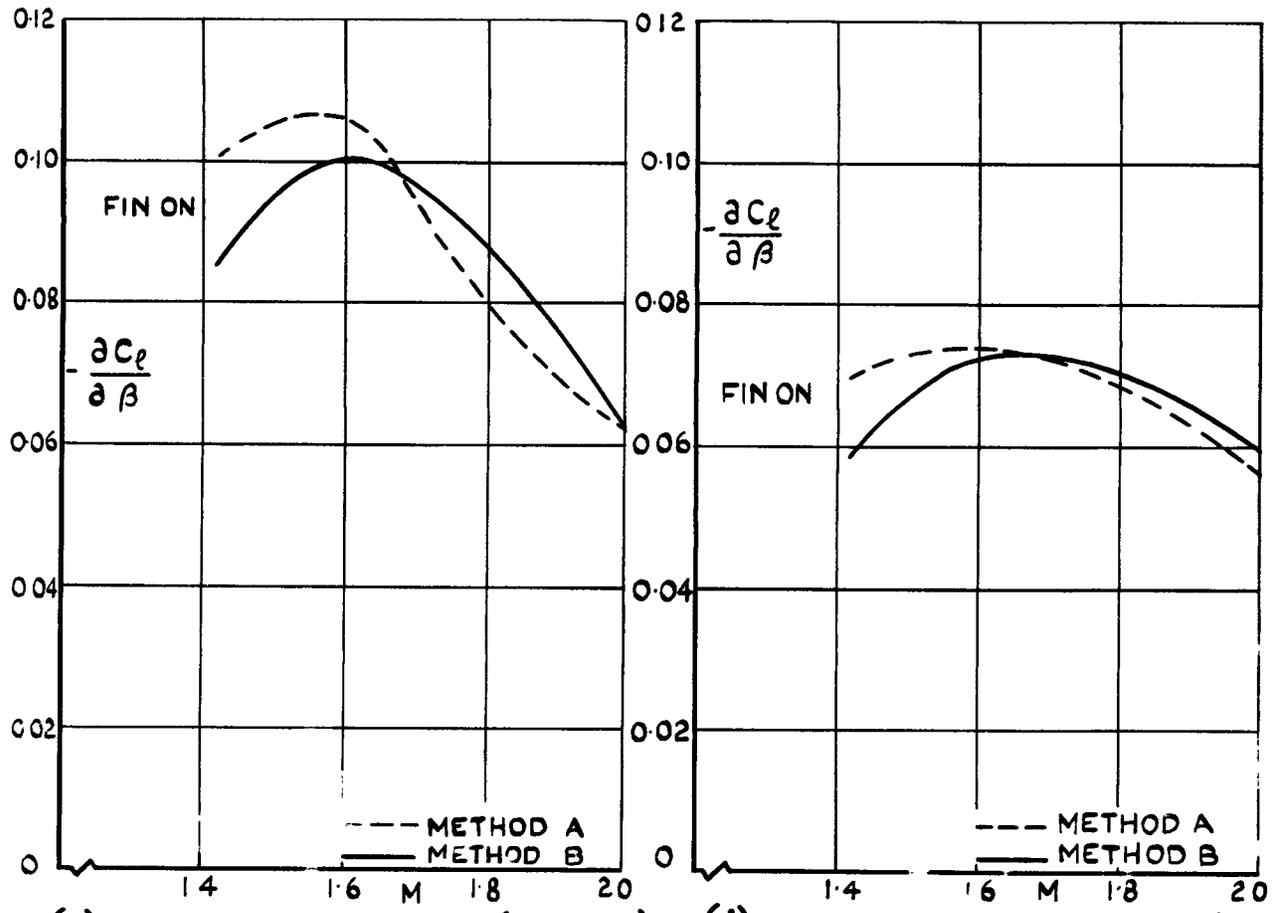

(c) WITH VENTRAL TANK ($\eta=-10°$) (d) WITH AIRBRAKES ($\eta=-10°$)

FIG.36. ROLLING MOMENT DUE TO SIDESLIP (AT $\alpha=0°$) – VARIATION WITH MACH NUMBER.

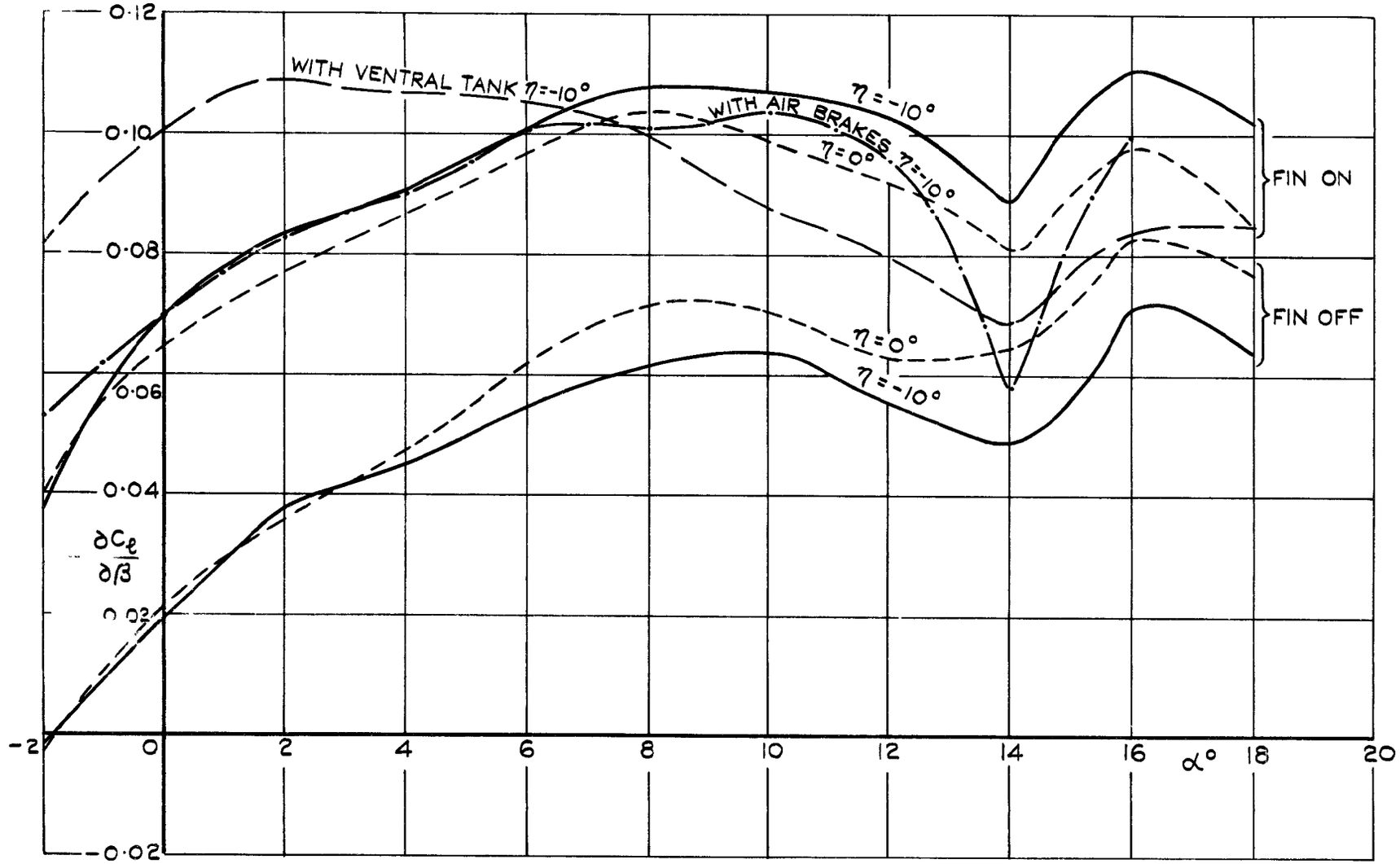

(a) M=1·42

FIG.37. ROLLING MOMENT DUE TO SIDESLIP—VARIATION WITH INCIDENCE AND MACH NUMBER.

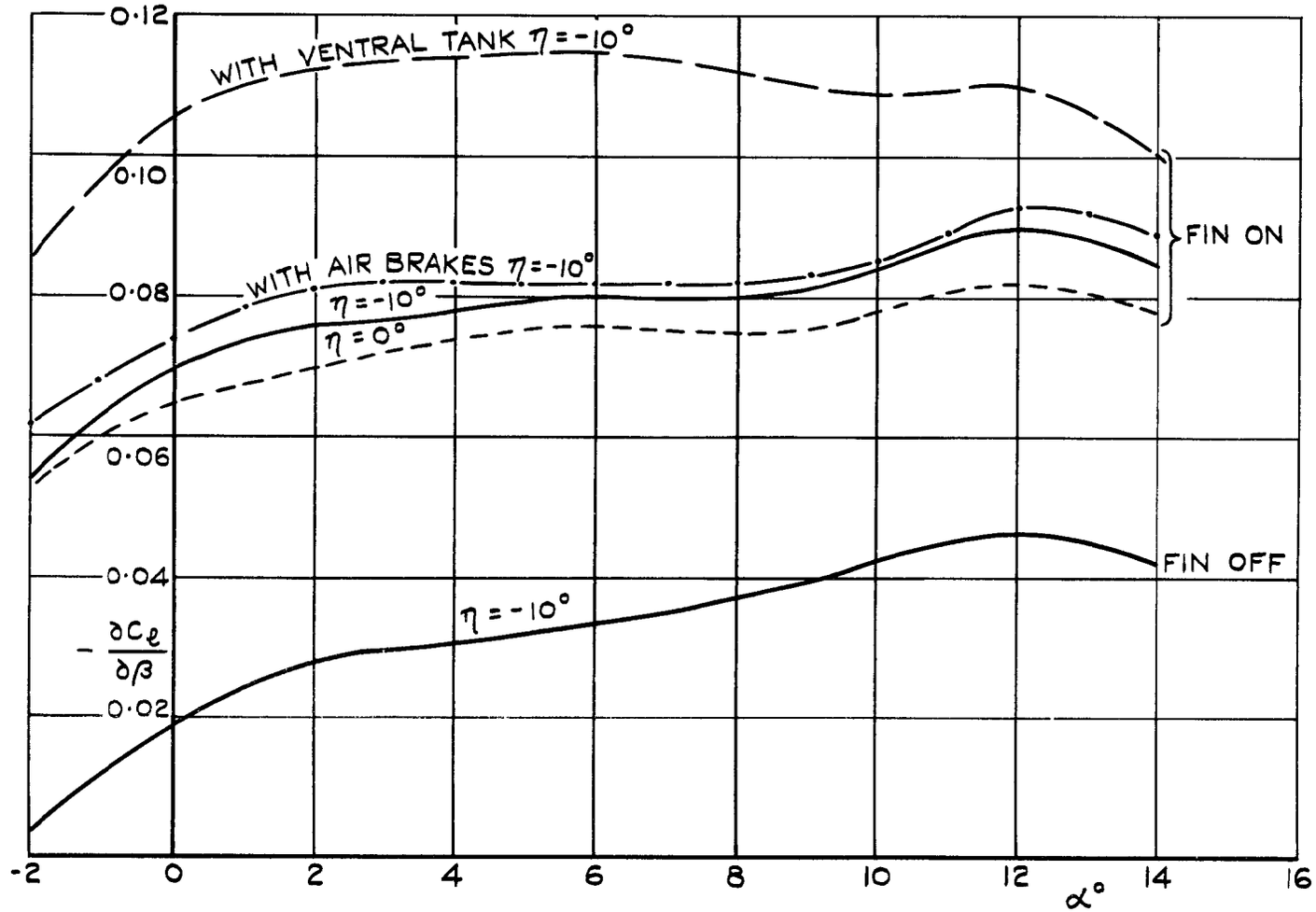

(b) M = 1·61.

FIG. 37 (CONTD.)

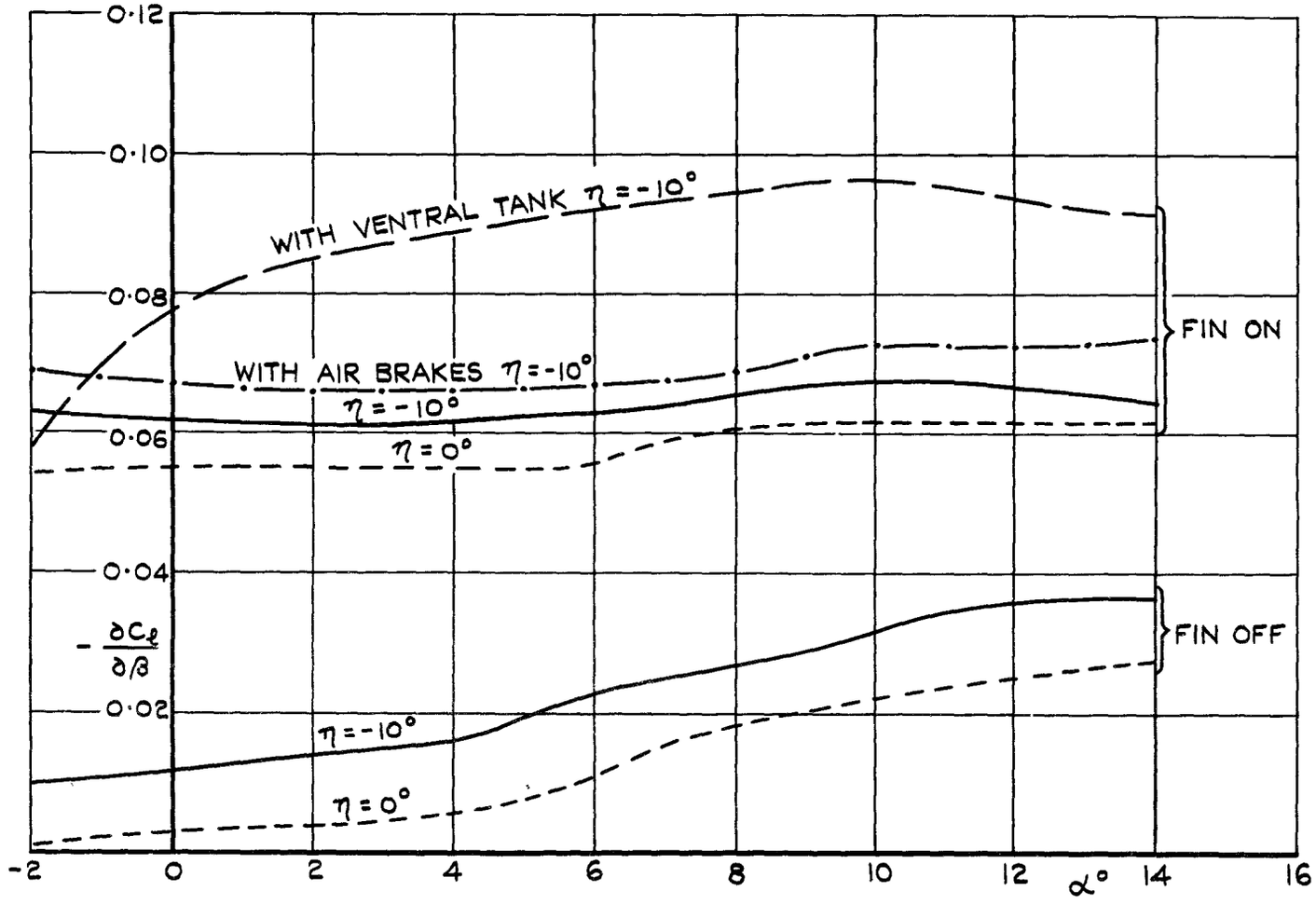

(C) M = 1·82.

FIG. 37. (CONTD.)

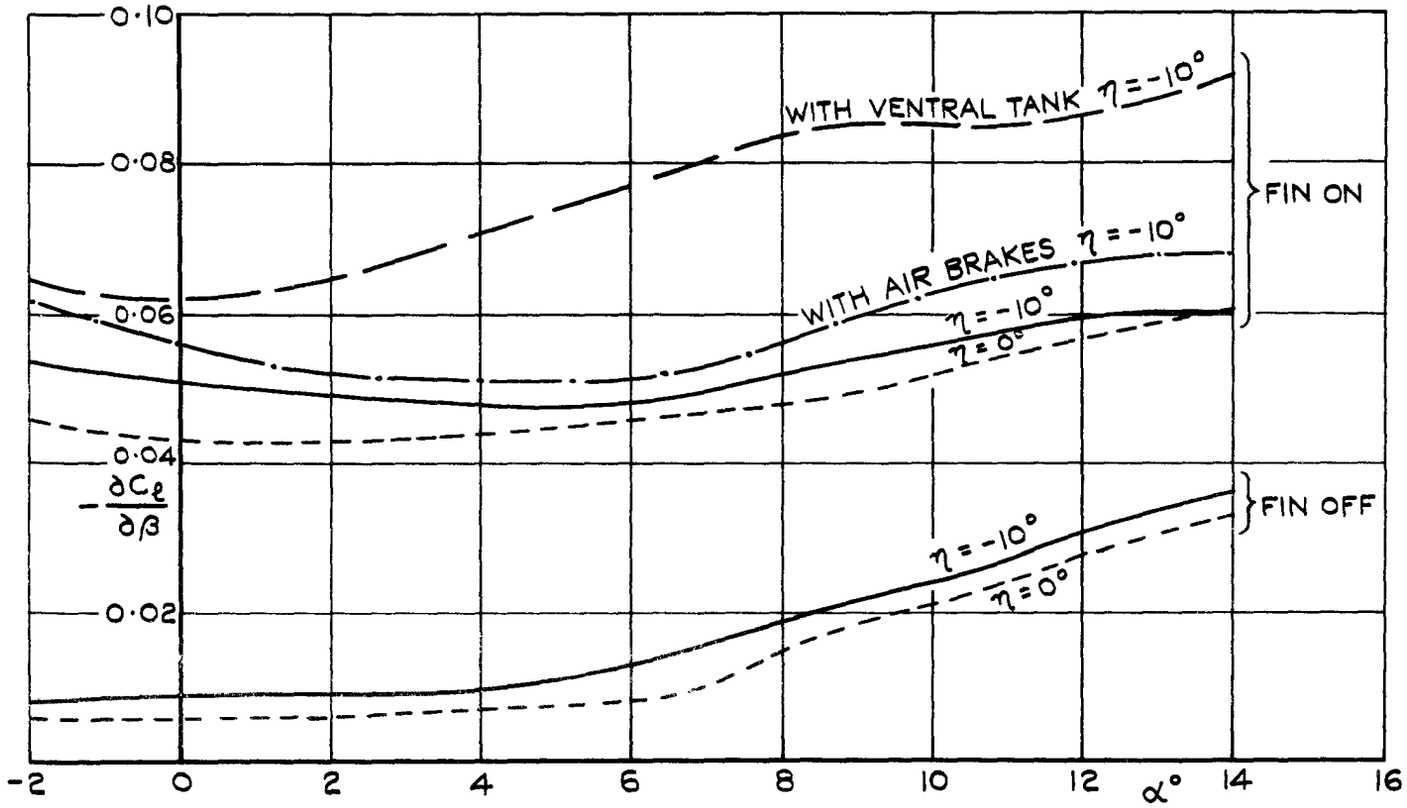

(d) M=2·00.

FIG. 37. (CONCLD.)

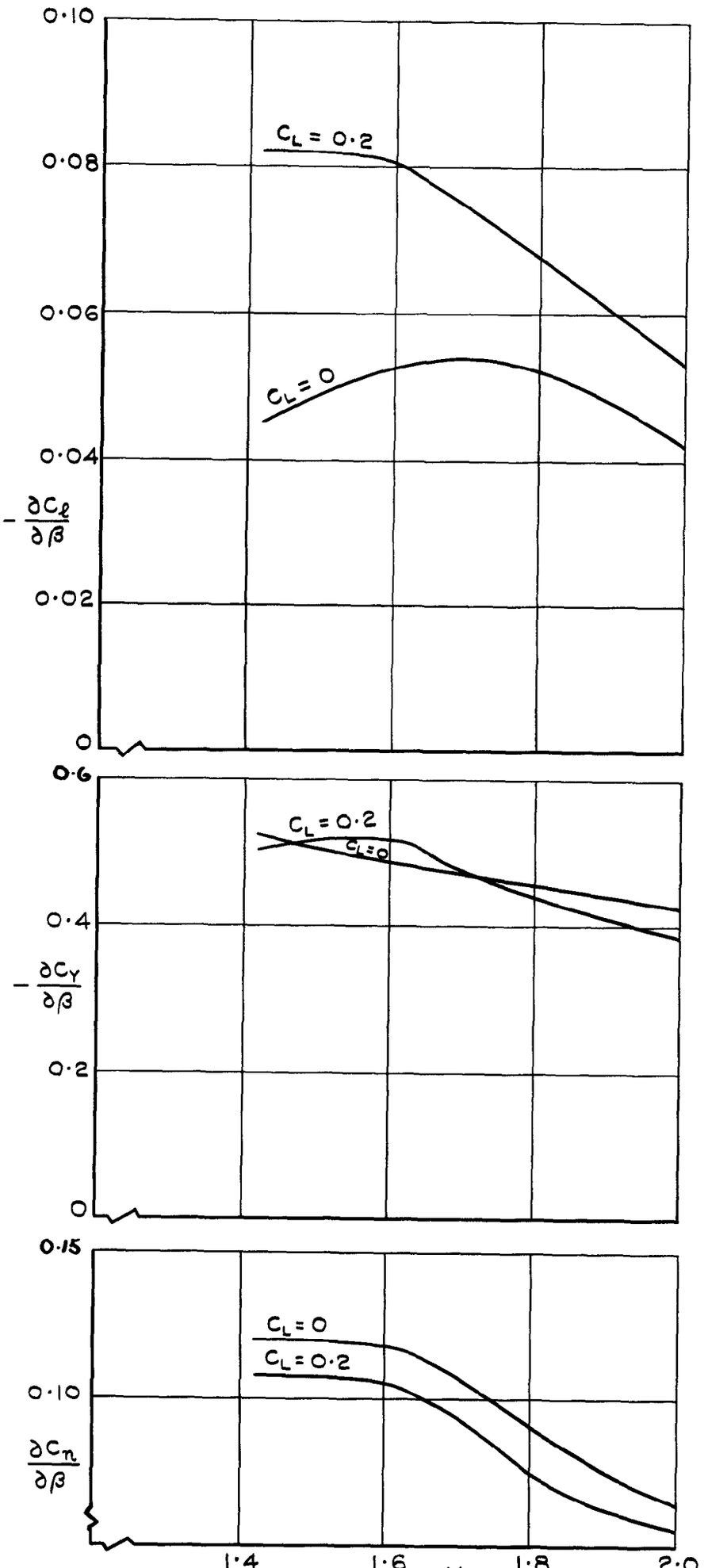

FIG. 38. SIDESLIP DERIVATIVES - VARIATION WITH MACH NUMBER AT CONSTANT LIFT COEFFICIENT.

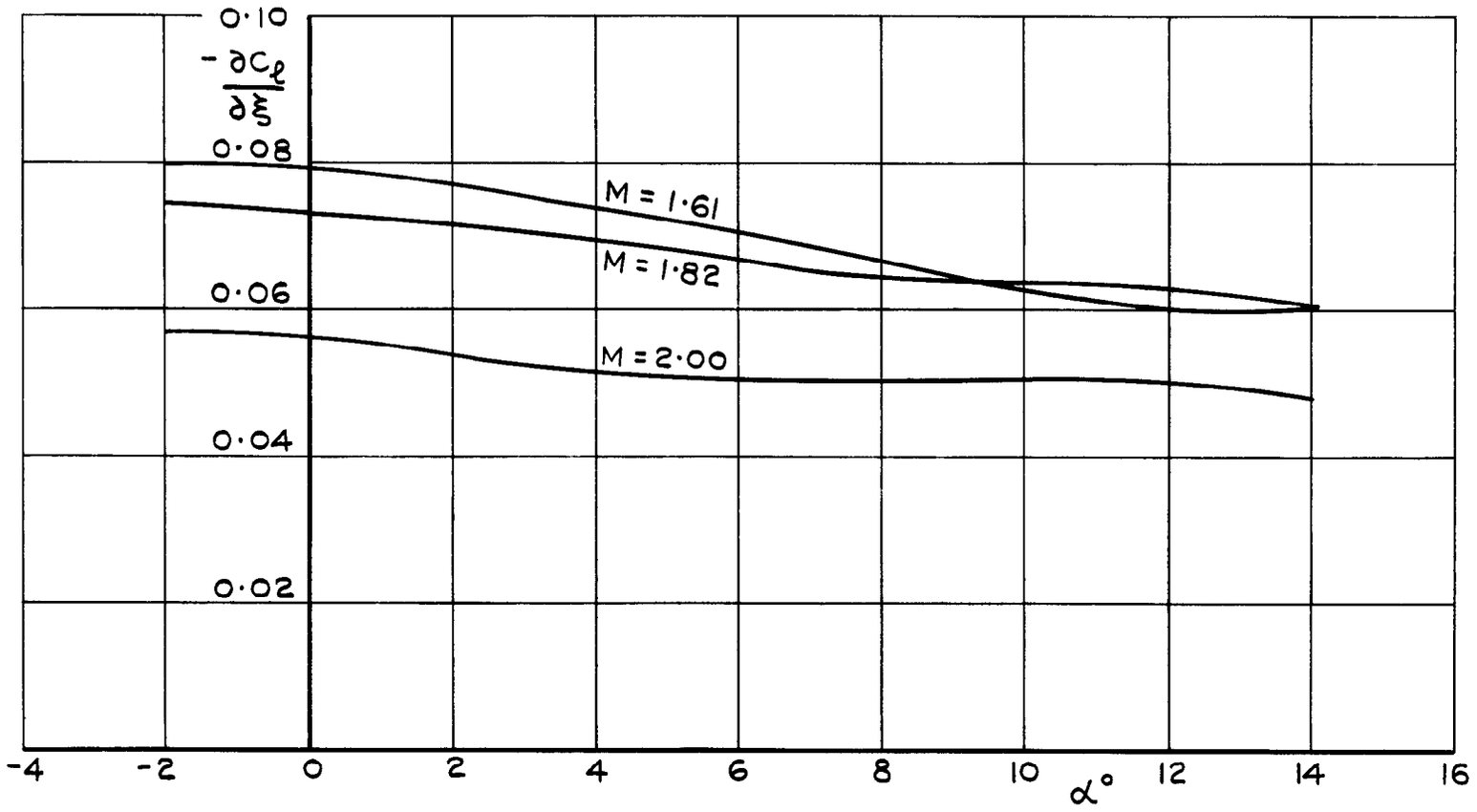

FIG. 39. AILERON EFFECTIVENESS - VARIATION WITH INCIDENCE AND MACH NUMBER, MODEL WITH $\eta = -4°$

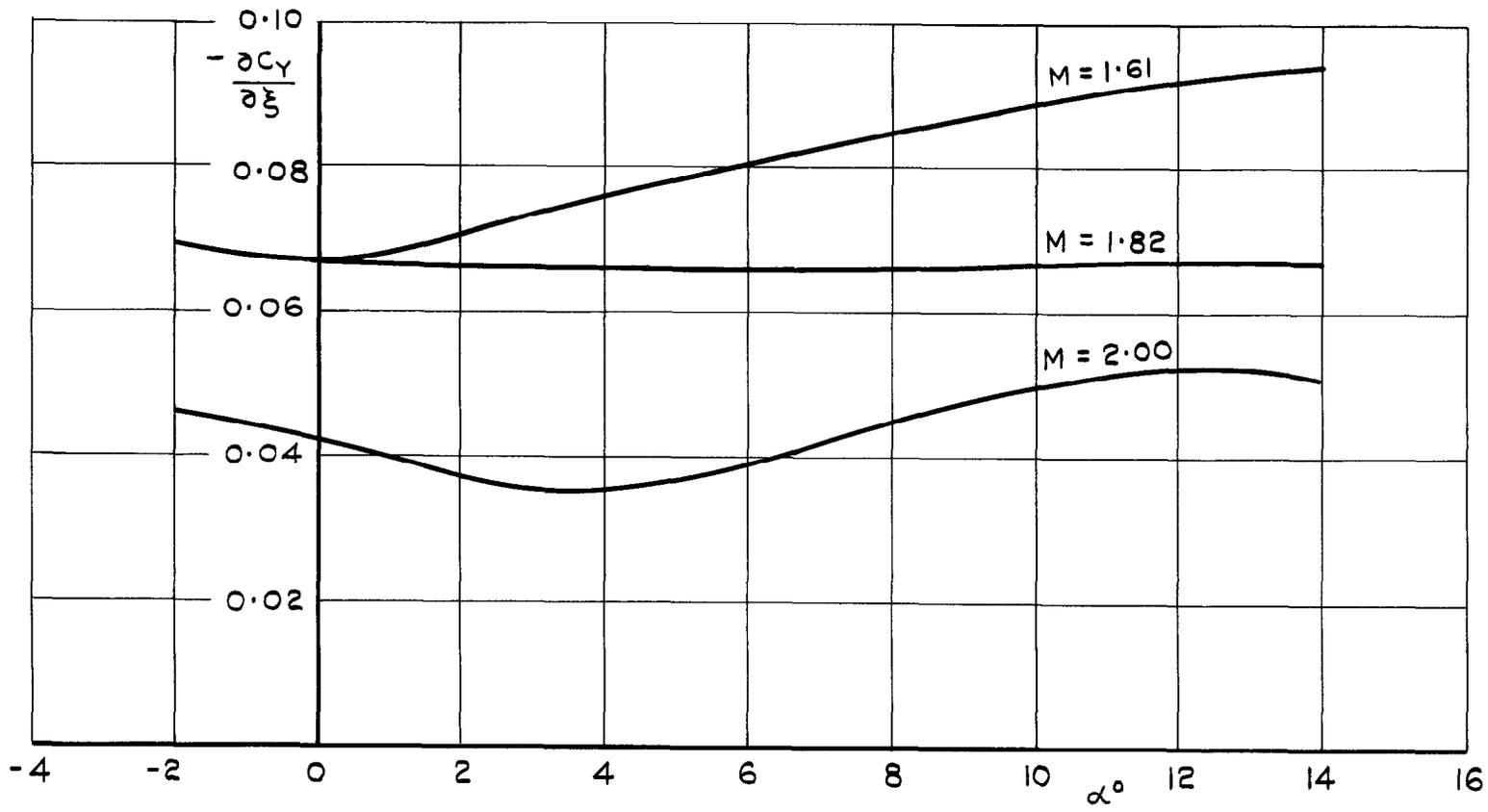

FIG.40. SIDEFORCE DUE TO AILERON—VARIATION WITH INCIDENCE AND MACH NUMBER, MODEL WITH $\eta = -4^{\circ}$.

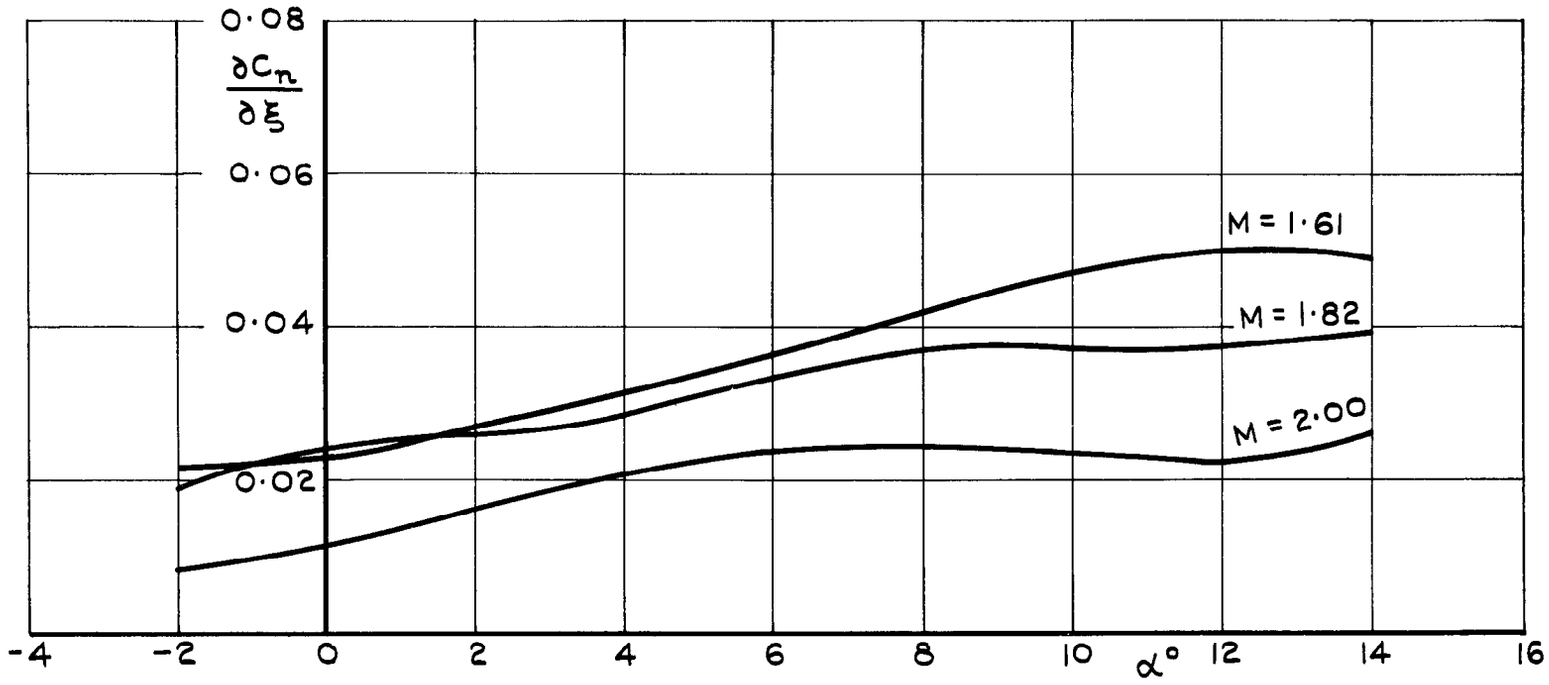

FIG. 41. YAWING MOMENT DUE TO AILERON—VARIATION WITH INCIDENCE AND MACH NUMBER, MODEL WITH $\eta = -4^\circ$

(8277)

A.R.C. C.P. No. 672

A.I.(42) Fairey Delta
533.6.013.1 :
533.6.011.5

WIND TUNNEL TESTS AT SUPERSONIC SPEEDS ON A MODEL OF THE FAIREY DELTA 2. Dobson, M.D. Oct. 1962.

Results are given of tests at Mach numbers from 1.42 to 2.00, on a 1/24 scale model of the Fairey Delta 2 aircraft. Lift, pitching moment, axial force, sideforce, yawing moment and rolling moment were measured, giving an assessment of the general stability characteristics, including the effects of airbrakes and a ventral fuel tank. Elevator effectiveness and aileron effectiveness were measured. Incremental values of drag were obtained resulting from separate addition of airbrakes and fuel tank, and the application of elevator and aileron. No absolute values of drag are presented owing to difficulties in measuring the internal drag of the intake system.

(Over)

A.R.C. C.P. No. 672

A.I.(42) Fairey Delta
533.6.013.1 :
533.6.011.5

WIND TUNNEL TESTS AT SUPERSONIC SPEEDS ON A MODEL OF THE FAIREY DELTA 2. Dobson, M.D. Oct. 1962.

Results are given of tests at Mach numbers from 1.42 to 2.00, on a 1/24 scale model of the Fairey Delta 2 aircraft. Lift, pitching moment, axial force, sideforce, yawing moment and rolling moment were measured, giving an assessment of the general stability characteristics, including the effects of airbrakes and a ventral fuel tank. Elevator effectiveness and aileron effectiveness were measured. Incremental values of drag were obtained resulting from separate addition of airbrakes and fuel tank, and the application of elevator and aileron. No absolute values of drag are presented owing to difficulties in measuring the internal drag of the intake system.

(Over)

A.R.C. C.P. No. 672

A.I.(42) Fairey Delta
533.6.013.1 :
533.6.011.5

WIND TUNNEL TESTS AT SUPERSONIC SPEEDS ON A MODEL OF THE FAIREY DELTA 2. Dobson, M.D. Oct. 1962.

Results are given of tests at Mach numbers from 1.42 to 2.00, on a 1/24 scale model of the Fairey Delta 2 aircraft. Lift, pitching moment, axial force, sideforce, yawing moment and rolling moment were measured, giving an assessment of the general stability characteristics, including the effects of airbrakes and a ventral fuel tank. Elevator effectiveness and aileron effectiveness were measured. Incremental values of drag were obtained resulting from separate addition of airbrakes and fuel tank, and the application of elevator and aileron. No absolute values of drag are presented owing to difficulties in measuring the internal drag of the intake system.

(Over)

The model was stable in pitch and the position of the aerodynamic centre remained constant at 0.51 $\bar{\bar{c}}$ (0.67 centre line chord) throughout the incidence range at all Mach numbers. The addition of airbrakes caused a rearward movement of the aerodynamic centre of 0.02 $\bar{\bar{c}}$ at all Mach numbers.

In all configurations the model was directionally stable at low lift, though the stability decreased with increase of incidence and in some cases the model became directionally unstable at high incidence. Directional stability was appreciably improved by opening the airbrakes but was reduced by the addition of the ventral fuel tank.

The model was stable in pitch and the position of the aerodynamic centre remained constant at 0.51 $\bar{\bar{c}}$ (0.67 centre line chord) throughout the incidence range at all Mach numbers. The addition of airbrakes caused a rearward movement of the aerodynamic centre of 0.02 $\bar{\bar{c}}$ at all Mach numbers.

In all configurations the model was directionally stable at low lift, though the stability decreased with increase of incidence and in some cases the model became directionally unstable at high incidence. Directional stability was appreciably improved by opening the airbrakes but was reduced by the addition of the ventral fuel tank.

The model was stable in pitch and the position of the aerodynamic centre remained constant at 0.51 $\bar{\bar{c}}$ (0.67 centre line chord) throughout the incidence range at all Mach numbers. The addition of airbrakes caused a rearward movement of the aerodynamic centre of 0.02 $\bar{\bar{c}}$ at all Mach numbers.

In all configurations the model was directionally stable at low lift, though the stability decreased with increase of incidence and in some cases the model became directionally unstable at high incidence. Directional stability was appreciably improved by opening the airbrakes but was reduced by the addition of the ventral fuel tank.

Printed and published by
HER MAJESTY'S STATIONERY OFFICE

To be purchased from
York House, Kingsway, London w.c.2
423 Oxford Street, London w.1
13A Castle Street, Edinburgh 2
109 St. Mary Street, Cardiff
39 King Street, Manchester 2
50 Fairfax Street, Bristol 1
35 Smallbrook, Ringway, Birmingham 5
80 Chichester Street, Belfast 1
or through any bookseller

Printed in England

C.P. No. 672

S.O. Code No. 23-9013-72